Assessing and Optimizing the Performance of Photoredox-Mediated Metal-Free Ring-Opening Metathesis Polymerization in Batch and Flow Reactors

By

Vincent P. Rigoglioso

A dissertation submitted in partial fulfillment of

the requirements for the degree of

Doctor of Philosophy

(Chemistry)

at the

UNIVERSITY OF WISCONSIN–MADISON

2024

Date of final oral examination: 01/30/2024

The dissertation is approved by the following members of the Final Oral Committee:

Andrew J. Boydston, Professor, Chemistry (Materials Chemistry)
Clark R. Landis, Professor, Chemistry (Inorganic Chemistry)
Tehshik P. Yoon, Professor, Chemistry (Organic Chemistry)
Jeffrey D. Martell, Assistant Professor, Chemistry (Chemical Biology)

Acknowledgements

My PhD journey has been testing, and I truly would not have made it through graduate school without the support, kindness, and love from those around me. There are so many more names that have helped me through this process than I have space to acknowledge, but know that I've only met extraordinary people during my time at UW-Madison.

I'll lead off by saying stating some advice that I'd received regarding graduate school… "If you can like 2 of the following 4, you can make it through grad school: advisor, lab mates, research, and location." I've been fortunate to love all 4 of these.

To Clark, Tehshik, and Jeff, thank you for being on my committee and supporting me through my PhD journey.

To AJ, thank you for your extreme kindness and patience. I admire you as a presenter, scientist, educator, and person (in increasing order of admiration). I hadn't known that you'd be at UW-Madison when I accepted my PhD offer, but I couldn't have found a better research advisor. You've truly let me make my PhD into what I wanted it to be. Thank you.

To my Boydston Group lab mates, thank you for being my family in the Midwest. I've loved camping, playing sports, doing game nights, and socializing with y'all for these past 5 years. I'd list names, but then I'd just end up writing out all Group members, past and present, so I'll limit my specific shout out to my cohort—Cody, Rachel, and Sean (alphabetical order). I'm so lucky to have joined the Group at the same time as y'all, and I've enjoyed all of our scientific and personal conversations.

To Chang-Uk, thank you for the countless personal, philosophical, and silly discussions that we've shared. You've been a wonderful lab mate, office mate, and friend.

To Oliver, Lydia, Becky, Matthew, and Megan, thank you for being my squad. I've enjoyed all of our sports and random hangouts. Thank you for being my friends.

To Tess, Basil, and Roman, I never could've imagined starting a family in grad school, but that's exactly what we did. Thank you for all the new experiences and love you've shared with me.

To Dad, Domenic, Vanessa, Wally, and Bobi, thank you for letting me experience an independent life in Madison. I wish I could've been in two places at once, or that you could've came out here and experienced this with me. I felt like I had a heart in 2 different places. Friends would mention how quickly they got bored of home when they visited for breaks, but I never had that problem. Thank you for making it so effortless to love you.

To Mom, thank you everything. We always talked, and you always let me know how loved and supported I was no matter what. I hope you can see this. I love you <3

Table of Contents

Abstract

Photoredox-mediated metal-free ring-opening metathesis polymerization (MF-ROMP) is a convenient metal-free method to produce a variety of ROMP polymers. Though simple to implement in small-scale batch experiments, attempts to study and improve this photomediated radical cationic polymerization have been profoundly complex.

This dissertation will motivate the research of MF-ROMP, and describe (1) the development of methods for assessing the mechanism of MF-ROMP, (2) the discovery and characterization of novel copolymer systems within MF-ROMP, and (3) the design and optimization of flow reactor setups enabling continuous production for MF-ROMP.

Ultimately, the information herein provides methods and insights in expanding the utility and functionality of MF-ROMP. A chapter summarizing this research for the general public is included at the end of this dissertation.

Chapter 1: Background and Motivation

The global market for polymers is currently valued at over $700 million and is expected to reach over $1,000 million by the end of 2030.[1] In plastic products alone, this corresponds to a consumption of over 390 million tonnes in 2021 alone, and the demand is expected to rise to one billion tonnes by 2050.[2,3] In order to sustainably mass-produce polymers at the rate required by humanity, polymer scientists need to develop novel, efficient, and scalable polymerization methods.

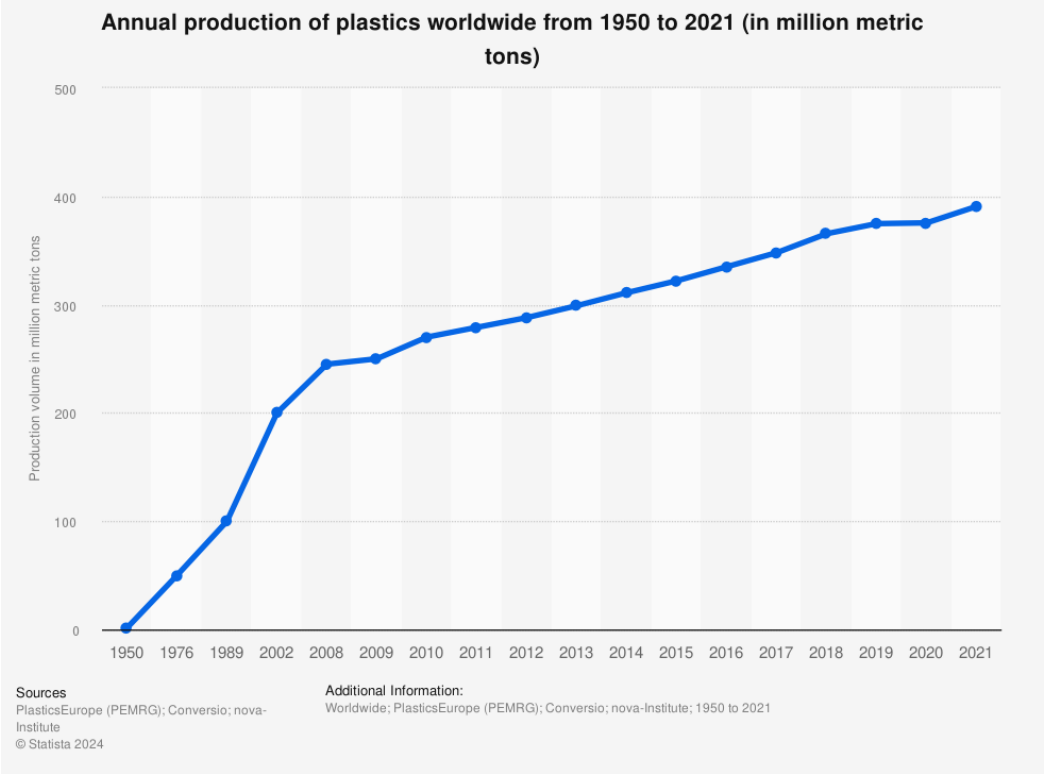

Figure 1. Annual plastic production through 2021. Chart and data from Statista (2024).

Ring-opening metathesis polymerization (ROMP) is a relatively modern polymerization that was enabled by the development of olefin metathesis. ROMP polymers—like poly(norbornene) (pNB or Norsorex®, a sound-proofing material), poly(dicylopentadiene) (pDCPD or Telene®, a common car plastic), and poly(tetracyclododecene) (pTD or Zeonex®, an optics material)—are predominantly produced using metal-mediated mechanisms that employ

well-established metal−alkylidene initiators or transition metal salts (precatalysts).[4–14] By using monomer feedstocks consisting of inexpensive cyclic alkenes, ROMP polymer products also tend to be inexpensive at higher molecular weights. Using metals like ruthenium, molybdenum, and tungsten, metal-mediated ROMP achieves rapid, highly-controlled polymerizations. However, due to the high cost of these metals, producing lower molecular weight polymers—where one mole of metal is needed to initiate one mole of polymer—becomes more costly. Removal of the metal from the polymer also becomes a significant cost-driver in metal-sensitive fields like biotechnology or electronics. See Figure 2 for a summary of considerations regarding ROMP.

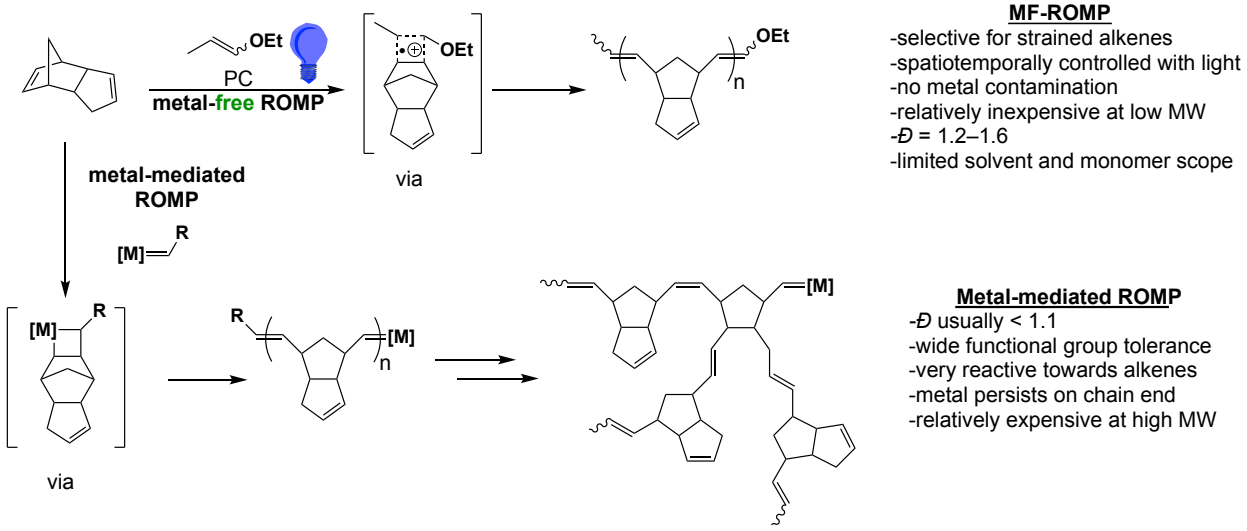

Figure 2. Comparison of metal-mediated v. metal-free ROMP for poly(dicyclopentadiene). Typically M = Mo, W, Ru.

In 2015, the Boydston Group improved the utility of ROMP and reported the novel photoredox-mediated metal-free ring-opening metathesis polymerization (MF-ROMP), a complementary ROMP pathway that is mechanistically distinct from its metal-mediated counterpart.[15] As shown in Figure 3a, MF-ROMP proceeds through a radical cationic polymerization pathway that uses organic monomers, initiators, and photocatalysts. In this polymerization pathway, the 2,4,6-tris(4-methoxyphenyl)pyrylium tetra-fluoroborate

photocatalyst (2) serves as a photooxidant to generate the radical cationic enol ether (3) from the ethyl-1-propenyl ether initiator (1). This radical cationic intermediate engages and opens the strained bicyclic intermediate (4) to produce a ring-opened olefin (5). This newly formed olefin maintains its radical cationic enol ether, which can go on to engage other monomer units to produce ROMP polymers. During this process, back-electron transfer from the reduced photocatalyst and degenerative electron transfer from neutral enol ethers are each envisioned, offering a photo-mediated, spatiotemporally controlled polymerization with living characteristics.[15] As MF-ROMP is a radical cationic polymerization, its performance is unsurprisingly affected by the presence of oxygen in the reaction headspace, performing best under ambient conditions and worse under atmospheres of entirely nitrogen or oxygen, based upon total monomer conversion.[16] Also noteworthy, only highly-strained alkenes show conversion in MF-ROMP leaving less strained alkenes intact, enabling access to valuable ROMP polymers that are typically difficult to produce via metal-mediated pathways, such as linear poly(dicyclopentadiene) (pDCPD).[17–24] MF-ROMP has been demonstrated to produce high-conversion linear pDCPD with the caveat of requiring low temperatures. See Figure 2 for a comparison between metal-mediated and metal-free ROMP.

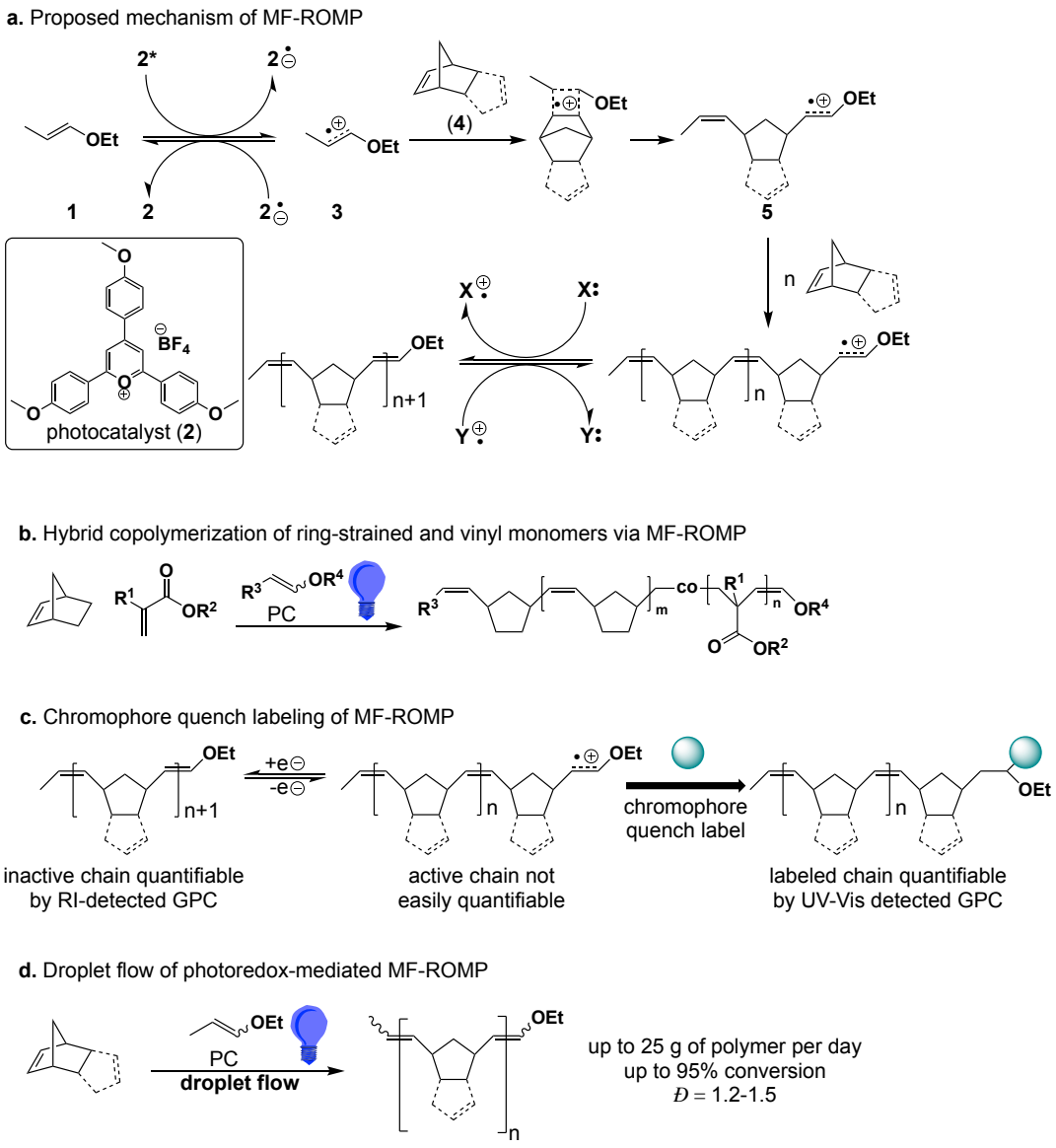

Figure 3. Areas of research for MF-ROMP. (a) Proposed mechanism of MF-ROMP. (b) Expansion of monomer scope for MF-ROMP (see Chapter 2). (c) Development of analytical techniques for MF-ROMP (see Chapter 3). (d) Scale-up of MF-ROMP via a droplet flow reactor setup.

Because of MF-ROMP's novelty, there are a swath of challenges that had yet to be addressed. For instance, MF-ROMP has only been shown to work with norbornyl monomers prior to 2019, which severely limits its utility compared to metal-mediated ROMP. Additionally, MF-ROMP polymer molecular weight dispersities, $Đ$, rarely are below 1.2, signaling decreased control relative to its metal-mediated counterpart, which frequently produces polymers with $Đ$ <1.1. To

improve the mechanism of MF-ROMP, a better understanding of the propagating chain end and general mechanism is needed, though we currently lack ways to analyze how different reaction conditions affect these aspects. Finally, since MF-ROMP requires adequate light penetration, thermal control, and effective mixing, scaleup attempts had been limited to using larger batch reactors at significantly decreased efficiencies to that of smaller scales. To develop MF-ROMP into a more efficient and useful polymerization method, we must achieve new (co)polymerizations with MF-ROMP, increasing its control, and improving its. I will address these goals in the coming chapters.

Chapter 1 References

1. PlasticsEurope (PEMRG). (December 2, 2022). Annual production of plastics worldwide from 1950 to 2021 (in million metric tons). In *Statista*. Retrieved January 21, 2024, from https://www.statista.com/statistics/282732/global-production-of-plastics-since-1950/

2. Polymers Market - Global Industry Analysis, Size, Share, Growth, Trends, Regional Outlook, and Forecast 2023-2032. Report code 2271. *Precedence Research.* **2023**. https://www.precedenceresearch.com/polymers-market

3. GRID-Arendal UNEP. Global plastic production, accumulation and future trends. In *From Pollution to Solution: A Global Assessment of Marine Litter and Plastic Pollution.* **2021.** https://grida.no/resources/15041

4. Mol, J. C. Industrial applications of olefin metathesis. *Journal of Molecular Catalysis A: Chemical* **2004,** *213,* 39–45.

5. Schrock, R. R. Synthesis of stereoregular polymers through ring-opening metathesis polymerization. *Acc. Chem. Res.* **2014**, *47*, 2457−2466.

6. Sutthasupa, S.; Shiotsuki, M.; Sanda, F. Recent advances in ring-opening metathesis polymerization, and application to synthesis of functional materials. *Polym. J.* **2010**, *42*, 905−915.

7. Bielawski, C. W.; Grubbs, R. H. Living ring-opening metathesis polymerization. *Prog. Polym. Sci.* **2007**, *32*, 1−29.

8. Rosebrugh, L. E.; Marx, V. M.; Keitz, B. K.; Grubbs, R. H. Synthesis of highly cis, syndiotactic polymers via ring-opening metathesis polymerization using ruthenium metathesis catalysts. *J. Am. Chem. Soc*. **2013**, *135*, 10032−10035.

9. Jeong, H.; Kozera, D. J.; Schrock, R. R.; Smith, S. J.; Zhang, J.; Ren, N.; Hillmyer, M. A. Z-Selective Ring-Opening Metathesis Polymerization of 3-Substituted Cyclooctenes by Monoaryloxide Pyrrolide Imido Alkylidene (MAP) Catalysts of Molybdenum and Tungsten. *Organometallics* **2013**, *32*, 4843−4850.

10. Forrest, W. P.; Axtell, J. C.; Schrock, R. R. Tungsten oxo alkylidene complexes as initiators for the stereoregular polymerization of 2, 3-dicarbomethoxynorbornadiene. *Organometallics* **2014**, *33*, 2313−2325.

11. Chauvin, Y. Olefin metathesis: The early days (Nobel lecture). *Angew. Chem., Int. Ed*. **2006**, *45*, 3740−3747.

12. Schrock, R. R. Multiple metal–carbon bonds for catalytic metathesis reactions (Nobel lecture). *Angew. Chem., Int. Ed*. **2006**, *45*, 3748−3759.

13. Grubbs, R. H. Olefin-metathesis catalysts for the preparation of molecules and materials (Nobel lecture). *Angew. Chem., Int. Ed.* **2006**, *45*, 3760−3765.

14. Autenrieth, B.; Schrock, R. R. Stereospecific Ring-Opening Metathesis Polymerization (ROMP) of Norbornene and Tetracyclododecene by Mo and W Initiators. *Macromolecules* **2015**, *48*, 2493–2503.

15. Ogawa, K. A.; Goetz, A. E.; Boydston, A. J. Metal-Free Ring-Opening Metathesis Polymerization. *J. Am. Chem. Soc.* **2015**, *137*, 1400.

16. Lu, P.; Kensy, V. K.; Tritt, R. L.; Seidenkranz, D. T.; Boydston, A. J. Metal-Free Ring-Opening Metathesis Polymerization: From Concept to Creation. *Acc. Chem. Res*. **2020**, *53*, 2325–2335.

17. Abadie, M. J.; Dimonie, M.; Couve, C.; Dragutan, V. New catalysts for linear polydicyclopentadiene synthesis. *Eur. Polym. J.* **2000**, *36*, 1213–1219.

18. Autenrieth, B.; Jeong, H.; Forrest, W. P.; Axtell, J. C.; Ota, A.; Lehr, T.; Buchmeiser, M. R.; Schrock, R. R. Z-Selective and Syndioselective Ring-Opening Metathesis Polymerization (ROMP) Initiated by Monoaryloxidepyrrolide (MAP) Catalysts. *Macromolecules* **2015**, *48*, 2480–2492.

19. Hayano, S.; Kurakata, H.; Tsunogae, Y.; Nakayama, Y.; Sato, Y.; Yasuda, H. Stereospecific Ring-Opening Metathesis Polymerization of Cycloolefins Using Novel Molybdenum and Tungsten Complexes Having Biphenolate Ligands. Development of Crystalline Hydrogenated Poly(endo-dicyclopentadiene) and Poly(norbornene). *Macromolecules* **2003**, *36*, 7422–7431.

20. Hayano, S.; Takeyama, Y.; Tsunogae, Y.; Igarashi, I. Hydrogenated Ring-Opened Poly(endo-dicyclopentadiene)s Made via Stereoselective ROMP Catalyzed by Tungsten Complexes: Crystalline Tactic Polymers and Amorphous Atactic Polymer. *Macromolecules* **2006**, *39*, 4663–4670.

21. Dono, K.; Huang, J.; Ma, H.; Qian, Y. Ring opening metathesis polymerization of dicyclopentadiene catalyzed by titanium tetrachloride adduct complexes with nitrogen-containing ligands. *J. Appl. Polym. Sci*. **2000**, *77*, 3247–3251.

22. Steese, N. D.; Barvaliya, D.; Poole, X. D.; McLemore, D. E.; DiCesare, J. C.; Schanz, J. J. Synthesis and thermal properties of linear polydicyclopentadiene via ring-opening metathesis polymerization with a third generation grubbs-type ruthenium-alkylidene complex. *J. Polym. Sci., Part A: Polym. Chem*. **2018**, *56*, 359–364.

23. Dumrath, C.; Dumrath, A.; Neumann, H.; Beller, M.; Kadyrov, R. Practical Ruthenium Catalysts for the Synthesis of Cyclic Olefin Oligomers, Polymers, and their Hydrogenated Derivatives. *ChemCatChem* **2014**, *6,* 3101–3104.

24. Yao, Z. Wang, Z.; Yu, Y.; Zeng, C.; Cao, K. Facile synthesis and properties of the chemo-reversible and highly tunable metallogels based on polydicyclopentadiene. *Polymer* **2017**, *119*, 98–106.

Chapter 2

Hybrid Photo-induced Copolymerization of Ring-Strained and Vinyl Monomers Utilizing Metal-Free Ring-Opening Metathesis Polymerization Conditions

Reproduced from: Krappitz, T.; Jovic, K.; Feist, F.; Frisch, H.; Rigoglioso, V. P.; Blinco, J. P.; Boydston, A. J.; Barner-Kowollik, C. "Hybrid Photo-induced Copolymerization of Ring-Strained and Vinyl Monomers Utilizing Metal-Free Ring-Opening Metathesis Polymerization Conditions." *J. Am. Chem. Soc*. **2019**, *141*, 16605−16609.

Abstract

We introduce the hybrid copolymerization of two disparate monomer classes (vinyl monomers and ring-strained cyclic olefins) via living photopolymerization. The living character of the polymerization technique (metal-free photo-ROMP) is demonstrated by consecutive chain-extensions. Further, we propose a mechanism for the copolymerization and analyze the copolymer structure in detail by high-resolution mass spectrometry.

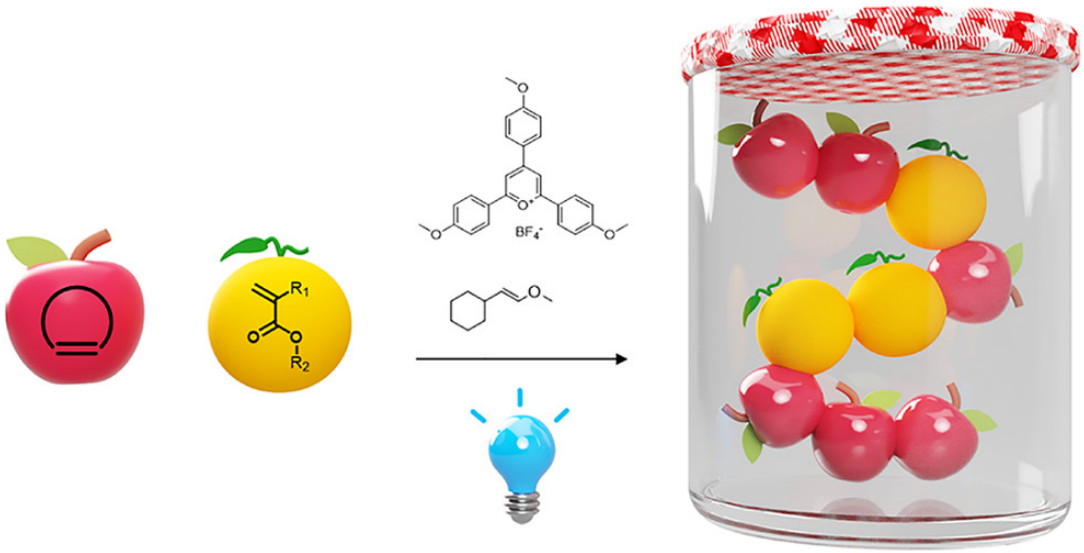

Introduction

Copolymerization within the same class of monomers, following the same polymerization mechanism, can be conducted for almost every polymerization technique. Hybrid copolymerization and interconversion between different polymerization mechanisms is rarely reported and mostly confined to block copolymer formation. Zhang et al. recently established an interconverting polymerization system using heat and light as triggers for the interconversion of anionic ring-opening polymerization (AROP) and photoinduced electron transfer reversible addition–fragmentation chain transfer polymerization (PET-RAFT), affording multiblock copolymers.[1] Despite the few reports on hybrid copolymerizations, some innovative approaches, such as tandem catalysis, afford block,[2–6] brush,[7–9] graft comb[10] or bridge-like[11] polymer structures. Buchmeiser and co-workers demonstrated a sophisticated tandem copolymerization of cyclic olefins with ethylene via a reversible interconversion of the catalyst to catalyze either ring-opening metathesis polymerization (ROMP) or vinyl-insertion polymerization (VIP) to construct the lateral chain.[12–16] The interconversion of two addition polymerizations, e.g. cationic- and radical polymerization of vinyl monomers was recently reported by Fors and co-workers.[17,18]

Metal-free ROMP (MF-ROMP) was demonstrated by Boydston and co-workers and follows a step-growth mechanism where the ω-chain end can be reversibly activated or deactivated by oxidizing the double bond or reducing the cationic radical.[19] Those authors presented random copolymerizations with different ring-strained monomers, the majority constituted of norbornene derivatives and dicyclopentadiene. Furthermore, copolymerization using a bifunctional initiator was shown, affording block copolymers.[20]

Our approach merges the rich variety of vinyl monomers in a hybrid copolymerization with ring-strained monomers utilizing MF-ROMP conditions and paves the way for new copolymer

structures not accessible by other means. The unsaturated backbone and side chains of these copolymers are synthetically readily accessible for functionalization.

Photoinduced homo- and copolymerization of norbornene with vinyl monomers under MF-ROMP conditions were performed utilizing ethyl-1-propenyl ether as well as (2-methoxyvinyl)cyclohexane as initiators and 2,4,6-tris(4-methoxyphenyl)pyrylium tetrafluoroborate ($MeOTPP^{+}BF4^{-}$) as the oxidizing photocatalyst.

The two structurally distinct monomer classes usually follow different polymerization mechanisms, involving radical cations or radicals as the reactive intermediates. Whereas in hybrid copolymerization one reactive species is generated that can add both ring-strained and vinyl monomers to the growing chain (Scheme 1).

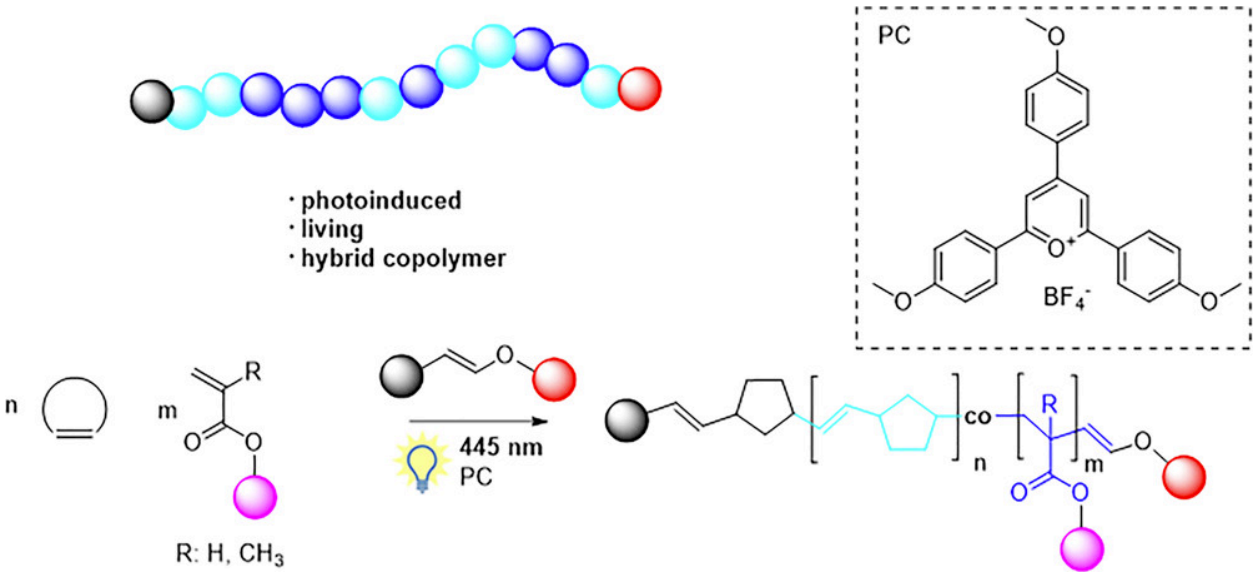

Scheme 1. Hybrid Copolymerization of Ring-Opening Cyclic Olefins with Vinyl Monomers via MF-ROMP Conditions.

Results and Discussion

A selection of the obtained polymers and the corresponding characteristics are summarized in Table 1. Methyl methacrylate and methyl acrylate were utilized as the main representative vinyl monomers and norbornene as the ring strained monomer. Styrenes as well as vinyl ethers are readily oxidized and cannot be polymerized using the same reaction conditions.[21] No quenching agents were required as the polymerization ceases in the dark due to reduction of the active chain end and regeneration of the catalyst.[19] Prior to the herein presented in-depth analysis, mass spectrometric studies have previously not been conducted on polymers obtained via MF-ROMP. For the norbornene homopolymer (entries 1 and 2, Table 1), solely consisting of the highly apolar norbornene repeating unit and the respective end groups originating from the utilized initiator, proton nuclear magnetic resonance (^{1}H NMR) spectroscopy clearly shows the anticipated α- and ω-chain ends as highlighted by Boydston and co-workers (Figure S5).[19]

Table 1. Different (Co)polymers Obtained Utilizing MF-ROMP Conditions[a]

entry	M1 (%)	M2[d]	M_{total}:I:PC	$[M]_0$ (mol·L^{-1})	conversion M1 (%)	conversion M2 (%)	time (min)	M_n (g·mol^{-1})	M_w (g·mol^{-1})	$Đ$
1[b,c]	100	/	108:1:0.05	2.3	44	/	100	17600	25900	1.5
2[b]	100	/	102:1:0.05	2.0	35	/	90	9900	15500	1.6
3[b]	50	MMA	100:1:0.05	2.6	36	0	90	/	/	/
4	50	MMA	100:1:0.03	2.3	14	3	60	3600	6000	1.7
5	50	MA	100:1:0.03	2.0	7	5	60	1700	4700	2.7
6	0	MMA	100:1:0.03	2.3	/	/	60	/	/	/
7	50	MMA	101:1:0.03	2.3	/	/	60	/	/	/
8	45	TFEMA	112:1:0.03	2.2	n.d.	n.d.	60	2100	4400	2.1
9	51	BA	97:1:0.03	1.9	13	5	60	3400	2200	2.2
10	51	IBA	97:1:0.03	1.9	24	3	60	2200	5600	2.6

[a]All reactions were performed in dry dichloromethane at 445 nm LED at 10 W (0.7 A, 8.85 V input) for the stated period of time. (2-methoxyvinyl)cyclohexane was utilized as initiator. The conversions were determined using ^{1}H NMR in CDCl3. [b]Non-deoxygenated. [c]Ethyl-1-propenyl ether. [d]Abbreviations: methyl methacrylate (MMA); methyl acrylate (MA); 2,2,2-trifluoroethyl methacrylate (TFEMA); n-butyl acrylate (BA); isobutyl acrylate (IBA).

A corresponding ionized species was not identified in the recorded electrospray ionization (ESI) mass spectra, most likely due to low ionization efficiencies, however, the correct repeating unit spacing of 94.08 Da was observed (refer to Figure S16). A possible explanation for the species in the mass spectrum could be the [2+2]-cycloaddition of the charged ω-chain end with a neutral initiator molecule, as is often observed in radical cation chemistry.[22] However, the corresponding species would inhibit the polymerization and would be in conflict with the ^{1}H NMR spectrum, therefore, the presence of the observed end group species may result from preferential ionization. After successful homopolymerization using MF-ROMP conditions, the possibility of orthogonal reactivities between MF-ROMP and radical polymerizations of vinyl monomers was investigated. Thus, a polymerization of norbornene via MF-ROMP in the presence of methyl methacrylate (MMA) was performed. The presence of MMA did not inhibit the ROMP, nor was it orthogonal to MF-ROMP, as can be seen in the ^{1}H NMR spectrum in Figure 1. The proton resonances of the methoxy group at 3.60 ppm, and for the methyl group at 0.84 ppm, are suitable signals for the identification of MMA units in the copolymer. The norbornene repeating unit can be readily identified via the resonances at 5.34 and 5.20 ppm, associated with the backbone double bonds formed during ROMP, as well as the CH resonances of the five-membered ring at 2.78 and 2.43 ppm.

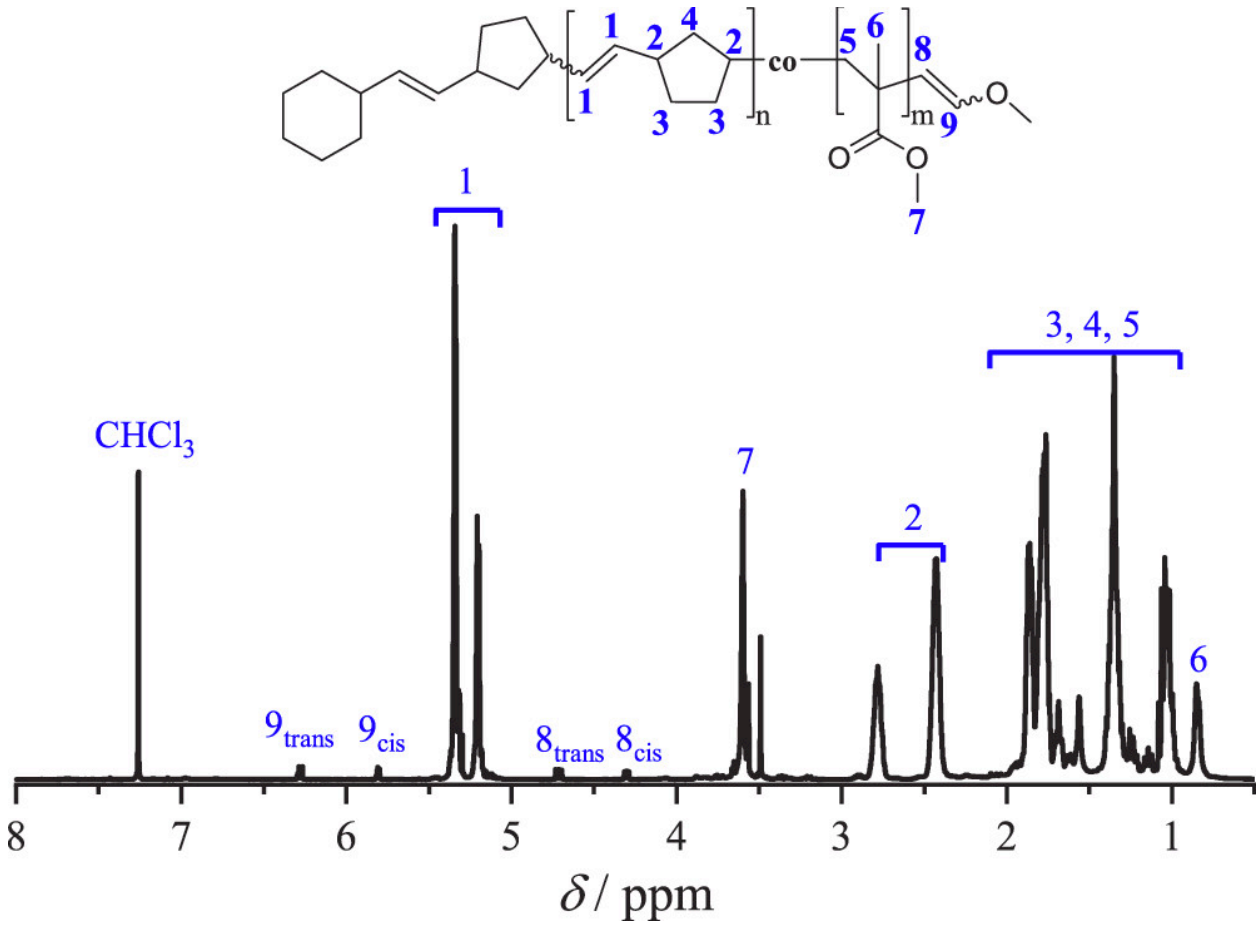

Figure 1. ^{1}H NMR spectrum of poly(norbornene-*co*-MMA), synthesized under MF-ROMP conditions with a 50/50 mixture of the two monomers in dichloromethane and (2-methoxyvinyl)cyclohexane as initiator.

The polymer sample contained 90% norbornene and 10% methyl methacrylate using (2-methoxyvinyl)cyclohexane as initiator. It is important to note that the same ω-chain end identified for a norbornene homopolymer was also identified via ^{1}H NMR (trans, 6.28 and 4.71 ppm; cis, 5.81 and 4.30 ppm). Critically, size exclusion chromatography (SEC) showed a monomodal shape with M_n = 3,700 g·mol^{-1} and M_w = 6,300 g·mol^{-1}, underpinning the copolymerization between norbornene and MMA. Experiments performed under the same conditions, yet without norbornene, did not result in the formation of poly(methyl methacrylate), indicating that norbornene has to generate cationic radicals to incorporate MMA units (entry 6, Table 1). The same observation applies in the absence of initiator (entry 7, Table 1).

While improved conversion in MF-ROMP using non-deoxygenated reaction mixtures was observed for the homopolymerization of norbornene,[23] the copolymerization with vinyl monomers requires inert reaction conditions. The incorporation of MMA in a copolymerization with norbornene completely ceased in the presence of oxygen (entry 3, Table 1). Any attempted copolymerization of norbornene with vinyl monomers (Table 1 and Figure S15) exhibited a higher conversion of norbornene compared to the vinyl monomer conversion, likely as a result of the high ring-strain of norbornene and the known fast polymerization kinetics in ROMP.[24]

Unambiguous evidence for the hybrid copolymerization between the two monomer classes was provided by SEC/ESI-MS analysis of the polymer samples (Figure 2).

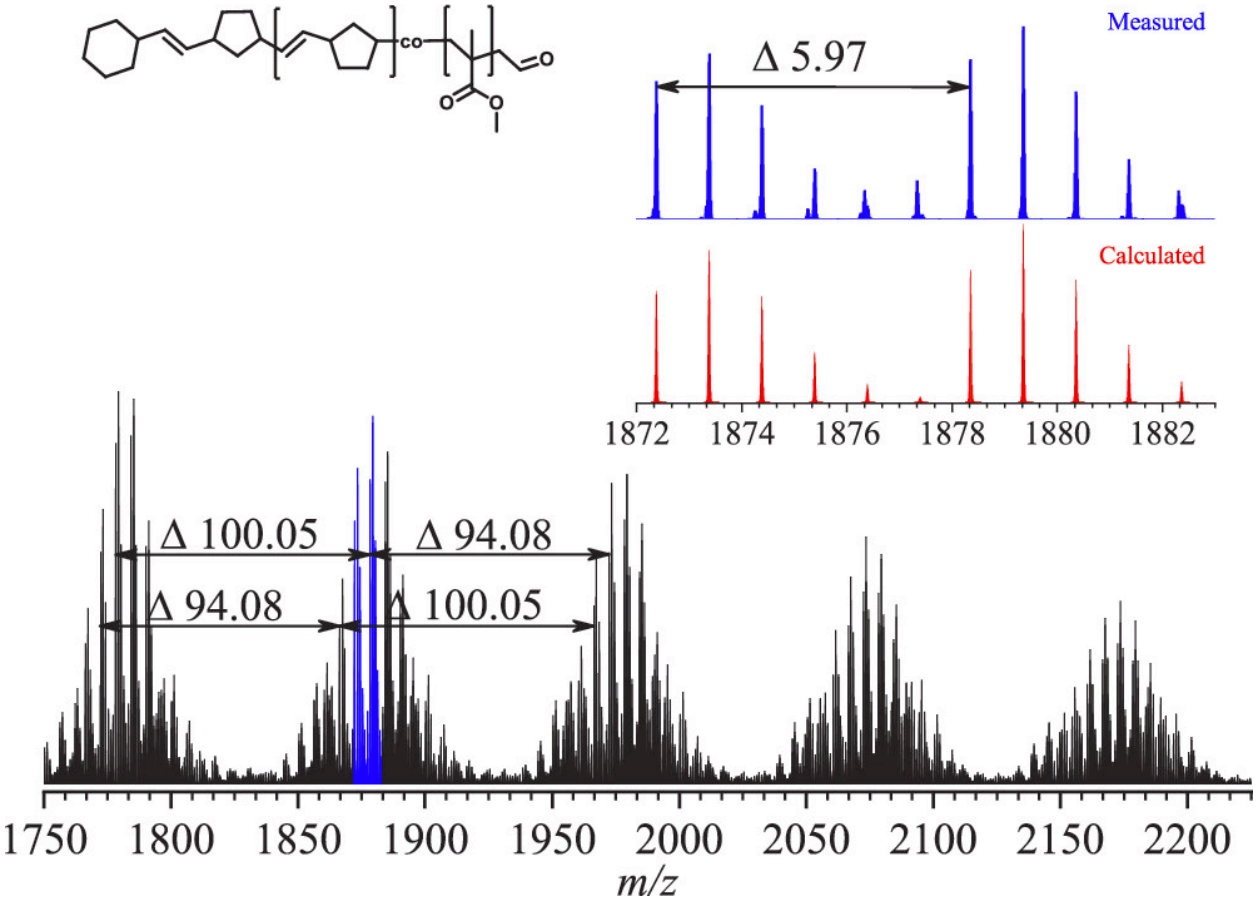

Figure 2. High-resolution mass spectrum of poly(norbornene-*co*-MMA) with spacings of the isotopic patterns corresponding to the exact masses of the repeating unit and the associated mass-

to-charge difference between the repeat units. The mass spectra were analyzed using pyMacroMS.[26]

This hyphenated technique enables separation of the polymer by chain length (SEC) and consecutive online recording of the mass spectrum by ESI-MS, facilitating the separation of the polymer fractions by different charge states—aiding an unambiguous identification of the macromolecular species according to their sum formula.[25] Contrary to the apolar norbornene homopolymer, species with multiple charges were observed indicating a copolymer consisting of MMA and norbornene. The copolymer exhibits a far better ionization due to the rather polar MMA repeating units.

The singly charged region (z = 1) was used for further analysis, whereas higher charged regions (e.g., z = 2) also exhibit the characteristic copolymer pattern. The mass spectrum contains repetitive signal patterns characteristic for copolymers, such as isotopic patterns with an m/z spacing corresponding to both monomers (norbornene, Δ = 94.08 Da; MMA, Δ = 100.05 Da) and the spacing of Δ = 5.97 Da between neighboring isotopic patterns, corresponding to the difference in mass between norbornene and MMA repeating units (Figure 2 inset). Comparison of the high-resolution mass spectra of poly(norbornene-*co*-MMA) obtained using either ethyl-1-propenyl ether or (2-methoxyvinyl)cyclohexane as initiators provided insight into the end group functionalities of the copolymers (Figures S17 and S18).

Matching sum formulas for the copolymer mass spectra were found if the α-chain end remains intact, while the ω-chain end is converted to an aldehyde under cleavage of the alkoxy group during ionization. The degradation yielding an aldehyde can also be observed for a norbornene homopolymer and the initiator under MF-ROMP conditions in acid containing solvents such as $CDCl_3$ (Figures S6 and S7).

A proposed mechanism for the copolymerization of norbornene and MMA is shown in Scheme 2. Similar to the mechanism proposed for the previously reported procedure for MF-ROMP, the copolymerization commences with the initiation of norbornene.[19] A subsequent metathesis of MMA with the active chain end, and release of an α-vinyl ether, results in an intermediate that can initiate the radical polymerization of MMA. The released α-vinyl ether does not initiate new chains as previously observed.[19]

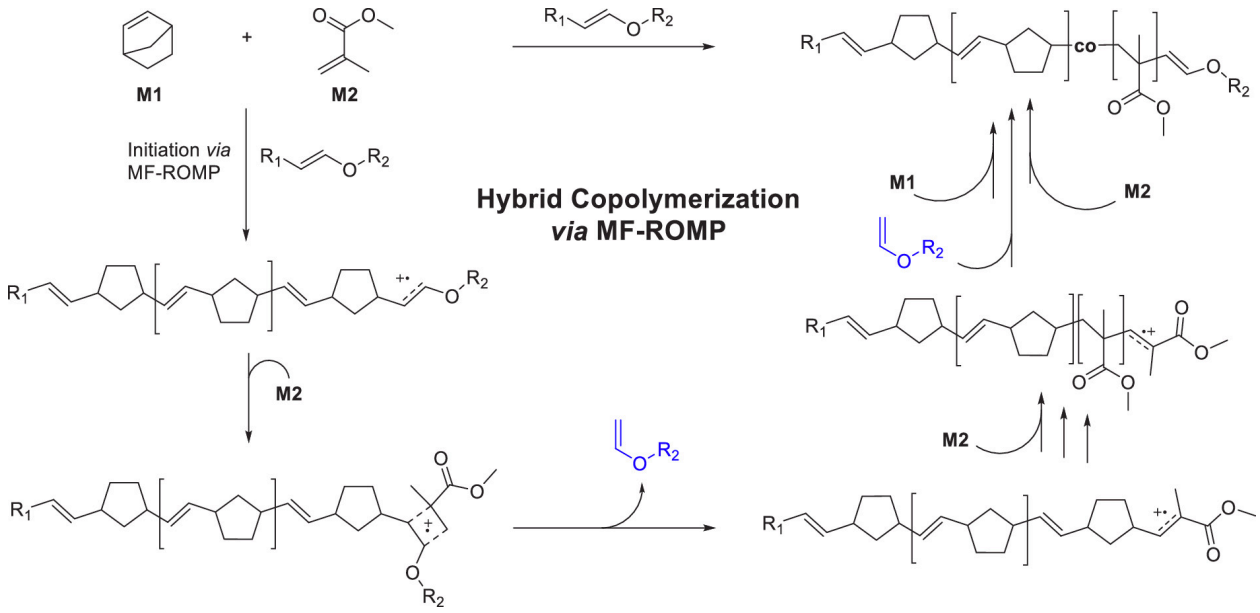

Scheme 2. Proposed Mechanism for the Hybrid Copolymerization of Norbornene (M1) and MMA (M2).

The nucleophilic addition of the prior released α-vinyl ether to the radical-cation of the active chain end will lead to the regeneration of the vinyl ether end group allowing for further norbornene addition. This assumption is in agreement with a recent publication of Huang and co-workers reporting the nucleophilic addition of a vinyl ether to a radical cation.[27] Importantly, the kinetics for a 50/50 mixture of MMA and norbornene reveal an increase of the conversion over time for both monomers, with norbornene being the predominantly incorporated monomer, especially during the early stages of the polymerization (Figure 3A, B).

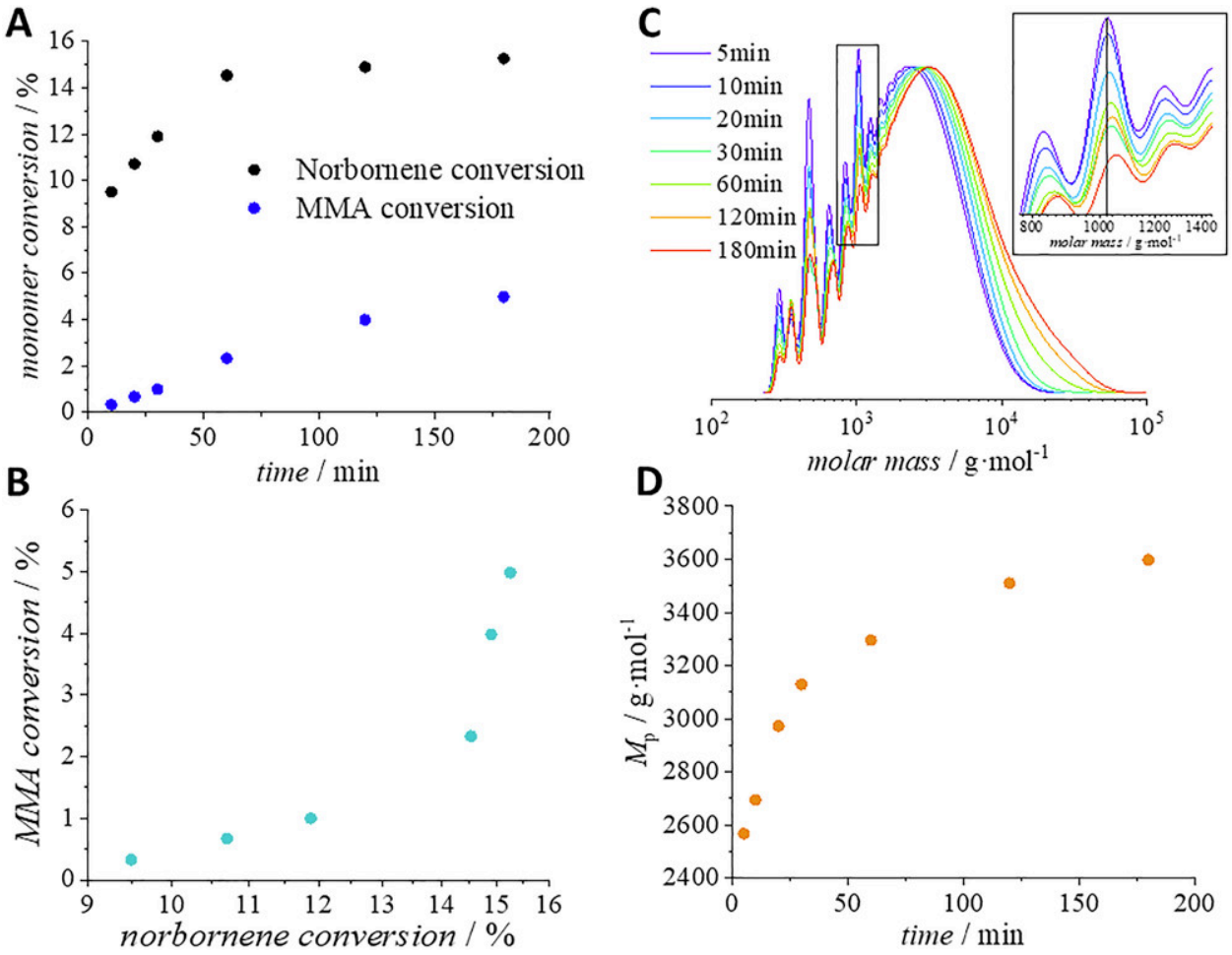

Figure 3. Conversions of norbornene and MMA at different times (A) and relative progress of the conversions (B). SEC traces at the corresponding times (C) showing a gradual increase in molecular weight Mp (D), while maintaining a monomodal distribution.

The conversion after 3 h reaches 15% of norbornene and 5% of MMA in the case of the experiment shown in Figure 3. The conversions and molecular weights obtained with the general procedure for hybrid copolymerization utilizing MF-ROMP conditions can be increased by sequential addition of the pyrylium salt (Table S1). The initially added pyrylium salt does not fully recover and thus the polymerization stops. Our kinetic data support a gradient copolymerization rather than a block copolymerization as MMA is incorporated into the polymer from the beginning and the entire molecular weight distribution—including the oligomer region—shifts toward higher molecular weights (Figure 3C, D). Furthermore, in the case of a polymer blend, a bimodal

distribution would be expected at a certain stage of the polymerization, which was not observed. Nonetheless, analysis via ^{13}C NMR spectroscopy points toward a high degree of blockiness, as no distinct resonances corresponding to the diad of norbornene adjacent to MMA were identified (Figures S8–S10). Caused by the relatively low percentage of incorporated vinyl monomer, the fraction of interconverting points in the polymer was too low to be detected via ^{13}C NMR.

In order to gain further information on the copolymerization mechanism, we attempted a chain extension of a copolymer consisting of MMA and norbornene. After purification of the copolymer the chain growth was successfully re-initiated by addition of a fresh norbornene feed and catalyst (Figure 4), proving the living character of the hybrid copolymerization. Critically, the complete molar mass distribution is shifted toward higher masses, starting from M_p = 4800 g·mol^{-1} and shifting to M_p = 58600 g·mol^{-1} after chain extension. The possibility of a chain extension further supports the hybrid copolymerization proposed in Scheme 2. The ^{1}H NMR spectra before and after chain extension also support hybrid copolymerization, showing an increase in the content of norbornene of the chain extended polymer, while the MMA content remains the same as prior to the chain extension (Figure S11).

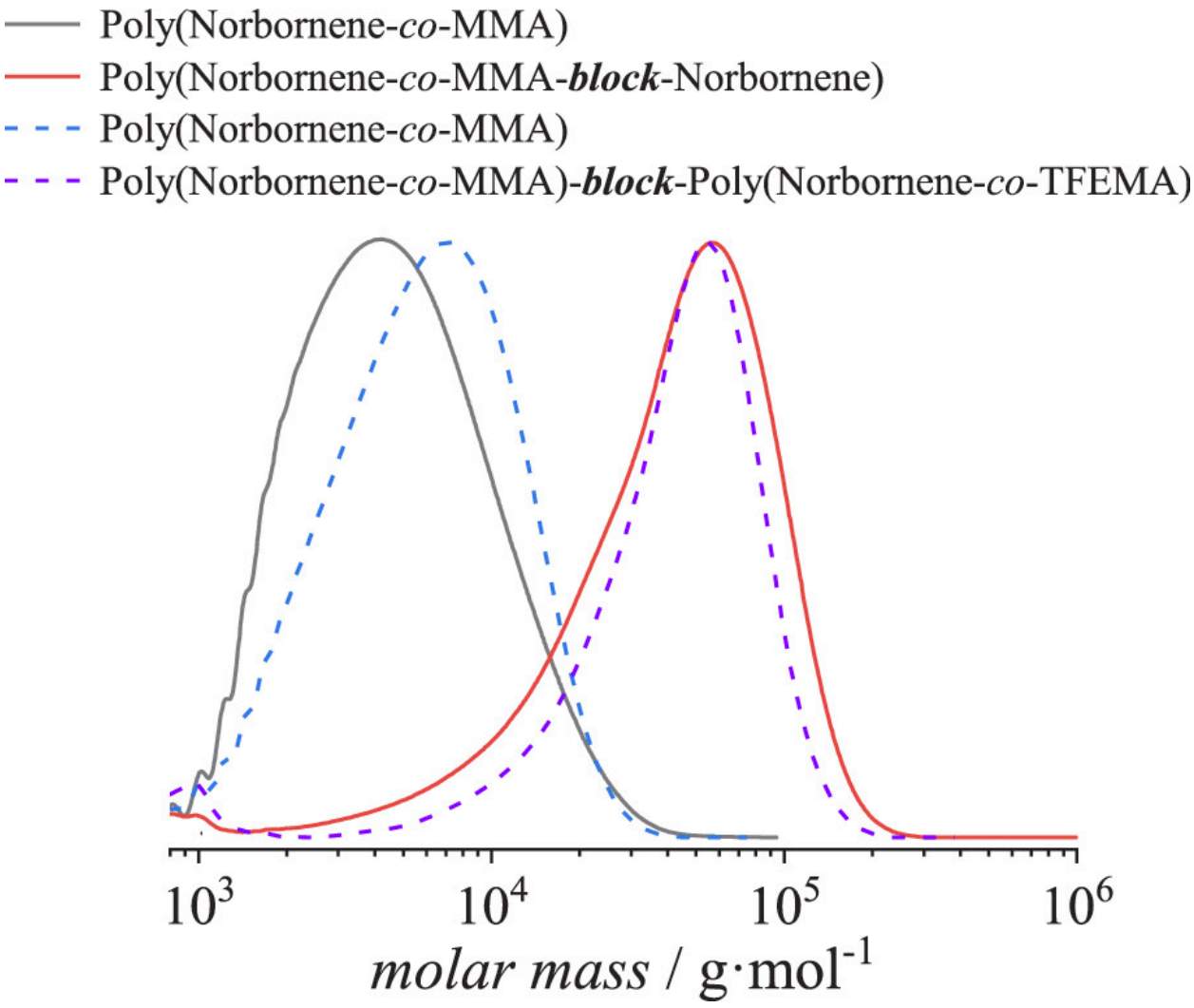

Figure 4. Chain extension of poly(norbornene-*co*-MMA) with norbornene (black and red lines) or a mixture of norbornene and 2,2,2-trifluoroethyl methacrylate (blue and purple dashed lines).

To demonstrate the living character and the end group fidelity of the developed technique, poly(norbornene-*co*-MMA) was chain extended with a mixture of 2,2,2-trifluoroethyl methacrylate and norbornene to obtain a terpolymer consisting of two blocks of different gradient copolymers—a microstructure unprecedented in literature (Figure 4, dashed lines, and Figure S12). A shift of the full mass distribution from M_p = 7500 g·mol^{-1} to 55700 g·mol^{-1} was observed.

Conclusions

In conclusion, we introduce the hybrid copolymerization of ring-strained monomers with vinyl monomers utilizing MF-ROMP conditions. The final copolymers contain a high proportion of the norbornene repeating unit. Monomers suitable for MF-ROMP but exhibiting less ring-strain compared to norbornene may enable a shift of the equilibrium further to the side of the vinyl monomer. The resulting copolymers are promising candidates for future applications, as the backbone, as well as the side chains, can be readily altered. For example, introducing a cleavable group into the lateral chain via the ring-strained monomer will open a promising avenue for materials with novel features, especially in the field of biodegradable polymers.[28]

Future Work

The proposed mechanism for incorporation of acrylates into MF-ROMP explains the observed results but is surprising. For the liberated vinyl enol ether to rebound back onto the polymer chain end seems unlikely. Furthermore, we have since shown that cross metathesis with terminal alkenes tends to leave produce a terminal alkene on the polymer and a beta-substituted enol ether, which is counter to the proposed mechanism of enol ether radical cations with methyl methacrylate that shows formation of a non-terminal alkene on the polymer chain end and a vinyl enol ether. This suggests that the proposed mechanism is inaccurate, or that the substitution pattern on the enol ether is greatly influenced by the alkene electronics more so than sterics in the case of methacrylates. Other potential polymerization pathways can also exist, for example the reduced pyryl radical or some other radical byproduct of MF-ROMP could plausibly initiate a radical polymerization of the methacrylate and then link onto one of the norbornyl alkenes on the polymer backbone. In either case, additional control experiments should be conducted to verify the currently proposed mechanism of acrylate incorporation.

Appendix A: Chapter 2 Experimental Procedures and Supporting Information

1 Materials

Ethyl-1-propenyl ether (928-55-2, Sigma Aldrich) and bicyclo[2.2.1]hept-2-en / norbornene (498-66-8, Sigma Aldrich) were used as received. The (meth)acrylates were filtered over basic aluminum oxide (brockmann type I) prior to use. The dry dichloromethane was obtained from a solvent purification system. The photoredox mediator 2.4,6-tris(4-methoxyphenyl)pyrylium tetrafluoroborate (**MeOTPP$^+$BF$_4^-$**) and the initiator (2-methoxyvinyl)cyclohexane were synthesized according to literature procedures.[19,29]

2 General procedures MF-ROMP (Co)-Polymerization

Catalyst **MeOTPP$^+$BF$_4^-$** (0.03 eq), norbornene (50 eq) and the respective comonomer (50 eq) were dissolved in dry dichloromethane (monomer concentration ~ 2 mol·L^{-1}). Subsequently, the respective initiator (1 eq) was added, the reaction vial closed and deoxygenated for 5 min by purging the solution with nitrogen gas. Finally, the stirred reaction mixture was irradiated for 1 hour with a blue LED (λ_{max} = 445 nm, 10 W) through the bottom of the vial with a 2 cm distance between LED and vial bottom. During the reaction time the set up was cooled with a fan to ensure ambient temperature. For purification, the solution was precipitated in cold methanol, centrifuged and the solid residue dried *in vacuo*.

3 Synthesis

Tris(4-methoxyphenyl)pyrylium tetrafluoroborate (MeOTPP$^+$BF$_4^-$)

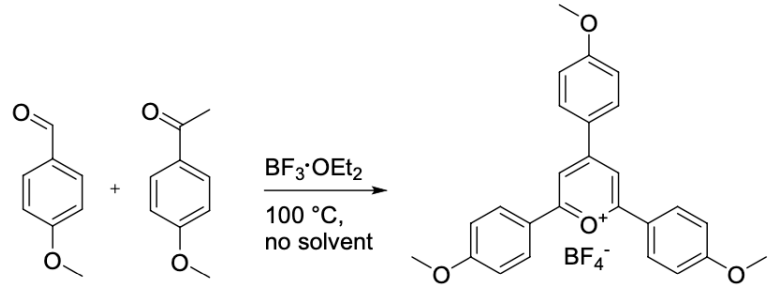

Synthesis adapted from reference[19]

7.6 mL (60 mmol, 2.4 eq) of BF_3•Et_2O was added slowly to a mixture of 3 mL (25 mmol, 1 eq) of 4-methoxybenzaldehyde and 7.5 g (50 mmol, 2 eq) of 4-methoxyacetophenone. The mixture was heated for 100 min at 100 °C and the oily product was dissolved in acetone and subsequently precipitated in diethyl ether. The residue was purified by three re-crystallizations from acetone to yield MeOTPP$^+$BF$_4^-$as an orange powder.

^{1}H NMR (600 MHz, DMSO-d^6) δ 8.73 (m, 2H), 8.60 (m, 2H), 8.48 (m, 4H), 7.28 (m, 6H), 3.97 (d, *J* = 10.6 Hz, 9H).
^{13}C NMR (150 MHz, DMSO-d^6) δ 56.04, 56.15, 111.09, 115.37, 115.40, 121.61, 124.68, 130.76, 132.43, 162.04, 164.50, 165.23, 168.07.

ESI-MS: $[M]^+$ = 399.1589 (m/z^{exp}); 399.1591 (m/z^{theo})

(2-Methoxyvinyl)cyclohexane

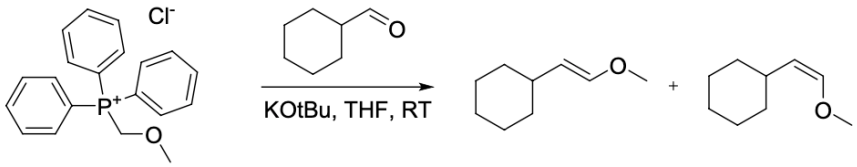

Synthesis adapted from reference[29]

2.93 g (26 mmol, 1.5 eq) of potassium *tert*-butoxide, 8.97 g (methoxymethyl)triphenylposphonium chloride (26 mmol, 1.5 eq) and 2.1 mL of cyclohexanecarboxyaldehyde (17 mmol, 1 eq) were dissolved in 80 mL of dry THF. The reaction mixture was continuously stirred at ambient temperature for 4 hours. After completion of the reaction THF was evaporated at 40 °C. Subsequently, the residue was diluted with *n*-hexane and filtered. The filtration product was washed three times with water. Next, any residual solvent was evaporated. The crude product was purified *via* column chromatography (SiO_2, ethylacetate:cyclohexane = 4:1 *v/v*).

^{1}H NMR (600 MHz, $CDCl_3$) δ 6.28 (d, J = 12.6 Hz, 1H), 5.78 (dd, J = 5.88 Hz, J = 1.0 Hz, 0.5H), 4.69 (dd, J = 12.6 Hz, J = 7.8 Hz, 1H), 4.22 (dd, J = 9.1 Hz, J = 6.3 Hz, 0.5H), 3.57 (s, 1.5H), 3.49 (s, 3H), 2.41 (m, 0.5H), 1.87 (m, 1H), 1.740.78 (m, $cyclohexane_{cis/trans}$).

^{13}C NMR (150 MHz, $CDCl_3$) δ 26.03, 26.12, 26.20, 33.43, 33.57, 34.47, 36.96, 55.83, 59.55, 109.79, 113.41, 144.55, 145.73.

ESI-MS: $[M+H]^+$ = 141.1272 (m/z^{exp}); 141.1274 (m/z^{theo})

4 Analysis

NMR spectra

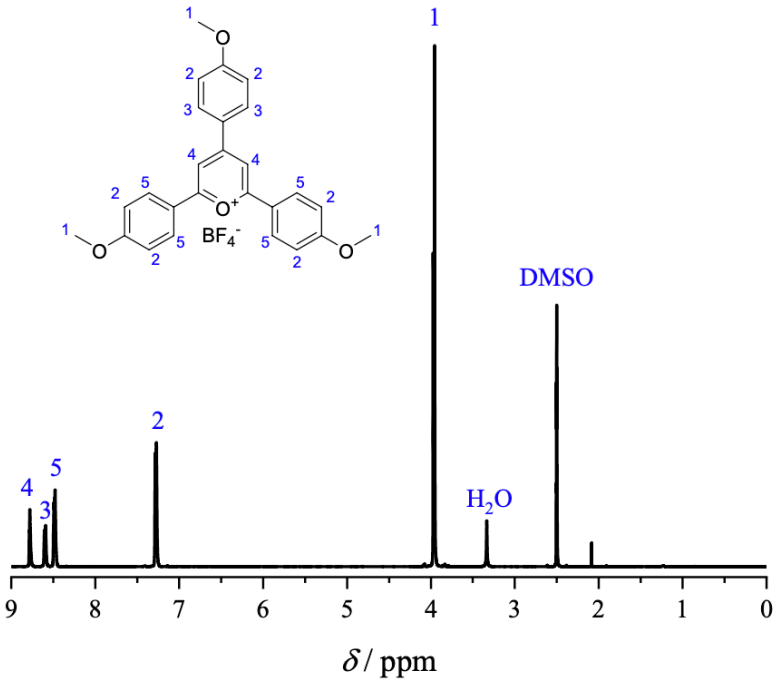

Figure S1. ^{1}H NMR spectrum of the photocatalyst MeOTPP^{+}BF$_4^{-}$ in DMSO-*d6*.

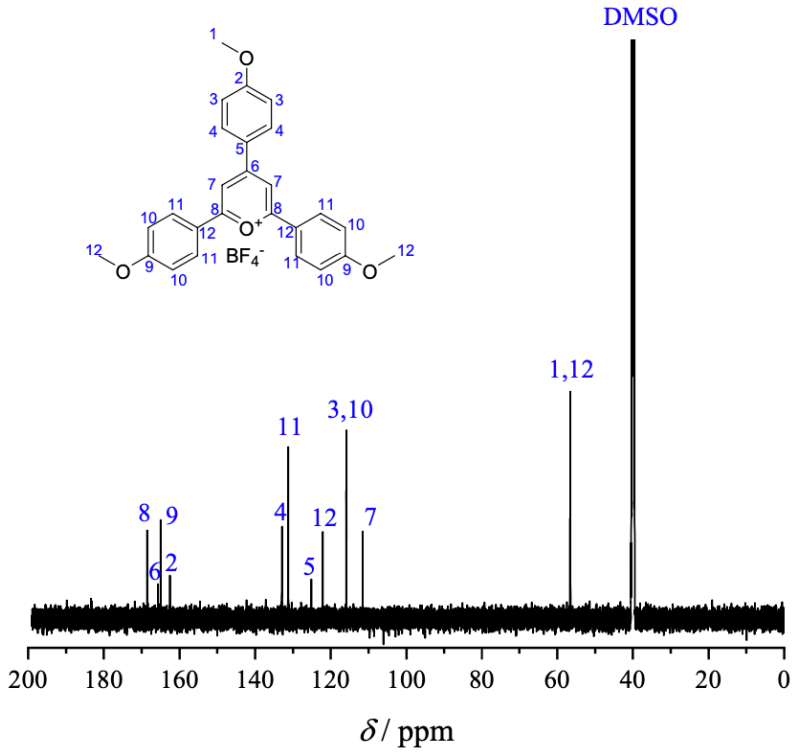

Figure S2. ^{13}C NMR spectrum of the photocatalyst MeOTPP^{+}BF$_4^{-}$ in DMSO-*d6*.

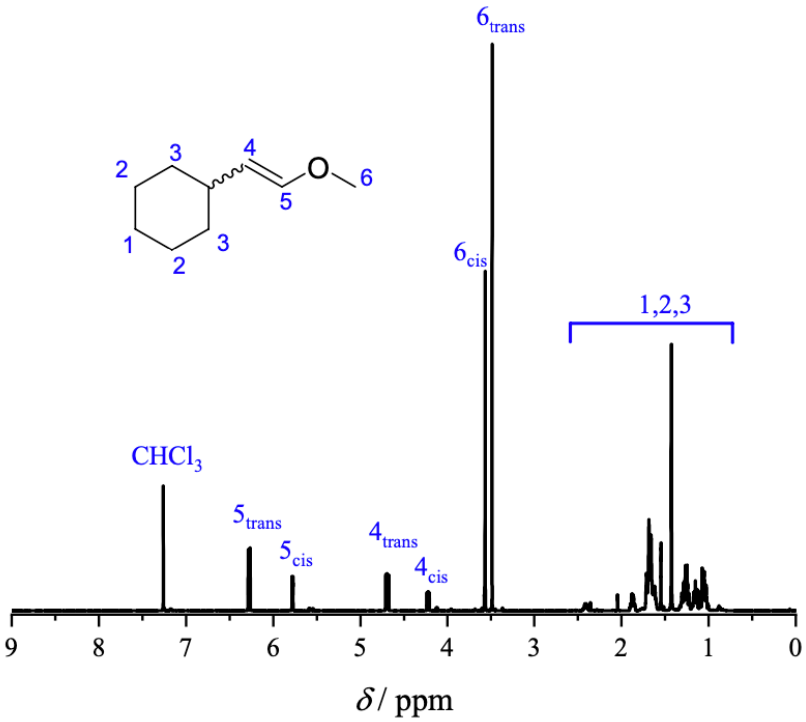

Figure S3. ^{1}H NMR spectrum of the initiator (2-methoxyvinyl)cyclohexane in $CDCl_3$.

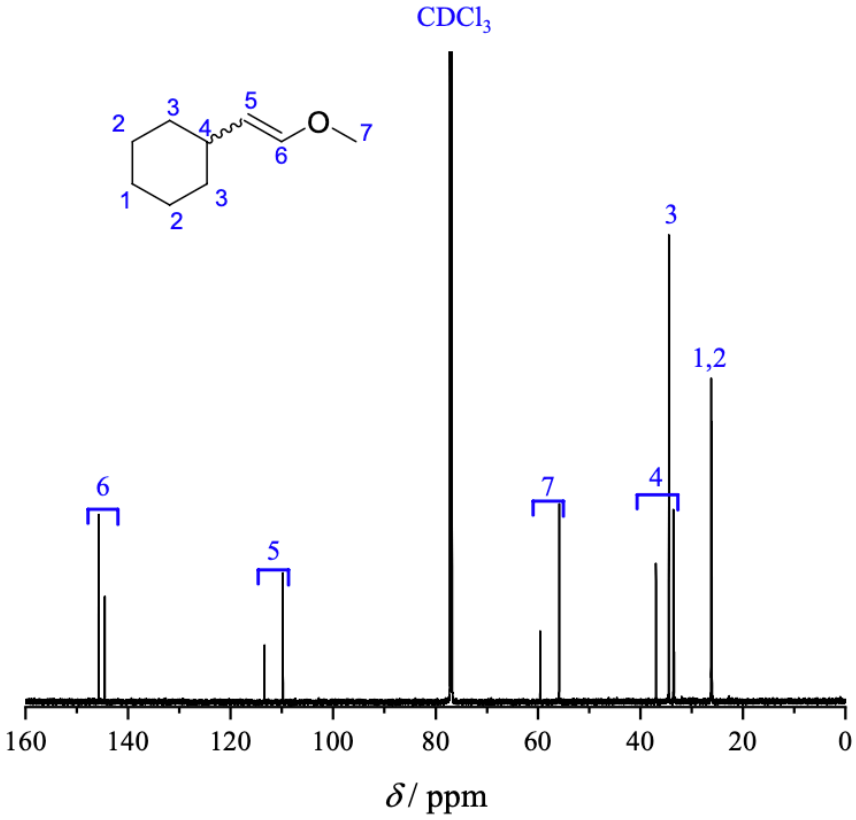

Figure S4. ^{13}C NMR spectrum of the initiator (2-methoxyvinyl)cyclohexane in $CDCl_3$.

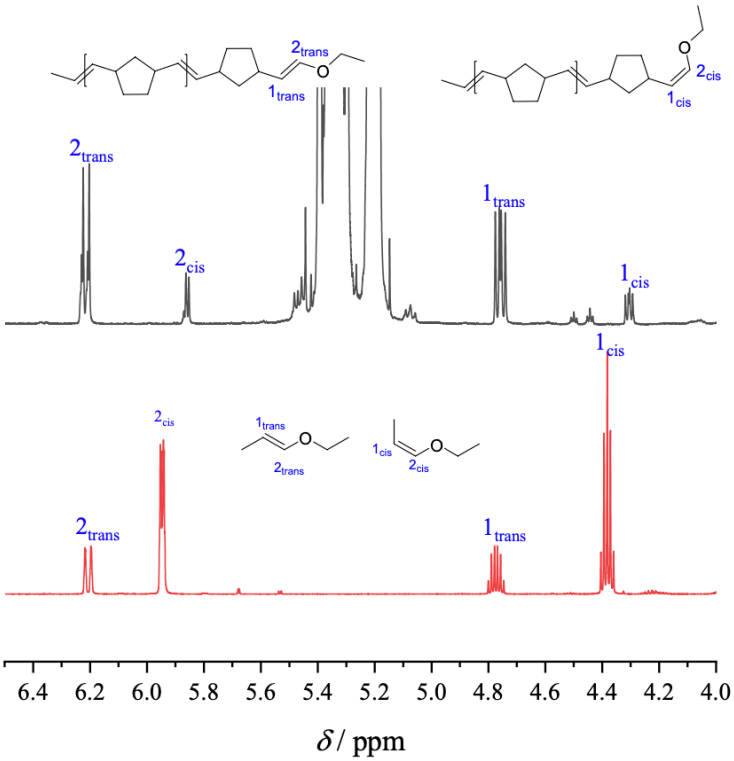

Figure S5. ^{1}H NMR spectrum of the initiator ethyl-1-propenyl ether (top) and norbornene homopolymer (bottom) obtained via MF-ROMP with ethyl-1-propenyl ether as initiator. The multiplicity of the *cis* and *trans* end group double bond resonances at 4.3 and 4.75 ppm changed from a higher order structure in ethyl-1-propenyl ether into a doublet of doublets in the polymer, evidencing the new connection of the initiator double bond to a norbornene unit at the ω-chain end.

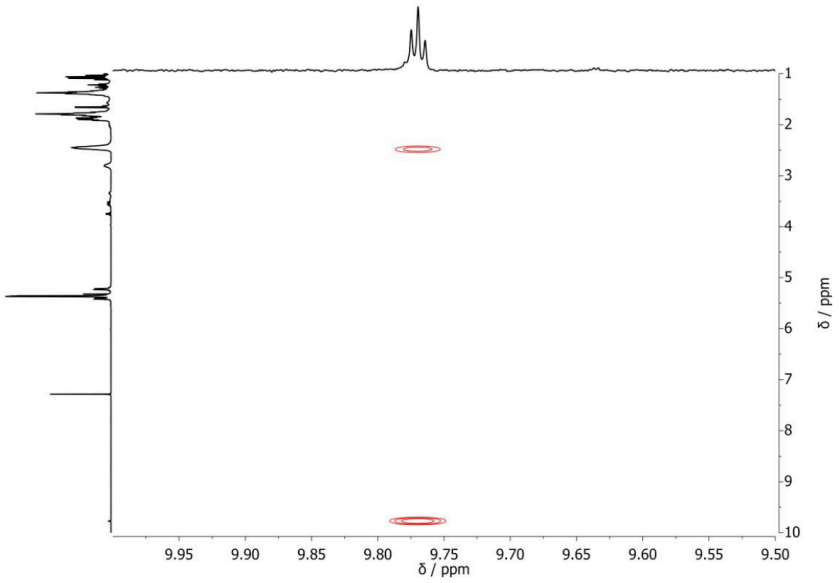

Figure S6. Zoomed region of the ^{1}H/^{1}H COSY of a norbornene homopolymer obtained via MF-ROMP with ethyl-1-propenyl ether as initiator. The feed ratio of norbornene:initiator: photocatalyst was 5:1:0.03. The sample was deoxygenated and irradiated at 445 nm in dry dichloromethane for 75 min. The aldehyde multiplicity is a triplet that couples to the alkyl region.

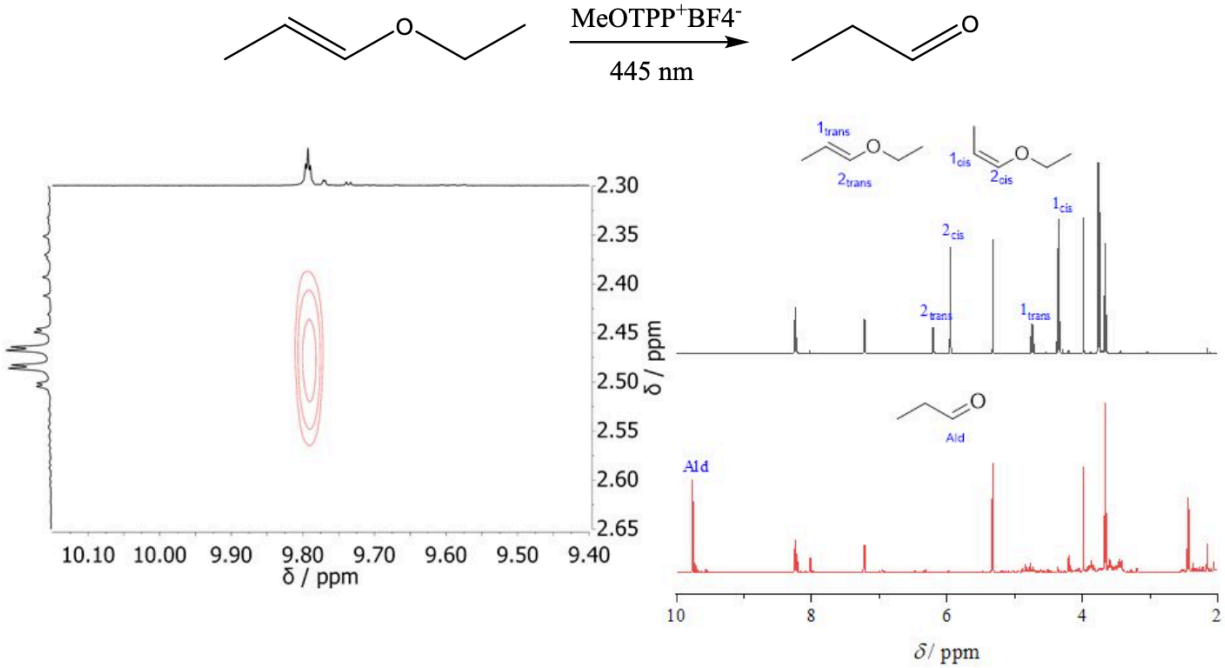

Figure S7. 'Cocktail experiment': ^{1}H NMR spectra of the reaction mixture before and after irradiation at 445 nm for 60 min. Reaction mixture consisting of 1 eq ethyl-1-propenyl ether and 0.03 eq MeOTPP^{+}BF4^{-} in deuterated dichloromethane without deoxygenation. Inset: Corresponding ^{1}H/^{1}H COSY spectrum. The reaction leads to aldehyde formation after cleavage of ethanol.

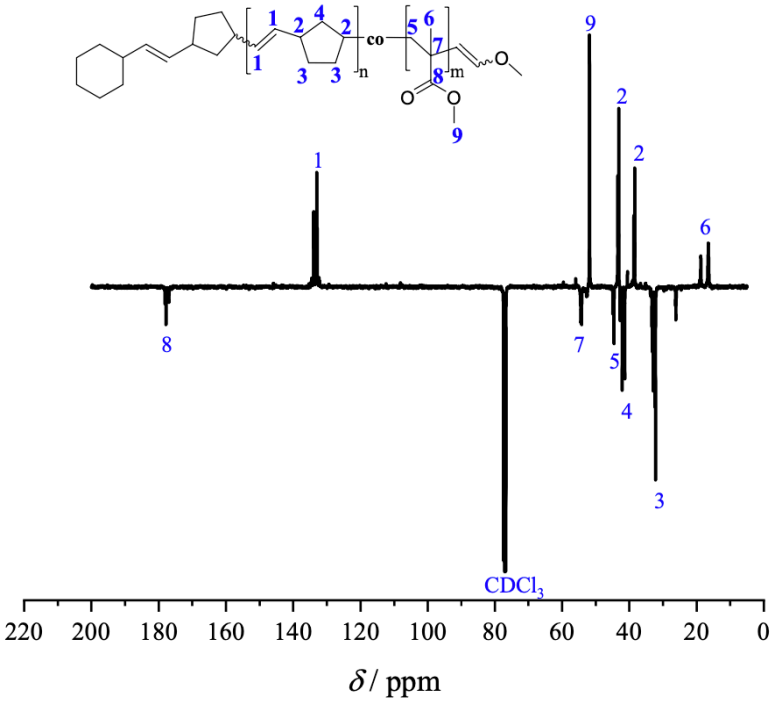

Figure S8. ^{13}C NMR spectrum of poly(norbornene-*co*-MMA) in $CDCl_3$.The copolymer was synthesized with (2-methoxyvinyl)cyclohexane as initiator and a 50/50 mixture of norbornene and MMA under constant irradiation at 445 nm for 180 min. The polymer was purified via precipitation in cold methanol.

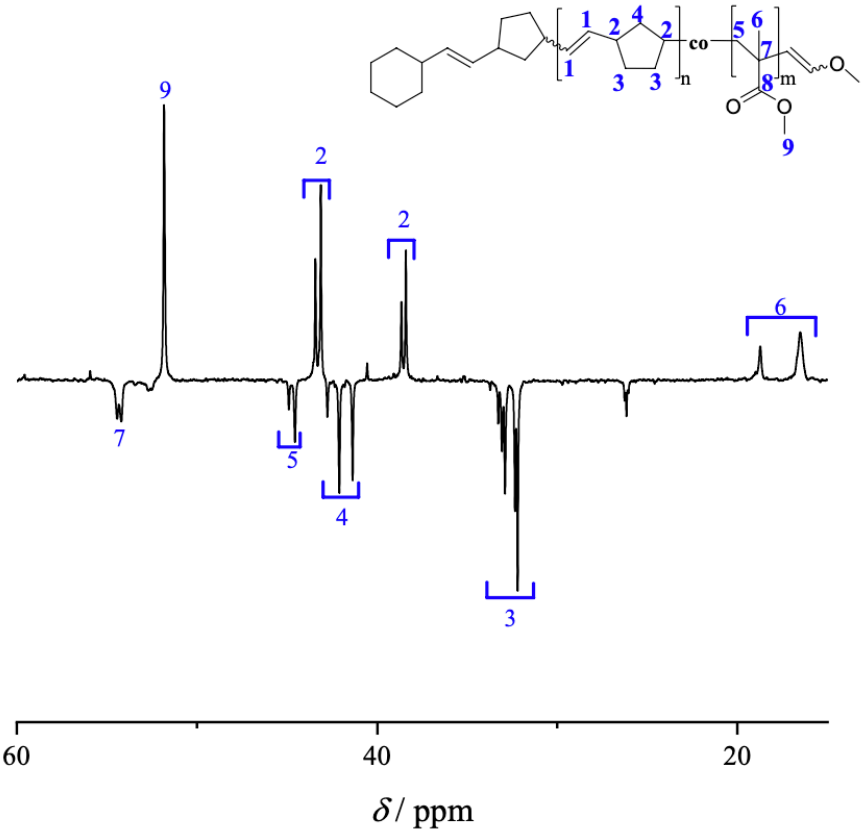

Figure S9. Zoomed part of the spectrum shown in Figure S8.

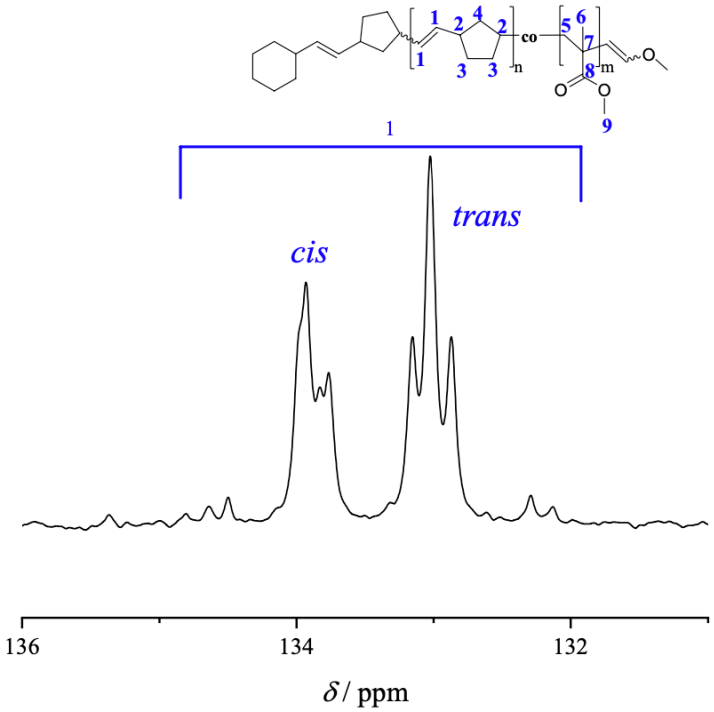

Figure S10. Zoomed part of the spectrum shown in Figure S9.

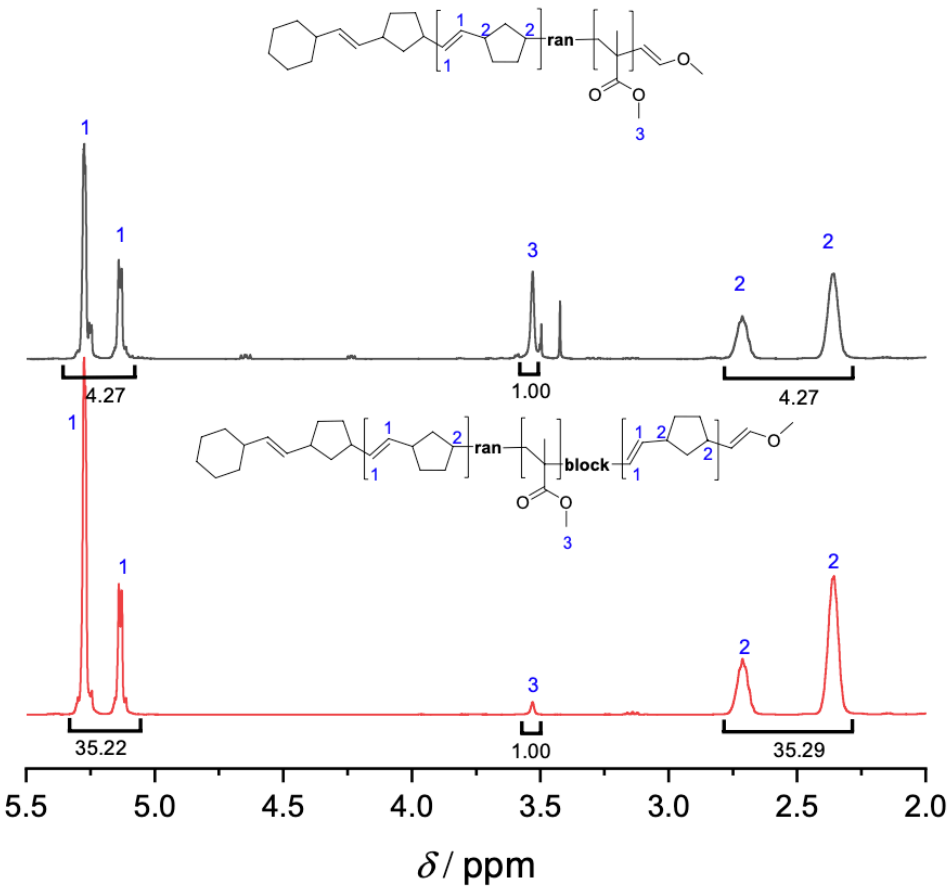

Figure S11. ^{1}H NMR spectra of the block chain extension of poly(norbornene-*co*-MMA) with norbornene affording poly(norbornene-*co*-MMA)-*block*-poly(norbornene). The precursor copolymer was synthesized with (2-methoxyvinyl)cyclohexane as initiator and a 50/50 mixture of norbornene and MMA under constant irradiation at 445 nm for 60 min. The precursor polymer was purified *via* precipitation in cold methanol. The chain extension was performed with freshly added norbornene, $MeOTPP^{+}BF_4^{-}$ and dry dichloromethane under constant irradiation for 60 min.

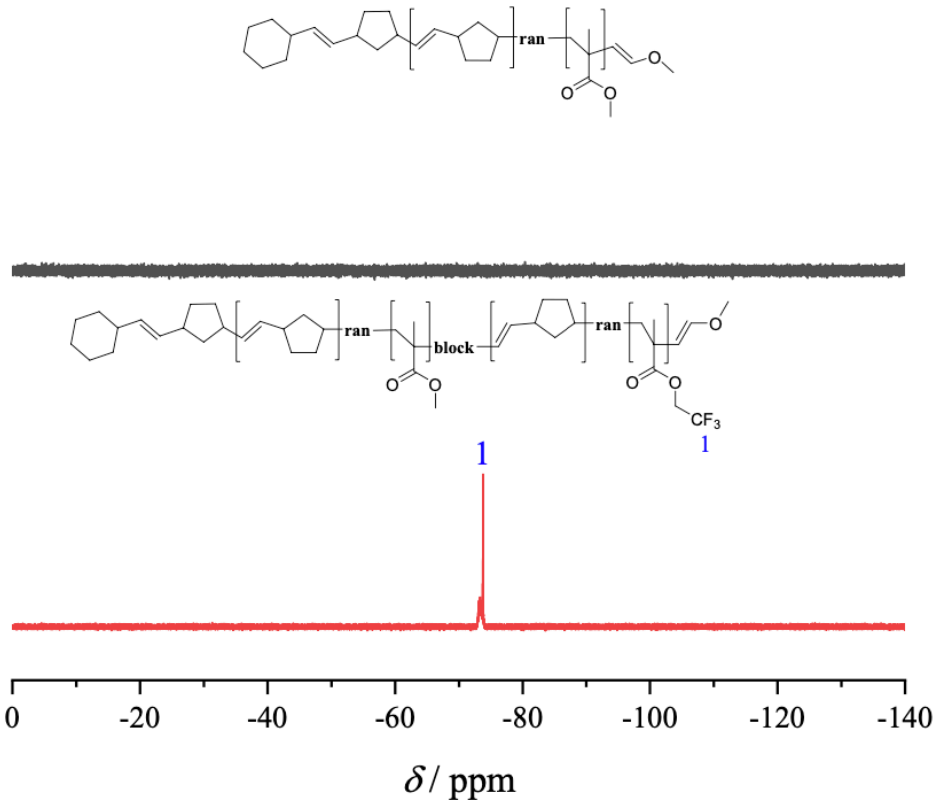

Figure S12. ^{19}F NMR spectra of the block chain extension of poly(norbornene-*co*-MMA) with norbornene and 2,2,2-trifluoroethyl methacrylate (TFEMA) yield poly(norbornene-*co*-MMA)-*block*-poly(norbornene-*co*-TFEMA). The precursor copolymer was synthesized with (2-methoxyvinyl)cyclohexane as initiator and a 50/50 mixture of norbornene and MMA under constant irradiation at 445 nm for 60 min. The precursor polymer was purified via precipitation in cold methanol. The chain extension was performed with a 50/50 mixture of norbornene and 2,2,2-trifluoroethyl methacrylate and fresh addition of $MeOTPP^+BF4^-$ and dry dichloromethane under constant irradiation for 60 min.

Size Exclusion Chromatography (SEC)

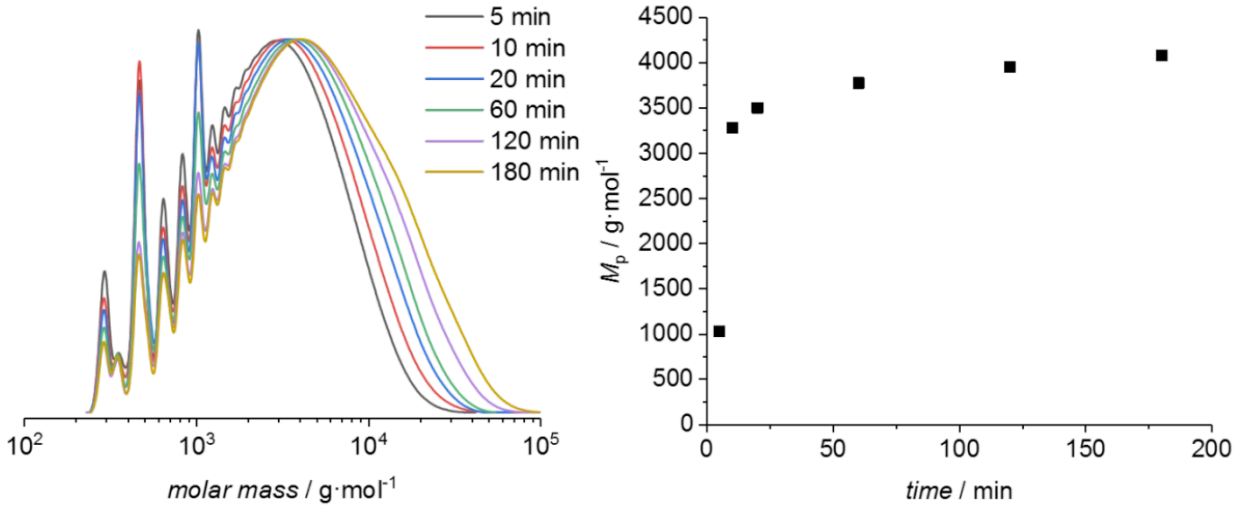

Fig. S14: Molar mass distribution (left) and increase of M_p (right) at several time intervals of a 50 % norbornene and 50% methyl acrylate copolymer utilizing (2-methoxyvinyl)cyclohexane as initiator. The typical copolymerization conditions of feed ratios of 100 eq monomer, 1 eq initiator and 0.03 eq catalyst were used. The reaction was performed for the stated times in dry dichloromethane using 445 nm LED light as an irradiation source.

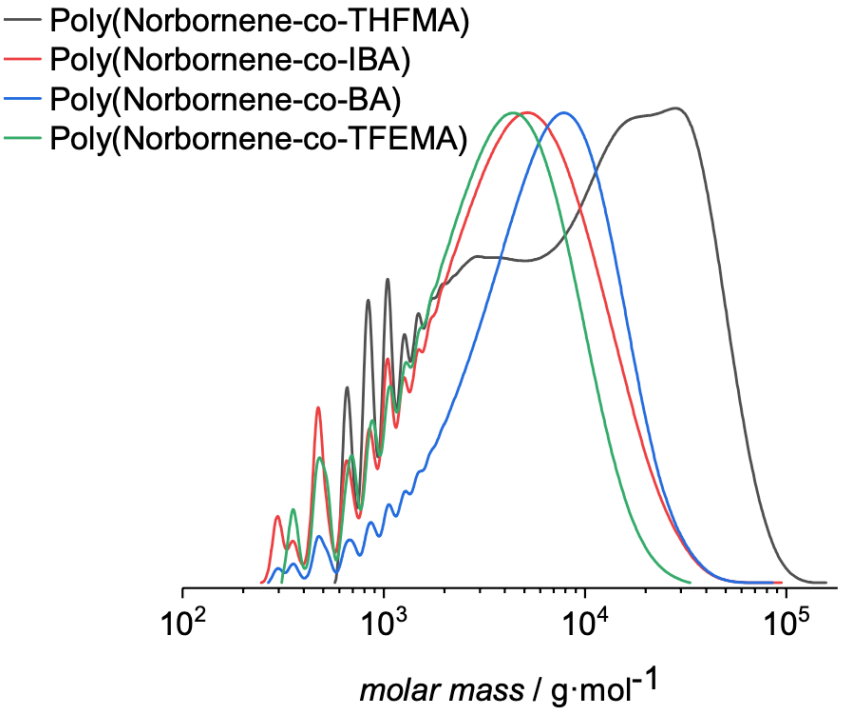

Figure S15. Molecular weight distribution of poly(norbornene-*co*-tetrahydrofurfuryl methacrylate) (black trace), poly(norbornene-*co*-isobutyl acrylate) (red trace), poly(norbornene-*co*-butyl acrylate) (blue trace) and poly(norbornene- *co*-trifluoroethyl methacyrlat) (green trace). Each copolymer was synthesized according to the standard procedure within 60 min with (2-methoxyvinyl)cyclohexane as initiator at 445 nm constant irradiation in dry dichloromethane.

SEC/HRESI – Mass Spectrometry

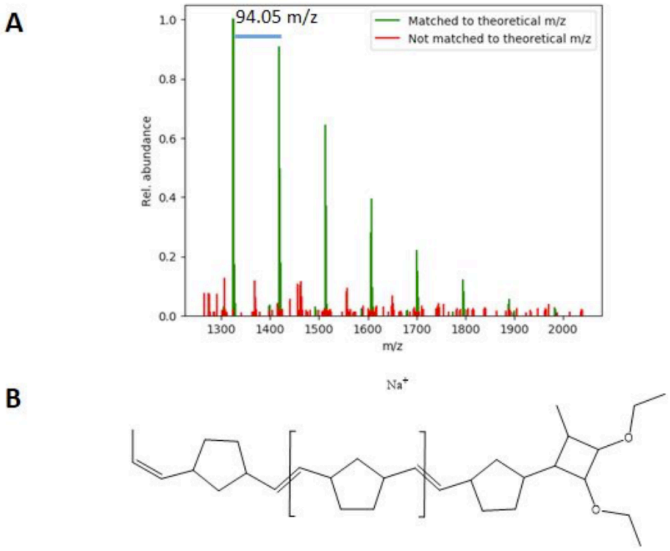

Figure S16: ESI-MS spectrum of a norbornene homopolymer synthesized with ethyl-1-propenyl ether as initiator. The sample was first fractionated *via* online SEC with THF as eluent and subsequently analyzed by ESI-MS using sodium iodide as doping agent. (A) Depiction of matching results (green peaks) and mismatched results (red peaks) between experimentally obtained pattern and simulated isotopic pattern of the proposed structure. (B) The proposed structure of the norbornene homopolymer with sodium as a positive counter ion was identified in the mass spectrum.

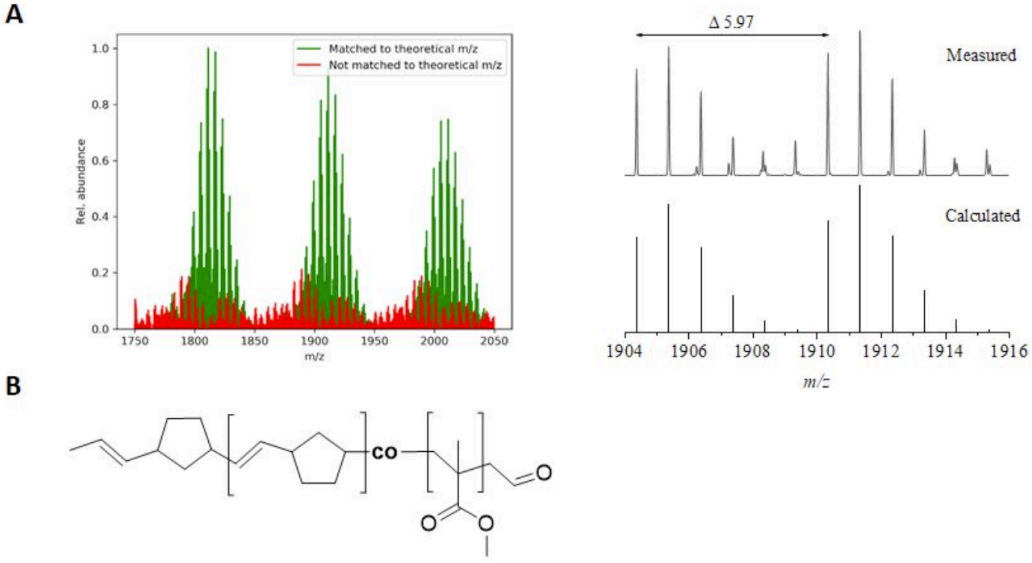

Figure S17: ESI-MS spectrum of a norbornene / methyl methacrylate copolymer (50:50) synthesized with ethyl-1- propenyl ether as initiator. The sample was first fractionated *via* online SEC with THF as eluent and subsequently analyzed by ESI-MS using sodium iodide as doping agent. (A) Depiction of matching results (green peaks) and mismatched results (red peaks) between experimentally obtained pattern and simulated isotopic pattern of the proposed structure. (B) The proposed structure of the norbornene/MMA copolymer with sodium as a positive counter ion was identified in the mass spectrum. A zoomed region of the spectrum shows the match of the experimental spectrum with the calculated one in greater detail.

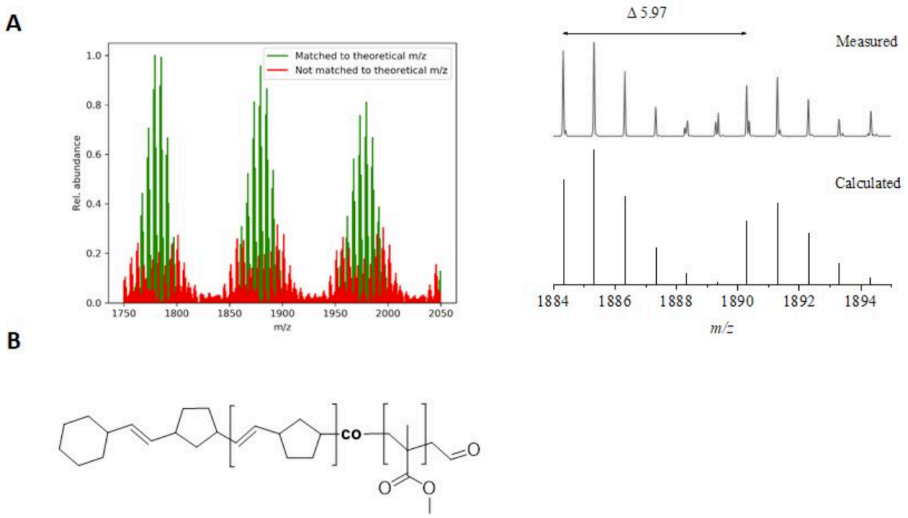

Figure S18: ESI-MS spectrum of a norbornene / methyl methacrylate copolymer (50:50) synthesized with (2-methoxyvinyl)cyclohexane as initiator. The sample was first fractionated *via* online SEC with THF as eluent and subsequently analyzed by ESI-MS using sodium iodide as doping agent. (A) Depiction of matching results (green peaks) and mismatched results (red peaks) between experimentally obtained pattern and simulated isotopic pattern of the proposed structure. (B) The proposed structure of the norbornene/MMA copolymer with sodium as a positive counter ion was identified in the mass spectrum. A zoomed region of the spectrum shows the match of the experimental spectrum with the calculated one in greater detail.

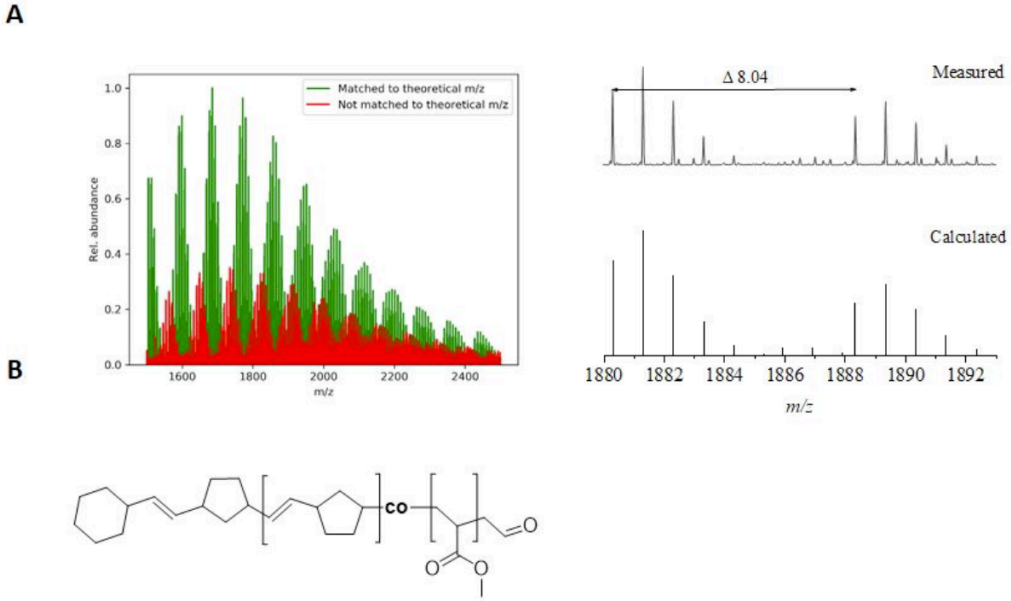

Figure S19: ESI-MS spectrum of a norbornene / methyl acrylate copolymer (50:50) synthesized with (2- methoxyvinyl)cyclohexane as initiator. The sample was first fractionated *via* online SEC with THF as eluent and subsequently analyzed by ESI-MS using sodium iodide as doping agent. (A) Depiction of matching results (green peaks) and mismatched results (red peaks) between experimentally obtained pattern and simulated isotopic pattern of the proposed structure. (B) The proposed structure of the norbornene/MA copolymer with sodium as a positive counter ion was identified in the mass spectrum. A zoomed region of the spectrum shows the match of the experimental spectrum with the calculated one in greater detail.

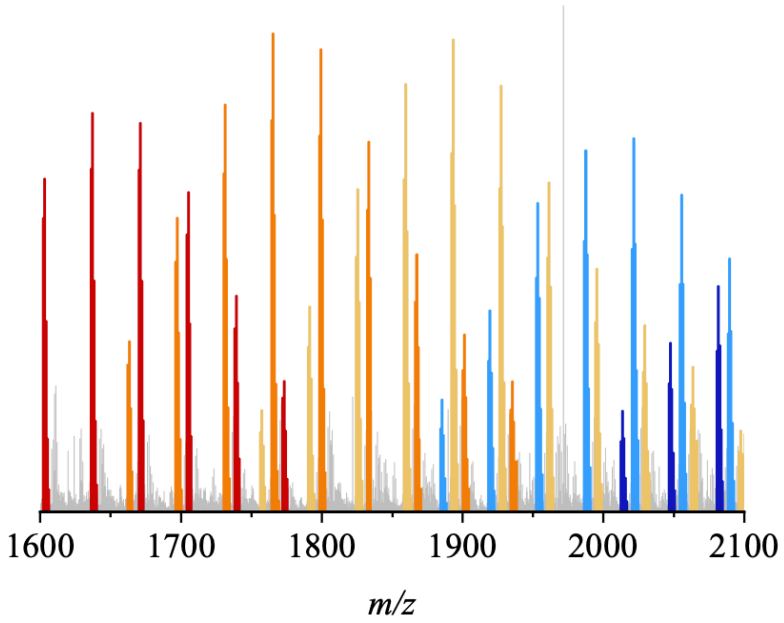

Figure S20: ESI-MS spectrum of a norbornene / butyl acrylate copolymer (50:50) synthesized with (2- methoxyvinyl)cyclohexane as initiator. The sample was first fractionated *via* online SEC with THF as eluent and subsequently analyzed by ESI-MS using sodium iodide as doping agent. The patterns of polymer chains with different degrees of polymerization (DP) overlap with each other and were color coded to guide the eye. The spacing between patterns of the same color is Δ34.01 *m/z*, corresponding to the difference of the repeating units 128.0837 Da (butyl acrylate) and 94.0783 Da (norbornene).

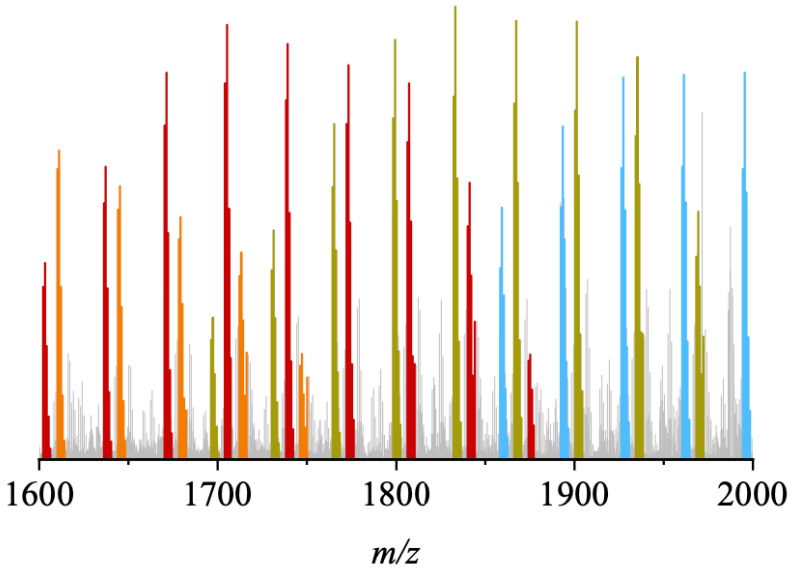

Figure S21: ESI-MS spectrum of a norbornene / isobutyl acrylate copolymer (50:50) synthesized with (2- methoxyvinyl)cyclohexane as initiator. The sample was first fractionated *via* online SEC with THF as eluent and subsequently analyzed by ESI-MS using sodium iodide as doping agent. The patterns of polymer chains with different degrees of polymerization (DP) overlap with each other and were color coded to guide the eye. The spacing between patterns of the same color is Δ34.01 *m/z*, corresponding to the difference of the repeating units 128.0837 Da (isobutyl acrylate) and 94.0783 Da (norbornene).

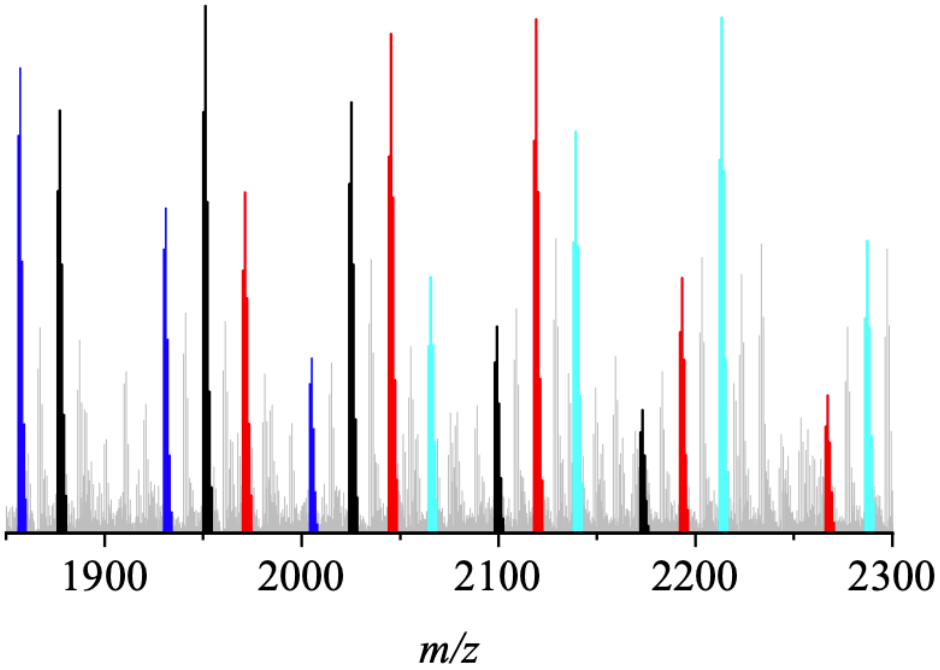

Figure S22: ESI-MS spectrum of a norbornene / 2,2,2-trifluoroethyl methacrylate copolymer (50:50) synthesized with (2-methoxyvinyl)cyclohexane as initiator. The sample was first fractionated *via* online SEC with THF as eluent and subsequently analyzed by ESI-MS using sodium iodide as doping agent. The patterns of polymer chains with different degrees of polymerization (DP) overlap with each other and were color coded to guide the eye. The spacing between patterns of the same color is Δ73.96 *m/z*, corresponding to the difference of the repeating units 168.0398 Da (2,2,2- trifluoroethyl methacrylate) and 94.0783 Da (norbornene).

In-situ UV/VIS absorbance measurements

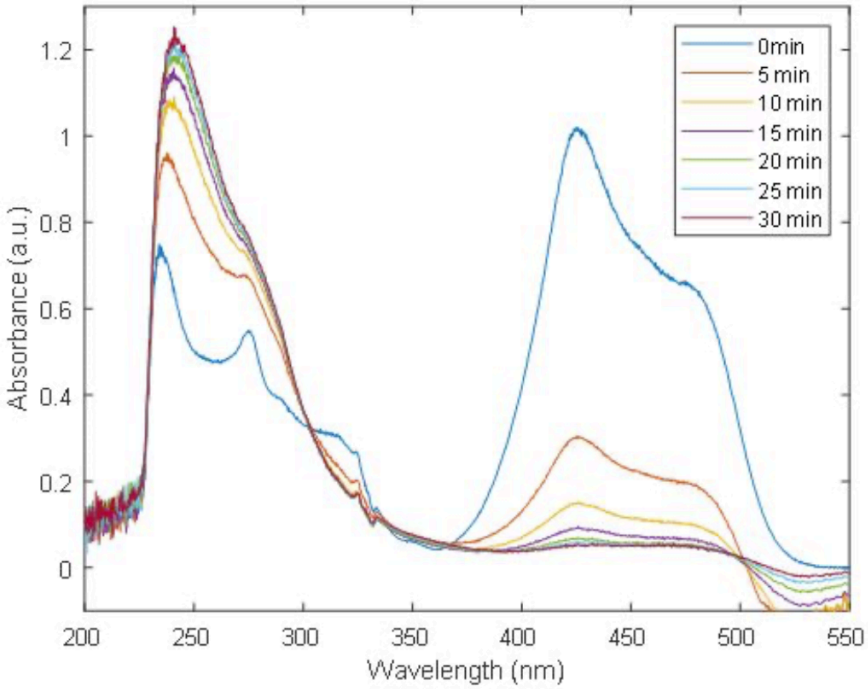

Figure S23. In-situ UV/Vis measurement of a norbornene homopolymerization mixture with 100 eq norbornene, 1 eq 2-cyclohexyl-1-methoxyethylene and 0.03 eq $MeOTPP^{+}BF_4^{-}$ in dichloromethane under constant irradiation with 445 nm blue light at ambient temperature. The dip in the absorbance above 500 nm can be explained by fluorescence of the catalyst.

Table S1. Higher conversions in the hybrid copolymerization of norbornene and MMA (50/50 feed ratio; 100 eq) utilizing MF-ROMP conditions with ethyl-1-propenyl ether (1 eq) as initiator and MeOTPP+BF4- (0.03 eq) in dichloromethane (2 mol·L-1)**.** After 60 min an aliquot was taken for ^{1}H NMR analysis. Afterwards, 1 mg of the pyrylium salt was dissolved in 2 mL dichloromethane and the solution degassed and subsequently added to the polymerization mixture. The same procedure was repeated after 180 min and the sample was irradiated for in total 420 min reaching higher conversions compared to experiments without sequential addition of pyrylium salt. The molecular weight distribution remained monomodal and leads towards higher molecular weights compared to the other molecular weights reported in table 1 of the main manuscript.

total reaction time (h)	**conversion norbornene (%)**	**conversion MMA (%)**	M_p^c **[kDa]**
1	4	4	/
2	15	7	10.6
3	22	13	13.1
4	25	16	13.4

5 Instrumentation

Nuclear Magnetic Resonance Spectroscopy (NMR)

^{1}H and ^{13}C NMR spectra were recorded on a Bruker System 600 Ascend LH, equipped with a BBO-Probe (5 mm) with z-gradient (^{1}H: 600.13 MHz, ^{13}C: 150.90 MHz). All measurements were carried out in deuterated solvents. The chemical shift (δ) is recorded in parts per million (ppm) and relative to the residual solvent protons. Coupling constants (J) were calculated in Hertz (Hz). *MestReNova* 12.0 software was used to analyze the spectra. The signals were quoted as follows: s = singlet, bs =broad singlet, d = doublet, t = triplet and m = multiplet.

Size-Exclusion Chromatography

The SEC measurements were conducted on a *PSS* SECurity[29] system consisting of a *PSS* SECurity Degasser, *PSS* SECurity TCC6000 Column Oven (35 °C), *PSS* SDV Column Set (8x150 mm 5 µm Precolumn, 8x300 mm 5 µm Analytical Columns, 100000 Å, 1000 Å and 100 Å) and an *Agilent* 1260 Infinity Isocratic Pump, *Agilent* 1260 Infinity Standard Autosampler, *Agilent* 1260 Infinity Diode Array and Multiple Wavelength Detector (A: 254 nm, B: 360 nm), *Agilent* 1260 Infinity Refractive Index Detector (35 °C). HPLC grade THF, stabilized with BHT, is used as eluent at a flow rate of 1 $mL \cdot min^{-1}$. Narrow disperse linear poly(styrene) (M_n: 266 $g \cdot mol^{-1}$ to $2.52 \cdot 10^6$ $g \cdot mol^{-1}$) and poly(methyl methacrylate) (M_n: 202 $g \cdot mol^{-1}$ to $2.2 \cdot 10^6$ $g \cdot mol^{-1}$) standards (*PSS* ReadyCal) were used as calibrants. All samples were passed over 0.22 µm PTFE membrane filters. Molecular weight and dispersity analysis was performed in *PSS* WinGPC UniChrom software (version 8.2).

SEC/HRESI-MS measurements

Spectra were recorded on a Q Exactive Plus (Orbitrap) mass spectrometer (Thermo Fisher Scientific, San Jose, CA, USA) equipped with an HESI II probe. The instrument was calibrated in the m/z range 74-1822 using premixed calibration solutions (Thermo Scientific) and for the high mass mode in the m/z range of 600-8000 using ammonium hexafluorophosphate solution. A constant spray voltage of 3.5 kV, a dimensionless sheath gas and a dimensionless auxiliary gas flow rate of 10 and 0 were applied, respectively. The capillary temperature was set to 320 °C, the S-lens RF level was set to 150, and the aux gas heater temperature was set to 125 °C. The Q Exactive was coupled to an UltiMate 3000 UHPLC System (Dionex, Sunnyvale, CA, USA) consisting of a pump (LPG 3400SD), autosampler (WPS 3000TSL), and a temperature controlled column department (TCC 3000). An aliquot (100 µL) of a polymer solution with a concentration of 2 $mg \cdot mL^{-1}$ in THF was separated on two mixed bed size exclusion chromatography columns (Agilent, Mesopore 250 × 4.6 mm, particle diameter 3 µm) with a precolumn (Mesopore 50 × 7.5 mm) operating at 30 °C. THF at a flow rate of 0.30 $mL \cdot min^{-1}$ was used as eluent. The mass spectrometer was coupled to the column in parallel to an UV detector (VWD 3400, Dionex), and a RI-detector (RefractoMax520, ERC, Japan) in a setup described earlier.[30] 0.27 $mL \cdot min^{-1}$ of the eluent were directed through the UV and RI-detector and 30 $\mu L \cdot min^{-1}$ were infused into the electrospray source after post-column addition of a 50 µM solution of sodium iodide in methanol at 20 $\mu L \cdot min^{-1}$ by a micro-flow HPLC syringe pump (Teledyne ISCO, Model 100DM).

Chapter 2. References

1. Zhang, Z.; Zeng, T. Y.; Xia, L.; Hong, C. Y.; Wu, D. C.; You, Y. Z. Synthesis of Polymers with On-Demand Sequence Structures via Dually Switchable and Interconvertible Polymerizations. *Nat. Commun*. **2018**, *9*, 1−9.

2. Bielawski, C. W.; Morita, T.; Grubbs, R. H. Synthesis of ABA Triblock Copolymers via a Tandem Ring-Opening Metathesis Polymerization: Atom Transfer Radical Polymerization Approach. *Macromolecules* **2000**, *33*, 678−680.

3. Bielawski, C. W.; Louie, J.; Grubbs, R. H. Tandem Catalysis: Three Mechanistically Distinct Reactions from a Single Ruthenium Complex. *J. Am. Chem. Soc.* **2000**, *122*, 12872−12873.

4. Mahanthappa, M. K.; Bates, F. S.; Hillmyer, M. A. Synthesis of ABA Triblock Copolymers by a Tandem ROMP-RAFT Strategy. *Macromolecules* **2005**, *38*, 7890−7894.

5. Nguyen, M. N.; Mougnier, S.-J.; Ibarboure, E.; Heroguez, V. Synthesis of Polynorbornene-Poly(tert-butyl Acrylate) Nanoparticles with Original Morphologies by Tandem ROMP and ATRP in Microemulsion. *J. Polym. Sci., Part A: Polym. Chem.* **2011**, *49*, 1471−1482.

6. Castle, T. C.; Hutchings, L. R.; Khosravi, E. Synthesis of Block Copolymers by Changing Living Anionic Polymerization into Living Ring Opening Metathesis Polymerization. *Macromolecules* 2004, *37*, 2035−2040.

7. Li, A.; Ma, J.; Sun, G.; Li, Z.; Cho, S.; Clark, C.; Wooley, K. L. One-Pot, Facile Synthesis of Well-Defined Molecular Brush Copolymers by a Tandem RAFT and ROMP, "Grafting-through" Strategy. *J. Polym. Sci., Part A: Polym. Chem*. **2012**, *50*, 1681−1688.

8. Kim, M. J.; Yu, Y. G.; Chae, C. G.; Seo, H. B.; Bak, I. G.; Mallela, Y. L. N. K.; Lee, J. S. ω-Norbornenyl Macromonomers: In Situ Synthesis by End-Capping of Living Anionic Polymers Using a Norbornenyl-Functionalized α-Phenyl Acrylate and Their Ring Opening Metathesis Polymerization. *Macromolecules* **2019**, *52*, 103−112.

9. Yu, Y. G.; Chae, C. G.; Kim, M. J.; Seo, H. B.; Grubbs, R. H.; Lee, J. S. Precise Synthesis of Bottlebrush Block Copolymers from ω-End-Norbornyl Polystyrene and Poly(4-tert-Butoxystyrene) via Living Anionic Polymerization and Ring-Opening Metathesis Polymerization. *Macromolecules* **2018**, *51*, 447−455.

10. Feast, W. J.; Gibson, V. C.; Johnson, A. F.; Khosravi, E.; Mohsin, M. A. Tailored Copolymers via Coupled Anionic and Ring Opening Metathesis Polymerization. Synthesis and Polymerization of Bicyclo[2.2.1]hept-5-ene-2,3-trans-bis(polystyrylcarboxylate)s. *Polymer* **1994**, *35*, 3542−3548.

11. Song, W.; Han, H.; Wu, J.; Xie, M. A Bridge-like Polymer Synthesized by Tandem Metathesis Cyclopolymerization and Acyclic Diene Metathesis Polymerization. *Polym. Chem.* **2015**, *6*, 1118−1126.

12. Zou, Y.; Wang, D.; Wurst, K.; Kühnel, C.; Reinhardt, I.; Decker, U.; Gurram, V.; Camadanli, S.; Buchmeiser, M. R. Group 4 Dimethylsilylenebisamido Complexes Bearing the 6-[2- (Diethylboryl)phenyl]pyrid-2-yl Motif: Synthesis and Use in Tandem Ring-Opening Metathesis/Vinyl-Insertion Copolymerization of Cyclic Olefins with Ethylene. *Chem. - Eur. J.* **2011**, *17*, 13832−13846.

13. Buchmeiser, M. R.; Camadanli, S.; Wang, D.; Zou, Y.; Decker, U.; Kühnel, C.; Reinhardt, I. A Catalyst for the Simultaneous RingOpening Metathesis Polymerization/Vinyl Insertion Polymerization. *Angew. Chem., Int. Ed*. **2011**, *50*, 3566−3571.

14. Wang, M.; Wang, D.; Widmann, L.; Frey, W.; Buchmeiser, M. R. Tandem Vinyl Insertion-/Ring-Opening Metathesis Copolymerization with ansa-6-[2-(Dimesitylboryl)-phenyl]pyrid-2-ylamido Zirconium Complexes: Role of Trialkylaluminum and MAO. *Polym. Chem*. **2016**, *7*, 1987−1998.

15. Buchmeiser, M. R. Tandem Ring-Opening Metathesis − Vinyl Insertion Polymerization: Fundamentals and Application to Functional Polyolefins. *Macromol. Rapid Commun.* **2017**, *38*, 1600672.

16. Wang, M.; Xu, G.; Wang, D.; Zou, Y.; Frey, W.; Buchmeiser, M. R. Group 4 Metal Complexes Bearing the Aminoborane Motif: Origin of Tandem Ring-Opening Metathesis/Vinyl-Insertion Polymerization. *Polym. Chem.* **2015**, *6*, 3290−3304.

17. Kottisch, V.; Michaudel, Q.; Fors, B. P. Photocontrolled Interconversion of Cationic and Radical Polymerizations. *J. Am. Chem. Soc.* **2017**, *139*, 10665−10668.

18. Peterson, B. M.; Kottisch, V.; Supej, M. J.; Fors, B. P. On Demand Switching of Polymerization Mechanism and Monomer Selectivity with Orthogonal Stimuli. *ACS Cent. Sci.* **2018**, *4*, 1228−1234.

19. Ogawa, K. A.; Goetz, A. E.; Boydston, A. J. Metal-Free Ring-Opening Metathesis Polymerization. *J. Am. Chem. Soc.* **2015**, *137*, 1400−1403.

20. Lu, P.; Boydston, A. J. Integration of Metal-Free Ring-Opening Metathesis Polymerization and Organocatalyzed Ring-Opening Polymerization through a Bifunctional Initiator. *Polym. Chem.* **2019**, *10*, 2975−2979.

21. Perkowski, A. J.; You, W.; Nicewicz, D. A. Visible Light Photoinitiated Metal-Free Living Cationic Polymerization of 4- Methoxystyrene. *J. Am. Chem. Soc*. **2015**, *137*, 7580−7583.

22. Meyer, S.; Metzger, J. O. Use of Electrospray Ionization Mass Spectrometry for the Investigation of Radical Cation Chain Reactions in Solution: Detection of Transient Radical Cations. *Anal. Bioanal. Chem.* **2003**, *377*, 1108−1114.

23. Goetz, A. E.; Pascual, L. M. M.; Dunford, D. G.; Ogawa, K. A.; Knorr, D. B.; Boydston, A. J. Expanded Functionality of Polymers Prepared Using Metal-Free Ring-Opening Metathesis Polymerization. *ACS Macro Lett*. **2016**, 5, 579−582.

24. Bielawski, C. W.; Grubbs, R. H. Living Ring-Opening Metathesis Polymerization. *Prog. Polym. Sci.* **2007**, *32*, 1−29.

25. Jovic, K.; Nitsche, T.; Lang, C.; Blinco, J. P.; De Bruycker, K.; Barner-Kowollik, C. Hyphenation of Size-Exclusion Chromatography to Mass Spectrometry for Precision Polymer Analysis-a Tutorial Review. *Polym. Chem.* **2019**, *10*, 3241−3256.

26. De Bruycker, K.; Krappitz, T.; Barner-Kowollik, C. High Performance Quantification of Complex High Resolution Polymer Mass Spectra. *ACS Macro Lett*. **2018**, *7*, 1443−1447.

27. Wu, F.; Wang, L.; Chen, J.; Nicewicz, D. A.; Huang, Y. Direct Synthesis of Polysubstituted Aldehydes via Visible-Light Catalysis. *Angew. Chem., Int. Ed*. **2018**, *57*, 2174−2178.

28. Becker, G.; Wurm, F. R. Functional Biodegradable Polymers: Via Ring-Opening Polymerization of Monomers without Protective Groups. *Chem. Soc. Rev*. **2018**, *47*, 7739−7782.

29. Martiny, M.; Steckhan, E.; Esch, T. Cycloaddition Reactions Initiated by Photochemically Excited Pyrylium Salts. *Chem. Ber.* **1993,** *126*, 1671-1682.

30. Gruendling, T.; Guilhaus, M.; Barner-Kowollik, C. Fast and Accurate Determination of Absolute Individual Molecular Weight Distributions from Mixtures of Polymers via Size Exclusion Chromatography- Electrospray Ionization Mass Spectrometry. *Macromolecules* **2009**, *42* (17), 6366–6374.

Chapter 3

Investigating the Reactivity of Photoredox-Mediated Metal-Free Ring-Opening Metathesis Polymerization with Quench Label Candidates

Abstract

Most chemists achieve molecular weight control over a polymerization by reducing the relative rate of propagation to termination. In metal-free ring-opening metathesis polymerization (MF-ROMP), the propagating chain ends continuously undergo deactivation and reactivation. This activation equilibrium makes it difficult to directly measure the population of propagating chain ends. This study probes the rates of activation and deactivation of MF-ROMP chain ends through the use of quench labeling, a method first used by the Landis group to determine active site counts on metal catalysts in olefin polymerizations. In this method, a UV-active quench is added to the polymerization such that it quickly and irreversibly binds and deactivates the active chain end, thus quenching the polymerization. The result is a population of labeled and unlabeled polymers, both of which are visible via gel permeation chromatography (GPC). From these GPC results, we can then calculate, along with other kinetic information, the equilibrium of active to inactive chain ends. Here, we look at different chromophoric quenchers and MF-ROMP reaction conditions, and how these variables affect the chain end equilibrium and control over MF-ROMP.

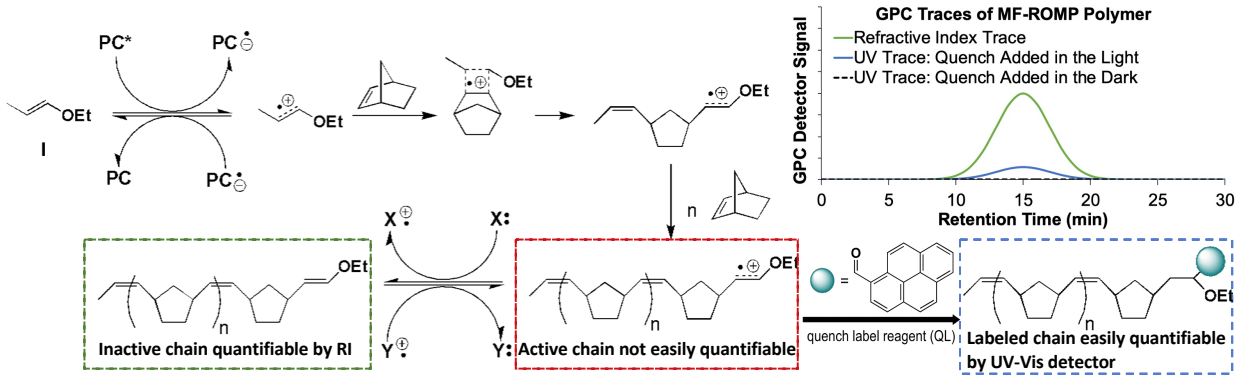

Author's preface: This project was the first of my graduate school career. I was drawn to it because it allowed me to dive into the mechanism and reactivity of MF-ROMP. Because of the complexity of MF-ROMP, I quickly ran into a variety of obstacles, made assumptions that were sometimes unfounded, and overlooked potentially viable solutions. Regardless, here are the results of this research reported from a more experienced perspective.

Introduction

Photomediated metal-free ring-opening metathesis polymerization (MF-ROMP) was developed by the Boydston group in 2015 as an alternative to the current metal-mediated polymerization processes.[18] As presented in Figure 1, MF-ROMP proceeds through a radical cationic polymerization pathway that uses organic monomers, initiators, and photocatalysts. In this polymerization pathway, the 2,4,6-tris(4-methoxyphenyl)pyrylium tetrafluoroborate photocatalyst (**2**) serves as a photooxidant to generate the radical cationic enol ether (**3**) from the ethyl-1-propenyl ether initiator (**1**). This radical cationic intermediate engages and opens the strained bicyclic intermediate (**4**) to produce a ring-opened olefin (**5**). This newly-formed olefin maintains its radical cationic enol ether which is now the propagating chain end. Other monomer units can be engaged by this chain end to produce ROMP polymers. During this process, back-electron transfer from the reduced photocatalyst and degenerative electron transfer from neutral enol ethers to the radical cationic chain end are each envisioned, affording a photomediated pathway to reversibly activate and deactivate the chain end. These mechanistic features make MF-ROMP a photomediated, spatiotemporally-controlled polymerization with living characteristics.

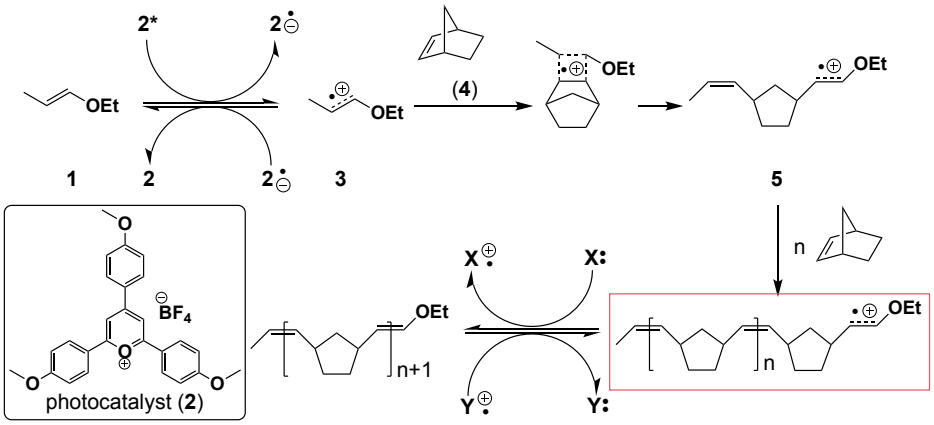

Figure 1. Proposed mechanism of MF-ROMP. Boxed in red is the active propagating species.

Despite MF-ROMP's living, controlled characteristics, its polymers' currently reported molecular weight dispersities range from 1.2–2.2. For many biological and industrial applications, it is important to have even lower dispersity polymers, where the polymer chain lengths are highly uniform. To afford better control over the polymer's dispersity, it is usually necessary to have a low concentration of propagating species to ensure uniform growth of chain ends.[9] Currently, there are no direct methods of measuring the population of active versus inactive chain ends in MF-ROMP. This makes it difficult to assess, and therefore tune, the control of this polymerization method. However in the field of catalytic olefin polymerizations, the Landis group has showcased the use of a quench label, which has greatly facilitated the study of active sites and dispersity during the course of polymerization.[10–15] Adaptation of the quench label method to MF-ROMP would be advantageous for quantifying the active chain end distribution during polymerization.

To establish a quench label method for MF-ROMP, the following needed to be developed: efficient quench label reagent; reproducible quench procedure; analysis procedure. A quench label reagent is a polymerization additive that irreversibly quenches and labels one of the key active species. When the concentration of the key species is too low to produce a strong signal via differential refractive index (RI)- or multiangle light-scattering (MALS)-detected gel permeation

chromatography (GPC), a more sensitive quantification technique is needed. Frequently, the quench label is chromophoric to offer more sensitive quantification techniques in the form of UV-Vis-detected GPC. With these GPC capabilities, one can determine a bulk, unlabeled molecular weight distribution via RI- and MALS-detected GPC and a quench labeled, active chain molecular weight distribution via UV-Vis-detected GPC for the polymerization.

As mentioned, for MF-ROMP it is desirable to know the active chain end distribution compared to the total chain end distribution at any given time during the polymerization. For a reagent to relay this information via RI- and UV-Vis-detected GPC, it needs to (1) irreversibly label active polymer chains during polymerization; (2) label an active chain only once; (3) show minimal reactivity towards inactive chains; (4) provide a strong UV-Vis handle.

Results and Discussion

To find a label reagent satisfying this criteria, different functionalities with literature precedence for reactivity with radicals, cations, or radical cations were screened in MF-ROMP. For example, [2+2], [4+2], nucleophilic, and radical additions are typical mechanisms that show reactivity with the radical cation enol ethers.[16–30] The following reagents shown in Figure 2 were expected to undergo these mechanisms, and were studied in MF-ROMP.

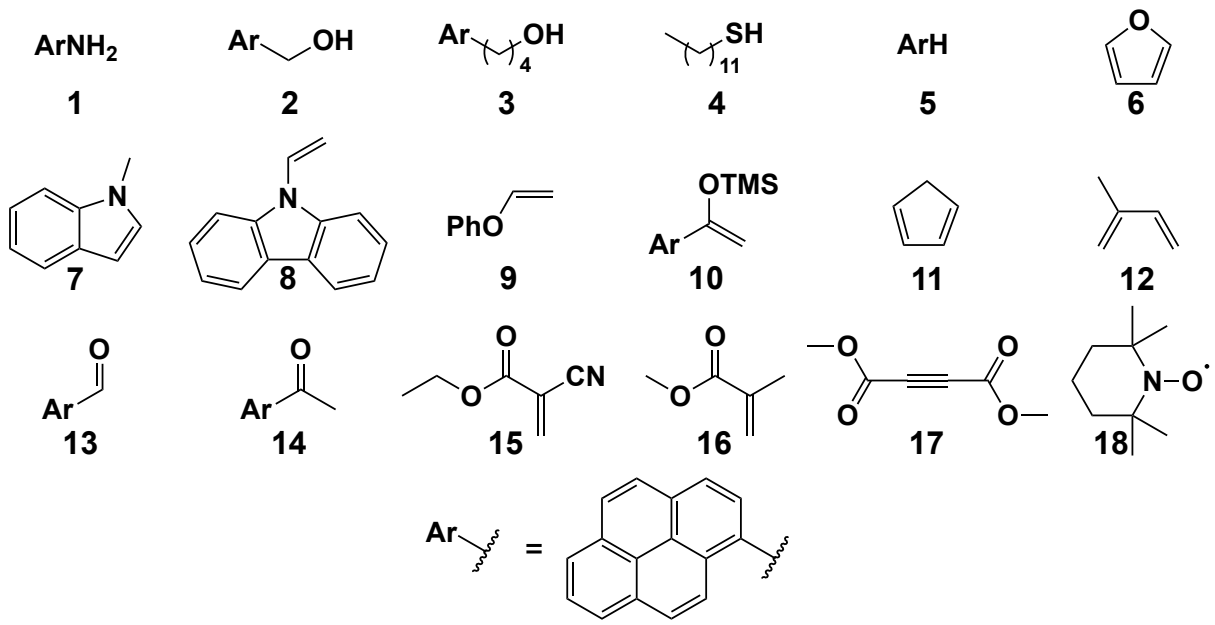

Figure 2. Quench label candidates. Ar = 1-pyrenyl.

To ensure that these quench label candidates would quench MF-ROMP, they were added mid-polymerization and monitored for increases in monomer conversion. If no significant increase in monomer conversion is detected, then the candidate passed this stage of screening and moved onto a labeling screening. The results to this screen are shown in Figure 3.

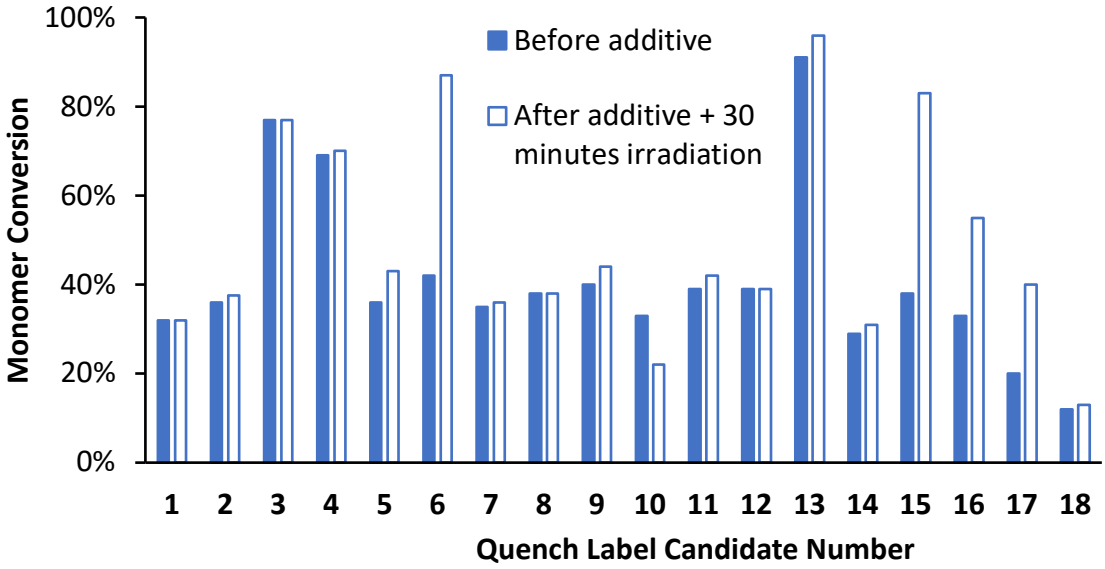

Figure 3. Quench label conversion screen results. Candidate numbering comes from Figure 2. Solid blue bar shows the norbornene conversion 3 minutes into polymerization (unless otherwise noted) before the quench candidate was added to the polymerization mixture; the blue outline/white infill bar shows the norbornene conversion after the quench candidate was added plus 30 minutes of irradiation (unless otherwise noted). (**4**) was added 30 minutes into irradiation and (**13**) at 10 minutes into irradiation; all other screening polymerizations were quenched at 3 min into irradiation. [NB]:[EPE]:[PC] = 50:1:0.1 for (**3**), 50:1:0.05 for (**15**), and 100:1:0.05 for all else. [EPE] = 20 mM.

The results indicate that, of the additives tested, furan (**6**) and ethyl 2-cyanoacrylate (**15**) do not inhibit the conversion of monomer, making them inviable quenchers. Dimethyl acetylenedicarboxylate (**17**), methyl methacrylate (**16**), and cyclopentadiene (**11**) retard polymerization but do not stop it, making them inviable quenchers. (**16**) had thereafter been shown to copolymerize with NB[9] in MF-ROMP albeit at a slower rate, which justifies the reduction in rate of polymerization. (**11**) undergoes oxidation, providing an off-target pathway for the polymerization which justifies the reduction in polymerization rate. 2,2,6,6-tetramethylpiperidine 1-oxyl (**18**) and isoprene (**12**) also demonstrated a halt in NB conversion, but the isolated polymer indicated no new chain end structure, supporting that these reagents stop polymerization and leave the propagating chain ends untagged, potentially through an oxidative pathway similar to (**11**).

Dodecyl mercaptan (**4**) halted conversion of NB. Further inspection supported labeling of the polymer backbone upon irradiation, making it an inviable quencher.[28,29]

The remaining reagents halted conversion of norbornene when added and were subjected to another screen to evaluate labeling of the polymer. This screen consisted of comparing the absorptivity of the unlabeled polymer to (i) the quenched polymer during irradiation and (ii) the quenched polymer after a dark period. From this screen, we determined if the polymer was labeled, if labeling happens during or after the polymerization, and the background reactivity of the quencher. The results from this screen are listed in Figure 4.

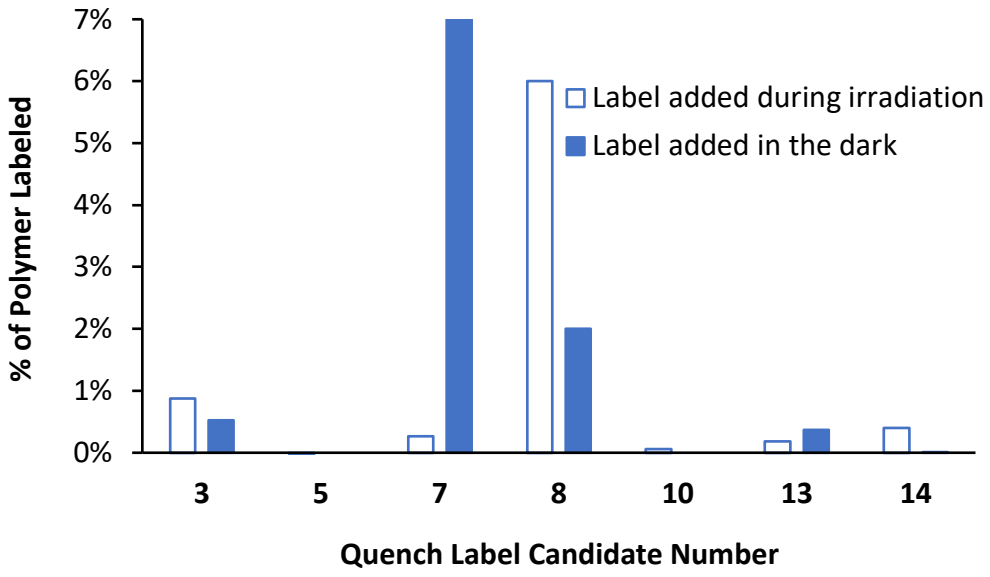

Figure 4. Label screening results. Candidate numbering comes from Figure 2. Polymerization was quenched at 3 min into irradiation unless otherwise noted. Blue solid bar indicates the calculated percentage of polymer labeled by adding the quench candidate in the absence of light; blue outline/white infilled bar indicates the calculated percentage of labeled polymer after a short period of irradiation. [NB]:[EPE]:[PC] = 50:1:0.1 for (**3**), 50:1:0.05 for (**14**), and 100:1:0.05 for all else. [EPE] = 20 mM.

1-acetylpyrene (**14**) and 1-pyrenecarboxaldehyde (**13**) labeled the polymer with little background labeling. Pyrene (**5**) and 1-pyrene-1-trimethylsiloxyethylene (**10**) did not significantly label the polymer. We observed conversion of (**10**) to (**14**) during the course of irradiation, so we hypothesize that (**10**) labels the polymer through (**14**)'s labeling mechanism. N-vinylcarbazole (**8**),

1-pryenebutanol (**3**), and N-methylindole (**7**) demonstrated moderate background labeling. Though 1-aminopyrene (**1**) was tested on a different detection setup, it also showed high levels of labeling in the dark relative to the amount it labeled in the light. Further studies on background labeling of these reagents must be done before they can be used as quench labels. Phenyl vinyl ether (**9**) is nonchromophoric and was not expected to provide a strong UV-Vis handle, and was not tested in this screen despite passing the conversion screen. 1-pyrenemethanol (**2**) was not further tested, it is expected to show reactivity similar to that of (**3**). Out of these quenches, (**13**) was further studied for its background reactivity. It was determined how quench loading relative to photocatalyst affects polymerization rate and how the polymer labeling increases during the course of irradiation. The percentage of labeled polymer grows to about 5% and levels off, as shown in Figure 5. Upon examination of the UV-Vis structure of the labeled polymer at 120 min, there was a clearly distinct band structure from that of the unlabeled polymer or from the initial quench label (Figure 6), indicating a change in functionality of the chromophore. The newly formed band structure is consistent with that of 1-pyrenebutanol, indicating that the aldehyde functionality of the quench label nay be consumed.

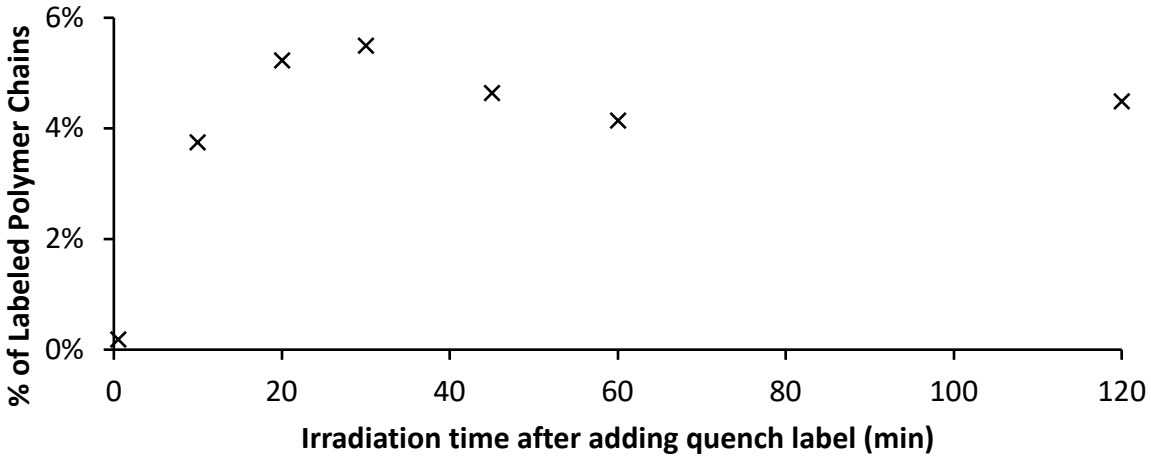

Figure 5. Polymer labeling time-course for 1-pyrenecarboxaldehyde in MF-ROMP. [NB]:[EPE]:[PC]:[**13**] = 100:1:0.05:10. [EPE] = 20 mM. Polymerization was irradiated for 3 minutes, at which point (**13**) was added and irradiation continued.

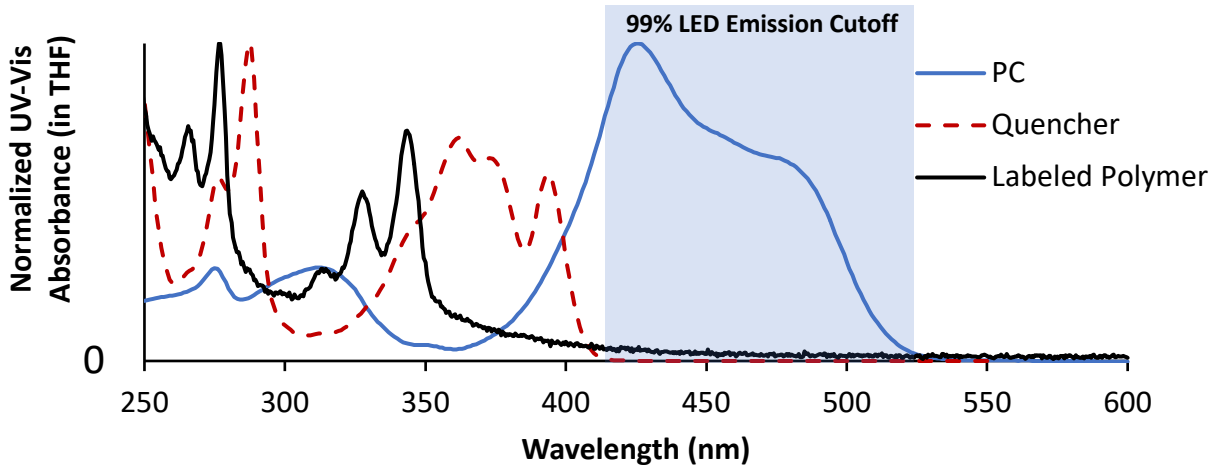

Figure 6. UV-Vis spectrum of the components of MF-ROMP. Solid blue region indicates the 99% emission cutoff of the blue LED used for irradiation; solid blue trace indicates the absorbance spectrum of the photocatalyst; dotted red trace indicates the absorbance spectrum of 1-pyrenecarboxaldehyde; solid black trace indicates the absorbance spectrum of the concentrated labeled polymer after about 120 minutes of irradiation. The black trace is also consistent with the UV-Vis trace of 1-pyrenebutanol.

Conclusions

Several candidates were tested for viability as quench label reagents for MF-ROMP. Though the mechanism is not clear yet, 1-aminopyrene (**1**), 1-pyrenebutanol (**3**), N-methylindole (**7**), 1-acetylpyrene (**14**), and 1-pyrenecarboxaldehyde (**13**) all displayed varying degrees of direct and background labeling. Further studies showed that (**13**) displays a clear change in molecular structure upon labeling. To complete this project, further studies into the chain end structure of the polymer should be conducted, and the other currently viable labels should be tested to measure each labeling rate in order to verify the calculated labeling percentage.

Appendix B: Chapter 3 Experimental Procedures and Supporting Information

All reagents were used as purchased unless otherwise stated.

Calculation of percentage labeled.
M_n = number average molecular weight (provided by GPC);
g = functional form of the GPC calibration curve of the chromophoric reagent;
f = initiator efficiency;
GPC injected mass is provided by the instrument using the RI trace and a known dn/dc of 0.1507 for PNB. GPC injected volume is known.

$$\%\ \text{labeled} = \frac{\text{concentration of labeled population}}{\text{concentration of entire population}} = \frac{g(\text{area of UV trace})}{M_n * \frac{\text{GPC injected mass}}{\text{GPC injected volume}}}$$

The % labeled should not be higher than the following…

$$\max\%\ \text{labeled} = \frac{\text{maximum amount of radical cation}}{\text{minimum possible moles of chain ends}} = \frac{[\text{PC}]}{\text{f}[\text{EPE}]}$$

In most cases, f > 0.4, and [PC]:[EPE] = 0.05, so we should see label percentages of less than 13%.

Control Experiments

Table S1. Control Experiments for 1-pyrenecarboxaldehyde

entry[a]	NB:I:PC:13	reaction time (min)	NB conv[b] (%)	M_n[c] [kDa]	polymer absorptivity ($M^{-1}cm^{-1}$)
1	50 : 1 : 0.05 : 0	10	93	5.6	95
2[d]	50 : 1 : 0.05 : 0.5	100	93	5.8	190
3[e]	50 : 1 : 0.05 : 0.5	180	96	7.0	1190
4	50 : 1 : 0.00 : 0.5	1180	0	--	--
5	15 : 0 : 0.05 : 2.5	150	0	--	--
6	0 : 1 : 0.12 : 1.5	30	--	--	--

[a]For all entries, 0% conversion of QL was observed.
[b]Conversion determined via ^{1}H NMR.
[c]Absorptivity determined via UV-detected GPC effluent at 328 nm.
[d]Entry 1 mixed with QL and left in the dark for 100 min.
[e]Entry 2 irradiated for 180 min.

These experiments show that (**14**) causes a significant increase in polymer absorptivity after irradiation despite having no reactivity outside of standard MF-ROMP conditions.

Quench Label Saturation Studies

The quench label can either label the chain end by being activated by photocatalyst and then labeling neutral chain end (undesirable) or by directly labeling active chain end (desirable) as depicted in Figure S1. We can check the quench candidates' saturation kinetics in MF-ROMP quenching. If the photocatalyst is activating the quench label before it reacts with chain-end, we should not see a dependence of quencher concentration on the labeling percentage. In the ideal quench-label case where the quench label reacts only with the active chain end, we should see a saturation dependence of quencher concentration on labeling percentage.

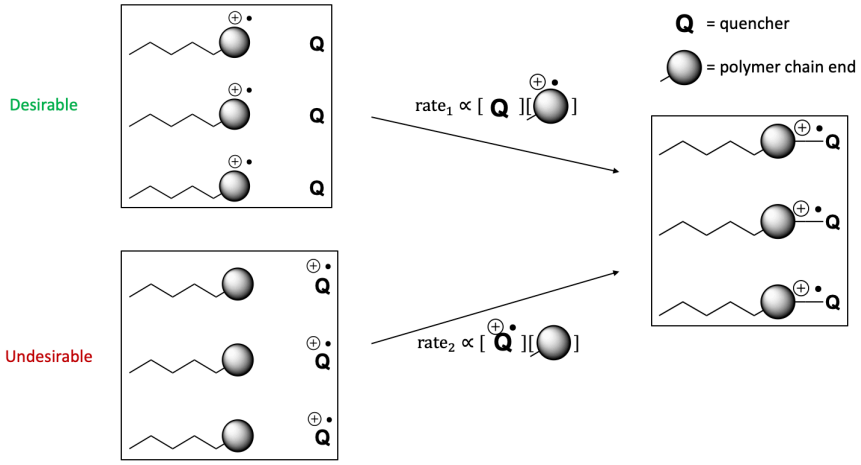

Figure S1. Potential pathways of quench-labeling chain end. This model assumes the radical cation concentration is some constant fraction of the amount of initial photocatalyst and that there is rapid e-transfer from activated photocatalyst.

Kinetic Models for Photoredox-Mediated MF-ROMP

Notes: For the following models, we will ignore photocatalyst relaxation but you can also assume that excited state photocatalyst relaxes with a significant rate (Step 5), which results in an additional term in the rate expression. Of the following models, Model A tends to be a good fit at early conversions, and Model B tends to fit for the entirety of the polymerization.

Abbreviations:
PC = pyrylium photocatalyst; EE = enol ether functionality; M = monomer; * = activated state; V = volume of reactor ; ϕ = quantum yield of excitation; F = Light flux into reactor; ε = molar absorbtivity; l = path length; f = initiator efficiency; k_n = rate constant of step n; X_t = monomer conversion at time t; $[N]_0$ = initial concentration of N; [N] = concentration of N at time t.

Step			Rate Expression
Initiation	(1)	$\mathrm{PC} \xrightarrow{h\nu} \mathrm{PC}^*$	$\text{rate} = \frac{\phi\,\mathrm{F}}{\mathrm{V}}(1 - 10^{-\varepsilon\, l\, [PC]})$
	(2)	$\mathrm{PC}^* + \mathrm{EE} \xrightarrow{k_i} \mathrm{PC}^{\bullet-} + \mathrm{EE}^{\bullet+}$	$\text{rate} = k_i[\mathrm{PC}^*][\mathrm{EE}]$
Propagation	(3)	$\mathrm{M} + \mathrm{EE}^{\bullet+} \xrightarrow{k_p} \mathrm{EE}^{\bullet+}$	$\text{rate} = k_p[\mathrm{M}][\mathrm{EE}^{\bullet+}]$
Termination	(4)	$\mathrm{PC}^{\bullet-} + \mathrm{EE}^{\bullet+} \xrightarrow{k_t} \mathrm{PC} + \mathrm{EE}$	$\text{rate} = k_t[\mathrm{PC}^{\bullet-}][\mathrm{EE}^{\bullet+}]$
Relaxation	(5)	$\mathrm{PC}^* \xrightarrow{k_r} \mathrm{PC}$	$\text{rate} = k_r[\mathrm{PC}^*]$

Model A: No Chain Death

Assumptions:

(i) Photocatalyst does not go through decomposition pathways.

(ii) Ground state and dead photocatalyst concentrations are significantly greater than excited and reduced photocatalyst concentrations; $[\mathrm{PC}] + [\mathrm{PC_{dead}}] >> [\mathrm{PC^{\bullet -}}] + [\mathrm{PC^{*}}]$.

(iii) Step 1 is the rate-determining step for initiation.

(iv) All radical cationic enol ethers react with a similar rate.

(v) All neutral enol ethers react with a similar rate.

(vi) Neutral enol ether concentration is significantly greater than radical cationic enol ether concentration; $[\mathrm{EE}] >> [\mathrm{EE^{\bullet +}}]$.

Mass balance:

$$[\mathrm{PC}]_0 = [\mathrm{PC}] + [\mathrm{PC^{\bullet -}}] + [\mathrm{PC^{*}}] + [\mathrm{PC_{dead}}] \approx [\mathrm{PC}] + [\mathrm{PC_{dead}}]$$

and

$$f[\mathrm{EE}]_0 = [\mathrm{EE}] + [\mathrm{EE^{\bullet +}}] \approx [\mathrm{EE}]$$

Charge balance: $$[\mathrm{PC^{\bullet -}}] = [\mathrm{EE^{\bullet +}}]$$

If RDS is Step 1: $\mathrm{rate_{init}} = \frac{\phi\,\mathrm{F}}{\mathrm{V}}(1 - 10^{-\varepsilon\, l\, [PC]}) \approx \frac{\phi\,\mathrm{F}}{\mathrm{V}}$ (based on our photocatalyst loadings)

$$\mathrm{rate_{term}} = k_t[\mathrm{PC^{\bullet -}}][\mathrm{EE^{\bullet +}}] = k_t[\mathrm{EE^{\bullet +}}]^2 \text{ (from the charge balance)}$$

For chain polymerizations, $\mathrm{rate_{init}} \approx \mathrm{rate_{term}} \rightarrow [\mathrm{EE^{\bullet +}}] \approx \sqrt{\frac{\phi\,\mathrm{F}}{k_t \mathrm{V}}}$

Therefore: $\mathrm{rate_{prop}} = -\frac{d[\mathrm{M}]}{dt} = k_p[\mathrm{M}][\mathrm{EE^{\bullet +}}] = k_p\sqrt{\frac{\phi\,\mathrm{F}}{k_t \mathrm{V}}}\,[\mathrm{M}] = k[\mathrm{M}]$

From calculus: $\frac{[\mathrm{M}]}{[\mathrm{M}]_0} = 1 - X_t = e^{-kt}$

A line of slope –k is produced for a plot of t vs. $Ln(1 - X_t)$

For chain polymerizations, rate of initiation ≈ rate of termination. [1] is the RDS for initiation (else we'd see a buildup of PC*)

If you include Step 5 and assumed a steady state concentration of excited state photocatalyst ($\frac{d[\mathrm{PC^{*}}]}{dt} = 0$), you'd now find…

$$\mathrm{rate_{prop}} = -\frac{d[\mathrm{M}]}{dt} = k_p[\mathrm{M}][\mathrm{EE^{\bullet +}}] = k_p\sqrt{\frac{\phi\,\mathrm{F}}{k_t \mathrm{V}} * \frac{k_i\, f[\mathrm{EE}]_0}{k_r\ + k_i\, f[\mathrm{EE}]_0}}\,[\mathrm{M}] = k[\mathrm{M}]$$

…in which case the rate constant, k, would include an additional term of k_r.

Model B: 1st Order Chain Death

Assumptions:

(i) Polymer chain end goes through first order decomposition pathway; $[\mathrm{EE}^{\bullet+}] \propto e^{-k_d t}$.

$$\text{Therefore: } \mathrm{rate}_{\mathrm{prop}} = -\frac{d[\mathrm{M}]}{dt} = k_p[\mathrm{M}][\mathrm{EE}^{\bullet+}] = k''[\mathrm{M}]\, e^{-k_d t}$$

$$\text{From calculus: } \frac{[\mathrm{M}]}{[\mathrm{M}]_0} = 1 - X_t = e^{(1-e^{-k\,t})*Ln(1-X_\infty)}$$

$$\text{A line of slope –k is produced for a plot of } t \text{ vs. } Ln\left[1 - \frac{Ln(1-X_t)}{Ln(1-X_\infty)}\right]$$

X_∞ = monomer conversion after an infinite amount of time, and can usually be approximated by the peak conversion attained after sufficient amounts of time.

Model C: 2nd Order Photocatalyst Chain Death

Assumptions:

(i) Polymer chain end goes through second order decomposition pathway; $[\mathrm{EE}^{\bullet+}] \propto \frac{1}{1+k_d\, t}$.

$$\text{Therefore: } \mathrm{rate}_{\mathrm{prop}} = -\frac{d[\mathrm{M}]}{dt} = k_p[\mathrm{M}][\mathrm{EE}^{\bullet+}] = k''[\mathrm{M}]\, \frac{1}{1+k_d\, t}$$

$$\text{From calculus: } \frac{[\mathrm{M}]}{[\mathrm{M}]_0} = 1 - X_t = (1 + k't)^{-k}$$

$$\text{A line of slope –k is produced for a plot of } Ln(1 - X_t) \text{ vs. } Ln(1 + k't)$$

Quench Label Poisoning Studies

These poisoning studies were conducted to determine the minimum amount of quench label needed to halt conversion in MF-ROMP. In these experiments, norbornene (NB), ethyl propenyl ether (EPE), pyrylium (PC) and the quench label reagent (same numbering as Figure 2 from main text) were mixed together in CH_2Cl_2 before being irradiated for 20 minutes. [NB]:[EPE]:[PC] = 100:1:0.05 at [EPE] = 20 mM.

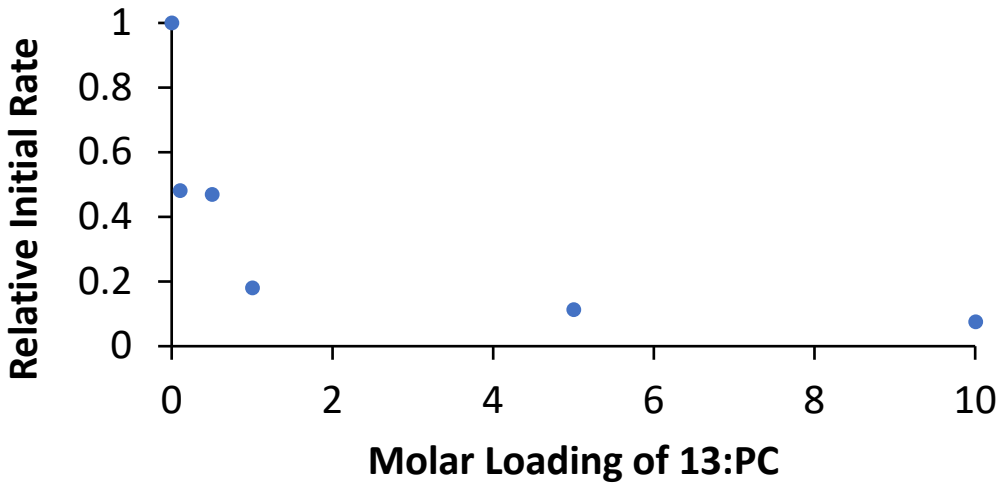

Figure S2. Poisoning study of N-vinylcarbazole (**8**) in MF-ROMP.

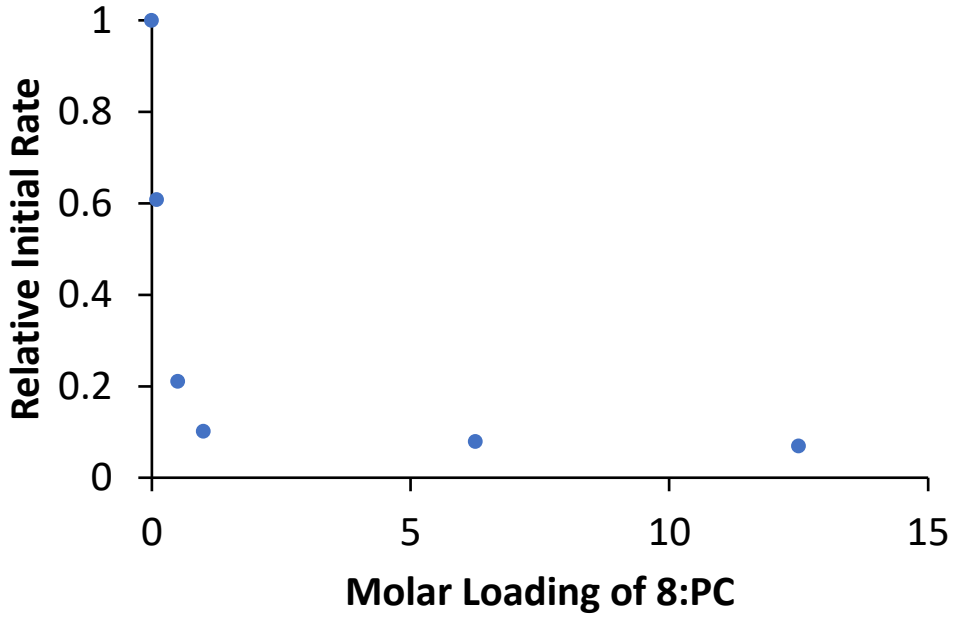

Figure S3. Poisoning study of N-vinylcarbazole (**8**) in MF-ROMP.

Polymerization of poly(norbornene) via MF-ROMP.

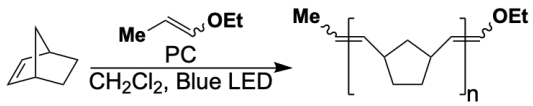

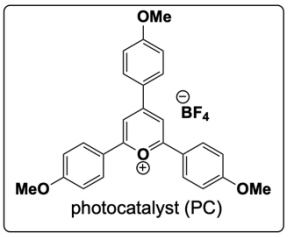

Sublimed norbornene (0.50 g, 5.31 mmol) and PC (1.3 mg, 0.0027 mmol) was added to a 2-dram vial. Dichloromethane (3.0 mL) was added. Ethyl propenyl ether (4.6 mg, 0.053 mmol) was added. The mixture is stirred and irradiated for 60 minutes. Crude aliquots are taken at various increments of the polymerization for analysis by ^{1}H NMR and GPC. Work up: dilute reaction mixture with dichloromethane (40 mL) and filter through alumina. Dry down filtrate to 10 mL, and precipitate in chilled methanol (75 mL). Analysis of the precipitated product is done using ^{1}H NMR and GPC.

Synthesis of 2,4,6-tri-(*p*-methoxyphenyl) pyrylium tetrafluoroborate photocatalyst.

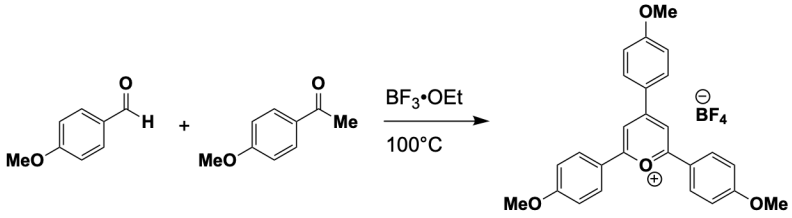

Following the literature preparation, acetanisole (2.50 mL, 20.6 mmol) and acetaldehyde (6.17 g, 41.2 mmol) were added to a 50 mL round bottom flask. After putting under the reagents under an atmosphere of nitrogen, boron trifluoride etherate (6.3 mL, 50.9 mmol) was slowly added over the course of a minute. The reaction was heated to 100 ºC and left for 2 hours. Work up: the reaction mixture was allowed to cool and diluted in 100 mL of acetone and 125 mL of diethyl ether. The dilution was filtered, the filtrite was washed with 80 mL of warm acetone. The filtrite was filtered and washed again before using.

^{1}H NMR in DMSO-*d6*

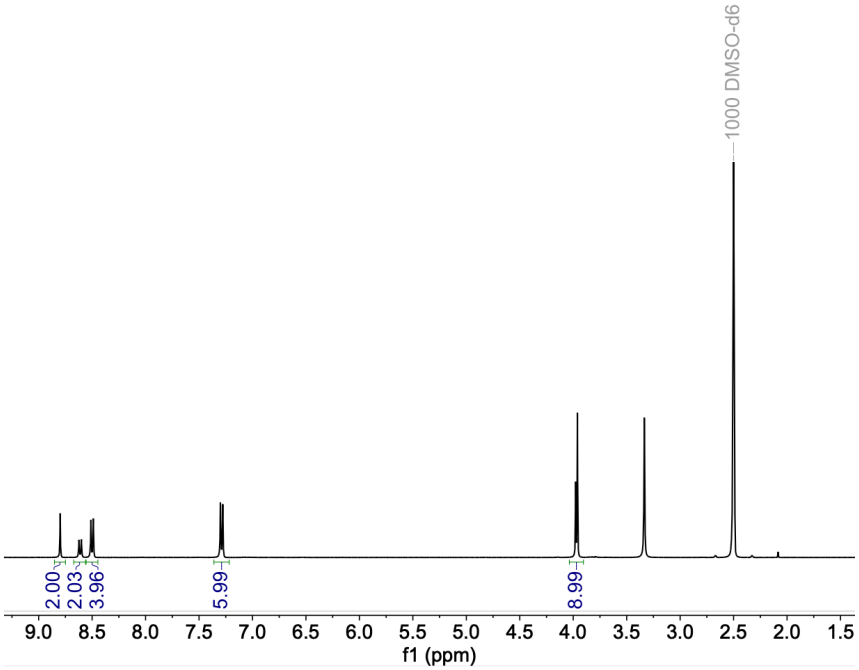

Synthesis of 1-pyrene-1-trimethylsiloxyethylene.

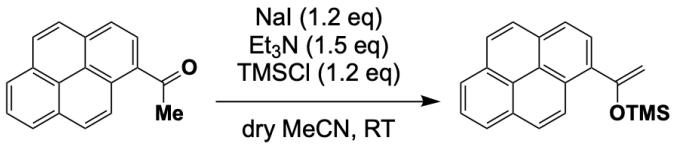

Adapted from I. Khan, B. G. Reed-Berendt, R. L. Melen, L. C. Morrill. *Angew. Chem. Int. Ed*. **2018**, *57*, 12356. 1-acetylpyrene (1.0 g, 4.1 mmol) and sodium iodide (740 mg, 4.9 mmol) were added to a 100 mL round bottom flask under nitrogen. Acetonitrile (50 mL) dried over 3Å mole sieves was added. The mixture was stirred for 5 minutes, and then triethylamine (0.86 mL, 6.1 mmol) was added. Chlorotrimethylsilane (0.52 mL, 4.9 mmol) was added slowly. The reaction was allowed to stir for 12 hours. Work up: the reaction mixture was diluted with chilled hexanes. The hexane layer was washed twice with chilled acetonitrile and water saturated with ammonium chloride. The resulting mixture was dried with sodium sulfate.

^{1}H NMR in CD_2Cl_2

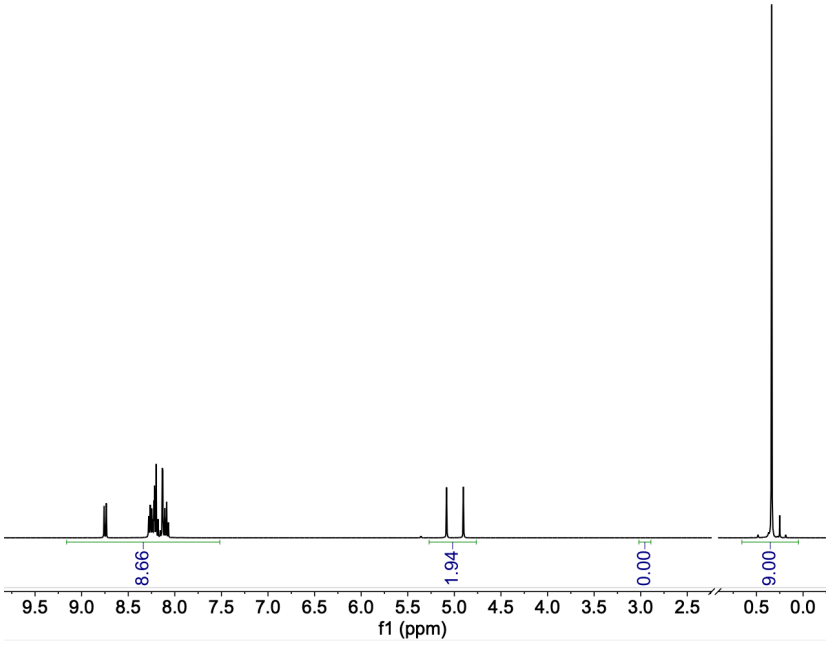

Chapter 3. References

1. Kelli A. Ogawa, K. A.; Goetz, A. E.; Boydston, A. J. Metal-Free Ring-Opening Metathesis Polymerization. *J. Am. Chem. Soc.* ***2015,*** *137* (4), 1400–1403.

2. Goetz, A. E.; Boydston, A. J. Metal-Free Preparation of Linear and Crosslinked Polydicyclopentadiene. *J. Am. Chem. Soc.* **2015**, *137*, 7572–7575.

3. Ogawa, K. A.; Goetz, A. E.; Boydston, A. J. Developments in Externally Regulated Ring-Opening Metathesis Polymerization. *Synlett* **2016**, *27*, 203–214.

4. Pascual, L. M. M.; Dunford, D. G.; Goetz, A. E.; Ogawa, K. A.; Boydston, A. J. Comparison of Pyrylium and Thiopyryium Photo-oxidants in Metal-Free Ring-Opening Metathesis Polymerization. *Synlett* **2016**, *27*, 759–762.

5. Goetz, A. E.; Pascual, L. M. M.; Dunford, D. G.; Ogawa, K. A.; Knorr, D. B., Jr.; Boydston, A. J. Expanded Functionality of Polymers Prepared Using Metal-Free Ring-Opening Metathesis Polymerization. *ACS Macro Lett.* **2016**, *5*, 579–582.

6. Lu, P.; Alrashdi, N. M.; Boydston, A. J. Bidirectional Metal-Free ROMP from Difunctional Organic Initiators. *J. Polym. Sci. A, Polym. Chem.* **2017**, *55*, 2977–2982.

7. Kensy, V. K.; Tritt, R. L.; Haque, F. M.; Murphy, L. M.; Knorr, D. B.; Grayson, S. M.; Boydston, A. J. Molecular Weight Control via Cross Metathesis in Photo-Redox Mediated Ring-Opening Metathesis Polymerization. *Angew. Chem., Int. Ed.*, **2020**, *59*, 9074–9079.

8. Lu, P.; Kensy, V. K.; Tritt, R. L.; Seidenkranz, D. T.; Boydston, A. J. Metal-Free Ring-Opening Metathesis Polymerization: From Concept to Creation. *Acc. Chem. Res*. **2020**, *53*, 2325–2335.

9. Plichta, A.; Zhong, M.; Li, W.; Elsen, A. M.; Matyjaszewski, K., Tuning Dispersity in Diblock Copolymers Using ARGET ATRP. *Macromol. Chem. Phys.* **2012,** *213*, 2659-2668.

10. Cueny, E. S.; Johnson, H. C.; Anding, B. J.; Landis, C. R. Selective Quench-Labeling of the Hafnium-Pyridyl Amido-Catalyzed Polymerization of 1-Octene in the Presence of Trialkyl-Aluminum Chain-Transfer Reagents. *J. Am. Chem. Soc*. **2017**, *139,* 11903−11912.

11. Nelsen, D. L.; Anding, B. J.; Sawicki, J. L.; Christianson, M. D.; Arriola, D. J.; Landis, C. R. Chromophore Quench-Labeling: An Approach to Quantifying Catalyst Speciation As Demonstrated for (EBI)ZrMe2/B(C6F5)3-Catalyzed Polymerization of 1-Hexene. *ACS Catal*. **2016**, *6,* 7398−7408.

12. Cueny, E. S.; Sita, L. R.; Landis, C. R. Quantitative Validation of the Living Coordinative Chain-Transfer Polymerization of 1-Hexene Using Chromophore Quench Labeling. *Macromolecules* **2020**, *53,* 5816–5825.

13. Cueny, E. S.; Johnson, H. C.; Landis, C. R. Selective Quench-Labeling of the Hafnium-Pyridyl Amido-Catalyzed Polymerization of 1-Octene in the Presence of Trialkyl-Aluminum Chain-Transfer Reagents. A*CS Catal.* **2018**, *8*, 11605–11614.

14. Y. Okada, K. Chiba. Electron transfer-induced four-membered cyclic intermediate formation: Olefin cross-coupling vs. olefin cross-metathesis. *Electrochimica Acta*. **2011**, *56,* 1037–1042.

15. Cueny, E. S.; Nieszala, M. R.; Froese, R. D. J.; Landis, C. R. Nature of the Active Catalyst in the Hafnium-Pyridyl Amido-Catalyzed Alkene Polymerization. *ACS Catal.* **2021**, *11*, 43014309.

16. Nelsen, S. F. Cation radical catalyzed chain oxygenation of alkylated olefins and dienes. *Acc. Chem. Res.* **1987**, *20*, 269.

17. Tatsuya, K.; Motoyuki, H.; Hirochika, S.; Katsumi, T. Oxygenation of Aromatic Vinyl Ethers. A Noticeable Formation of Epoxides and Reaction Mechanism. *Bull. Chem. Soc. Jpn.* **1981**, *54*, 2330.

18. Kawata, H.; Niizuma, S. Pyranyl Radicals and Their Dimers. *Bull. Chem. Soc. Jpn.* **1989**, *62,* 2279–2283.

19. Gaviña, P.; Lavernia, N. L.; Mestres, R.; Miranda, M. A. Deacetalization by Photoinduced Electron Transfer with a Pyrylium Salt: Effect of Limiting the Amounts of Water, Oxygen and Sensitizer. *Tetrahedron* **1996**, *52*, 4911.

20. Iijima, Y.; Obara, S.; Ohba, Y.; Kubo, K.; Sakurai, T. 2,4,6- triphenylpyrylium ion-mediated photooxidation of N,N-dibenzylhydroxylamine and its derivatives. *J. Photochem. Photobiol. A.* **2001**, *143*, 23−29.

21. Pang, Y.; Moser, D.; Cornella, J. Pyrylium Salts: Selective Reagents for the Activation of Primary Amino Groups in Organic Synthesis. *Synthesis* **2020**, *52*, 489–503.

22. Groenewold, G. S.; Gross, M. L. Reaction of the Vinyl Methyl Ether Cation Radical and 1,3-Butadiene: A Two-step Cycloaddition. *J. Am. Chem. Soc.* **1984,** *106,* 6575–6519.

23. Morse, P. D.; Nguyen, T. M.; Cruz, C. L.; Nicewicz D. A. Enantioselective counter-anions in photoredox catalysis: The asymmetric cation radical Diels-Alder reaction. *Tetrahedron* **2018**, *74*, 3266–3272.

24. Kuwata, S.; Shigemitsu, Y.; Odaira, Y. Photosensitized Dimerization of Phenyl Vinyl Ethers. *J. Org. Chem.* **1973***, 38***,** 3803–3805.

25. Bauld, N. L.; Bellville, D. J.; Harirchian, B.; Lorenz, K. T.; Pabon, R. A.; Reynolds, D. W.; Wirth, D. D.; Chiou, H. S.; Marsh, B. K. Cation Radical Pericyclic Reactions. *Acc. Chem. Res.* **1987**, *20,* 371–378.

26. Moeller, K. D. Using Physical Organic Chemistry To Shape the Course of Electrochemical Reactions. *Chem. Rev.* **2018**, *118*, 4817−4833.

27. Xu, T. C., Tu, K., Cheng, J. N., Ni, Y. Y., Zhang, L. F., Cheng, Z. P., Zhu, X. L. Organocatalytic Approach to Functional Semifluorinated Polymers Driven by Visible Light. *Macromol. Rapid Commun.* **2018**, *39*, 1800151.

28. Griesser, T.; Wolberger, A.; Daschiel, U.; Schmidt, V.; Fian, A.; Jerrar, A.; Teichert, C.; Kern, W. Cross-linking of ROMP derived polymers using the two-photon induced thiol–ene reaction: towards the fabrication of 3D-polymer microstructures. *Polym. Chem*. **2013**, *4*, 1708.

29. Lowe, A. B. Thiol–ene "click" reactions and recent applications in polymer and materials synthesis: a first update. *Polym. Chem.* **2014**, *5*, 4820.

30. Naumov, S.; Janovsky, I.; Knolle, W.; Mehnert, R. *Macromol. Chem. Phys*. **2003**, *204*, 2099–2104.

Chapter 4

Flow Optimization of Photoredox-Mediated Metal-Free Ring-Opening Metathesis Polymerization

Reproduced from: Rigoglioso, V. P. Boydston, A. J. "Flow Optimization of Photoredox-Mediated Metal-Free Ring-Opening Metathesis Polymerization." *ACS Macro Lett.* **2023**, *12*, 1479−1485.

Abstract

Photoredox-mediated metal-free ring-opening metathesis polymerization (MF-ROMP) is a convenient metal-free method to produce a variety of ROMP polymers. Transitioning MF-ROMP from a batch to a continuous flow process has yet to be demonstrated and could potentially benefit production efficiency, safety, and modularity of reaction conditions. We designed and evaluated continuous flow and droplet flow setups and compared the results for MF-ROMP across a short series of common monomers. By using the droplet flow reactor setup, we achieved flow conversions comparable to that of batch, and circumvented issues with diffusion-limited mixing and air exposure.

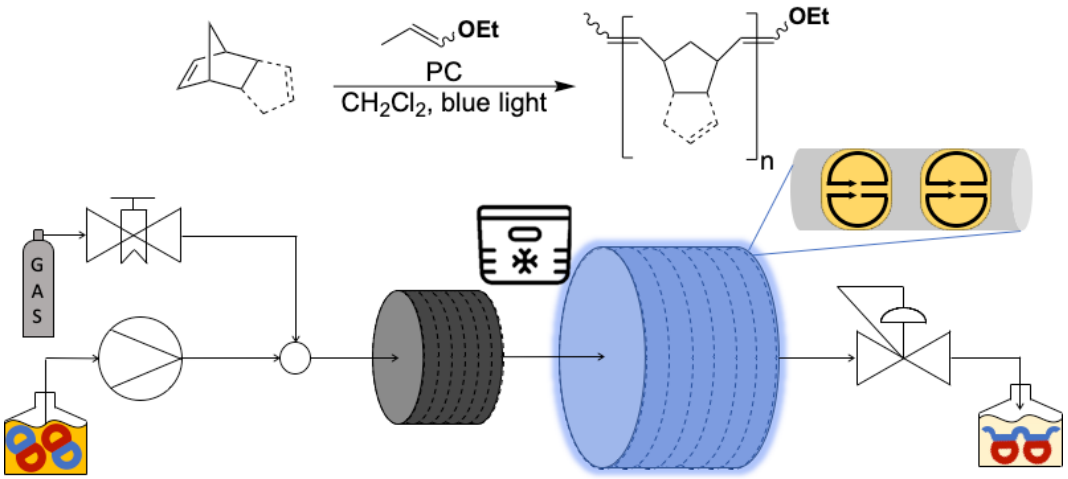

Introduction

In general, products of ring-opening metathesis polymerization (ROMP) are used industrially in applications where their material strength and chemical compatibility are featured.[1] Until recently, essentially all ROMP products were produced via metal-mediated mechanisms that employ any number of well-established metal-alkylidene initiators or transition metal salts (pre-catalysts).[2–11] Although metal-mediated ROMP has been integrated into flow chemistry production methods (Figure 1a), the metal-free variant, which features several mechanistic distinctions from metal-mediated ROMP, has not yet been reported in flow (Figure 1c).[12,13]

Flow chemistry is becoming increasingly more applicable for polymer production relative to batch reactor methods for its improved safety, ease of scale up, and compatibility with automation. As breakthroughs in catalysis continue to enable more efficient chemical syntheses, so too have flow reactor designs advanced to augment and facilitate manufacturing processes.[14–21] Of course, certain classes of reactions present greater potential benefits from moving into a flow reactor process in comparison with batch production. For example, photochemical methods are best conducted with sufficient light penetration throughout the reactor volume, which is better accommodated by narrow diameter flow paths than by large volume batch reactors.[22–24] Additionally, reaction parameters such as temperature, pressure, and thermal management can be compartmentalized to small volumes at any given time within a flow reactor design, whereas the entirety of a batch reactor must be subjected to the requisite conditions.[25–31] We found light penetration, temperature control, and gas dissolution (e.g., conducting a reaction under nitrogen versus ambient air) to be particularly alluring features of flow chemistry when considering potential scale-up of photoredox-mediated metal-free ring-opening metathesis polymerization (MF-ROMP). At present, MF-ROMP is best conducted using photoredox catalysis, provides the

highest yields for common monomers only when performed at low temperatures, and is particularly sensitive to the composition and concentration of gases in the reaction solvent.[32–36]

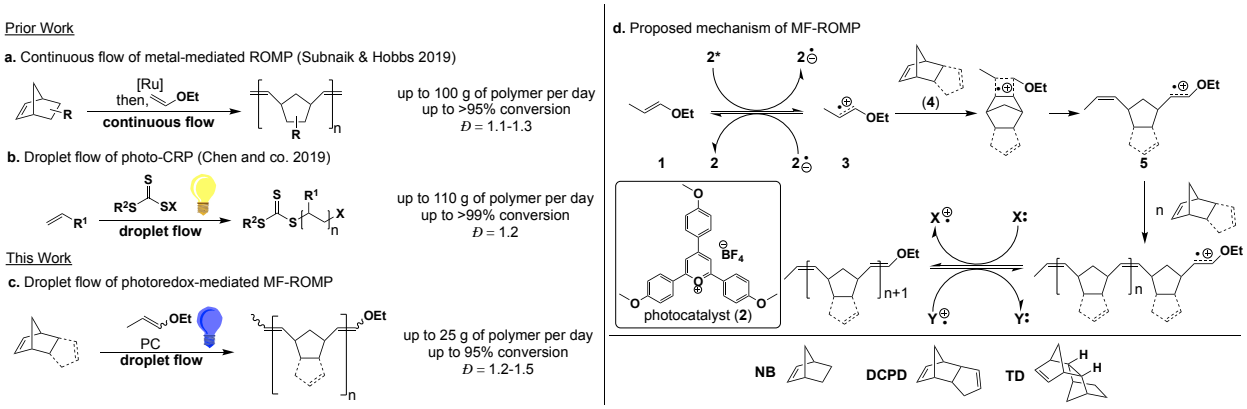

Figure 1. Supporting precedence for conducting MF-ROMP in a droplet flow setup. (a) The first literature example of metal-mediated ROMP in continuous flow.[12] (b) The first literature example of a photo-controlled radical polymerization (CRP) in droplet flow.[67] (c) This work. (d) Mechanism of MF-ROMP. X is the reduced pyryl radical or neutral enol ether; $Y^{\bullet+}$ is excited photocatalyst or oxidized enol ether. Evaluated monomers pictured on the bottom.

As presented in Figure 1d, MF-ROMP proceeds through a radical cationic polymerization pathway that uses organic monomers, initiators, and photocatalysts. The polymerization proceeds under ambient conditions and performs worse under atmospheres of entirely nitrogen or oxygen, based upon total monomer conversion.[33] In this polymerization pathway, the 2,4,6-tris(4-methoxyphenyl)pyrylium tetrafluoroborate photocatalyst (**2**) serves as a photooxidant to generate the radical cationic enol ether (**3**) from the ethyl-1-propenyl ether initiator (**1**). This radical cationic intermediate engages and opens the strained bicyclic intermediate (**4**) to produce a ring-opened olefin (**5**). This newly formed olefin maintains its radical cationic enol ether, which can go on to engage other monomer units to produce ROMP polymers. During this process, back-electron transfer from the reduced photocatalyst and degenerative electron transfer from neutral enol ethers are each envisioned, offering a photo-mediated, spatiotemporally controlled polymerization with living characteristics.[13] Also noteworthy, only highly-strained alkenes show conversion in MF-

ROMP leaving less strained alkenes intact, enabling access to valuable ROMP polymers that are typically difficult to produce via metal-mediated pathways, such as linear poly(dicyclopentadiene) (pDCPD).[37–44] MF-ROMP has been demonstrated to produce high-conversion linear pDCPD with the caveat of requiring low temperatures, which presents an opportunity for improvement with an appropriate flow process.

The scalability of linear pDCPD production and more generally of MF-ROMP, which is promoted by uniform irradiation and rapid cooling, would greatly benefit from the improved photophysics and heat transfer of flow chemistry relative to batch.[45–47] However, implementing MF-ROMP in flow has many of the obstacles associated with laboratory-scale flow reactors. Going from laboratory-scale batch photopolymerizations to laboratory-scale flow photopolymerizations is nontrivial, but there are well-defined parameters to consider when making the transition.[48–57] Mixing speed, irradiation setup, temperature control, reaction atmosphere, reactor size, and reaction time (among other things) must be considered in batch reactors. Similarly for flow reactors, flow rate, irradiation setup, temperature control, reactor pressure, tubing diameter, and residence time must be considered. Being at sub-industrial scales already creates further constraints and considerations for flow reactors. For transitioning MF-ROMP to a flow setup, we considered the benefits and limitations of both continuous and droplet flow reactor designs, which included quality of mixing, control over reaction atmosphere, and throughput of the reactor.

Continuous flow reactor designs are commonly used at research scales, and reagent quantities necessitate slower flow rates. These sub-industrial continuous flow reactors are typically limited to laminar flow, resulting in slow, diffusion-limited mixing within the reactor.[58–65] This is detrimental to photopolymerizations because light exposure is uneven across the flow reactor, leading to increased molecular weight dispersities, reduced initiation efficiencies, and reduced monomer conversions (Figure 2). Though these issues can be mitigated by decreasing the flow loop diameter to improve diffusive mixing, doing so can drastically raise the pressure of the flow system and increase the likelihood of clogging, especially in cases where the solution viscosity increases as the polymerization progresses. There is also limited air exposure in continuous flow which, after observing nontrivial effects of reaction atmosphere on MF-ROMP, we thought could affect catalyst turnover.[33] Based on these observations, we hypothesized that a droplet flow reactor could be an ideal setup for MF-ROMP.

Droplet flow—sometimes referred to as Taylor flow, segmented flow, or isolated plug flow—refers to a flow reactor setup where two immiscible fluids (such as liquid/liquid or liquid/gas) are driven through the same flow loop.[66–69] The two fluids travel through the loop as separate, alternating plugs causing each plug to circulate and mix within itself. In the case where one fluid is the reaction solution and the other fluid is a gas, the gas composition of the reaction solution can be maintained within the flow loop, thereby allowing one to probe the interaction of atmosphere with a reaction. For polymerizations, droplet flow setups have been shown to yield experimental results (like molecular weight dispersity, monomer conversion, and initiation efficiency) better than that of continuous flow setups and comparable to that of small-scale batch setups owing to more similar mixing dynamics to that of batch.[66,67] Droplet flow setups have also shown great compatibility with photo-controlled radical polymerizations (CRPs) (Figure 1b).[70,71]

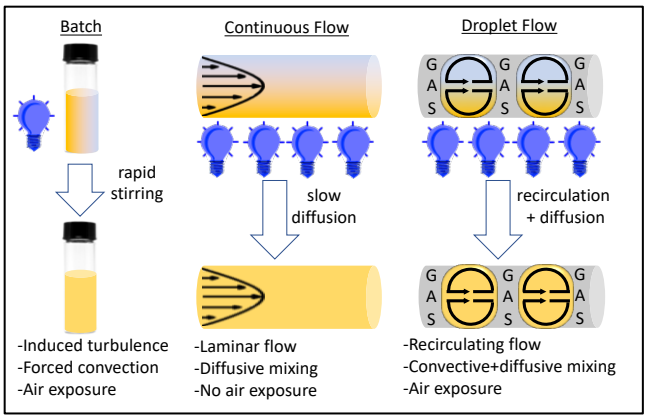

Figure 2. Comparison of batch, continuous flow (in the laminar flow regime), and droplet flow reactor setups when exposed to irradiation. Flow velocity profiles shown in black for continuous and droplet flow.

The droplet flow setup is more complex than its continuous flow counterpart. Pressure regulators, flow controllers, and other safety measures are essential to creating a safe, controlled droplet flow setup. Another feature intrinsic to droplet flow is a reduced active reactor volume relative to continuous flow since part of the reactor volume is taken up by gas pockets. Though not explicitly studied here, others have shown that decreasing the gas to liquid ratio can maintain the mixing benefits of droplet flow while increasing the amount of active reactor volume.[69] When the optimal reactor setup is droplet flow, the decreased active volume is compensated by increased quality of mixing translating to increased monomer conversion, increased initiator efficiency, and decreased dispersity relative to continuous flow. Based on our experience with MF-ROMP, droplet flow was viewed as a promising approach to outperform batch production methods. Herein, we report on laboratory-scale flow systems for MF-ROMP, which includes comparisons of continuous versus droplet flow designs, optimization of flow conditions, and demonstration of successful (co)polymerizations using commercially relevant monomers.

Results and Discussion

For our studies, we evaluated norbornene (NB) and dicyclopentadiene (DCPD) as representative monomers for MF-ROMP before evaluating tetracyclododecene (TD) in our optimized flow setup. Importantly, NB performs well at room temperature and with high rates of monomer conversion relative to other MF-ROMP monomers.[32,35] Therefore, NB is a good starting testbed for comparing flow reactor designs. DCPD requires more stringent reaction conditions in batch production, such as low temperature, which makes it an attractive target for vetting modifications to flow systems. MF-ROMP of TD is unreported and demonstrates the applicability of our optimized flow setup to other monomer systems.

We assembled a modular flow reactor ensemble (Figure 3) and evaluated 3 flow reactor configurations for each monomer system: (i) a continuous flow setup (CF) in which the reaction solution is pumped through the flow reactor; (ii) a droplet flow air setup (DF-Air) in which the reaction solution and dried air are pumped through the flow reactor; and (iii) a droplet flow nitrogen setup (DF-N_2) in which the reaction solution and dried nitrogen are pumped through the flow reactor. Within each flow setup the gas flow rate, liquid flow rate, temperature, and system pressure could be directly controlled. When surveying different reagent concentrations, we found that higher concentrations of monomer led to large changes in viscosity during polymerization, and that photocatalyst solubility was limited. Therefore, with our current designs we chose to study more dilute concentrations. We evaluated each monomer across the 3 different flow reactors to compare monomer conversion, product molecular weight, and polymer yield.

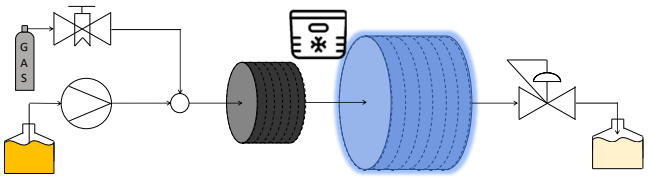

Figure 3. Flow Reactor Setup. The equipment shown on the scheme is: reagent solution storage vessel, liquid pump, gas supply, needle valve, tee joint, temperature equilibration zone, active irradiation zone, chiller, back pressure regulator, and product solution storage vessel.

As we began our investigations of flow systems, we first focused on CF as this design is comparatively simpler than DF. Although results with NB as monomer were initially encouraging (reaching 80% conversion), attempts to reach serviceable yields when using DCPD as monomer or comonomer (with NB) were met with limited success (Figure 4). We achieved only 37% conversion with DCPD alone (at 20 °C) and 45% conversion with a 1:1 feed ratio of NB and DCPD (at 20 °C). Much greater gains were found as we shifted focus to DF experiments, as described below.

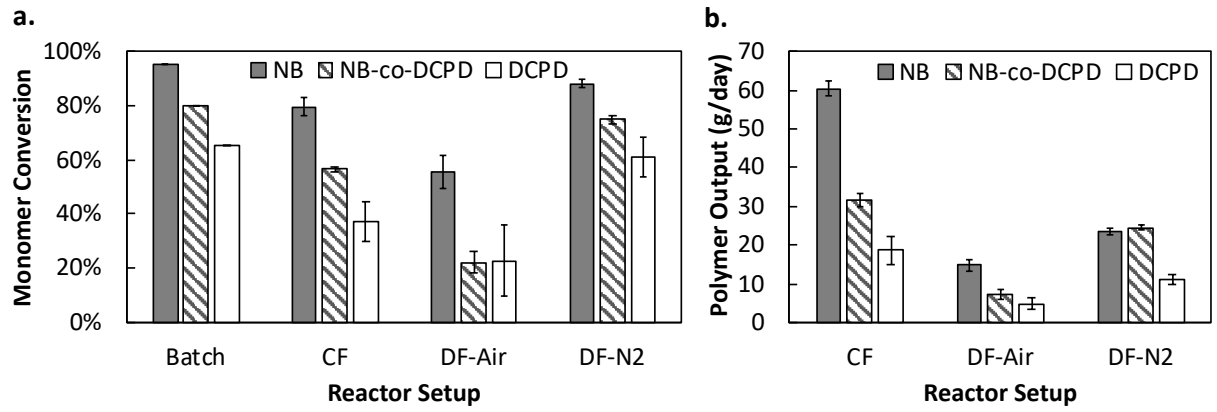

Figure 4. MF-ROMP Reactor Comparison: (a) Monomer conversion and (b) Equivalent polymer output. All values shown as average of 2 trials ± standard deviation. For the NB experiments (solid, gray)—NB:1:2 = 65:1:0.05; NB = 0.65 M; total flow rate for CF and DF = 0.9 mL/min; liquid flow rate for DF = 0.3 mL/min. For the DCPD experiments (solid, white)—DCPD:1:2 = 25:1:0.07; DCPD = 0.45 M; total flow rate for CF and DF = 0.6 mL/min; liquid flow rate for DF = 0.2 mL/min. For the NB-*co*-DCPD experiments (striped, gray)— NB:DCPD:1:2 = 25:25:1:0.07; [NB] = 0.3 M; total flow rate for CF and DF = 0.6 mL/min; liquid flow rate for DF = 0.2 mL/min.

The results from studying norbornene in DF as summarized in Figure 4, Figure 5, and elaborated in Table S3.1, revealed that using a backpressure regulator (BPR) with the DF-Air setup resulted in low monomer conversions and significant photobleaching for the reaction mixture, which we ascribed to decomposition of the pyrylium salt photocatalyst. Specifically, NB conversion dropped from 67% to 60% to 51% as BPR pressure increased from 5 to 20 to 40 PSI (Figure 5). In the absence of a BPR, monomer conversions varied broadly across experiments and the fickleness of the system precluded additional optimization. Lowering the temperature from room temperature to 0 °C at 40 PSI did not improve conversions when using the DF-Air setup (29% conversion, Table S3.1, entry 9). We observed color loss to a lesser extent after changing the gas from air to nitrogen, signifying less photocatalyst decomposition. Accordingly, monomer conversion also increased, reaching above 80% for the 5, 20, and 40 PSI BPR experiments. Across the different setups that used a BPR and N_2, no significant trends in conversion were observed when varying the BPR pressure. As mentioned previously, oxygen has a nontrivial effect on MF-ROMP, and presumably using BPRs to pressurize the system in our studies causes an increased O_2 concentration in the reaction solution, thereby causing an increased rate of photocatalyst decomposition. Decreasing solution temperature also increases dissolved O_2 concentration, and therefore the observations regarding monomer conversion, pressure, and temperature support the hypothesis that increasing dissolved O_2 concentration negatively affects the performance of these pressurized reactor setups. In general, when compared to continuous flow, droplet flow yielded better monomer conversions. The production of DF-N_2, as compared to continuous flow, was lower, as is expected when using the same total flow rate but about a one-third the solution flow rate.

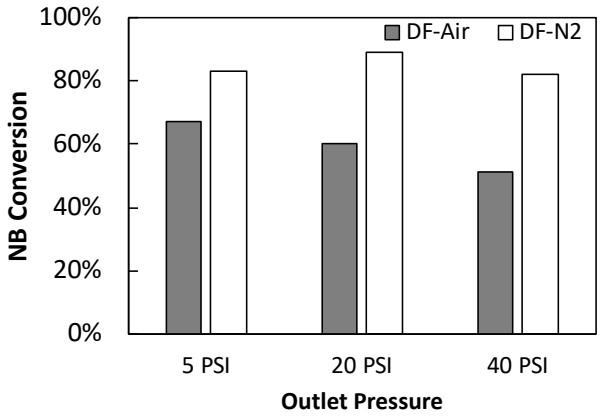

Figure 5. Droplet Flow Optimization: Gas, Pressure, and Temperature Trends. NB:1:2 = 65:1:0.05; [NB] = 0.65 M; total flowrate = 0.9 mL/min; liquid flow rate = 0.3 mL/min.

In the flow optimization of DCPD in Table S3.2, we noticed an influence of total flow rate on conversion. Figure S3.2 shows that an appropriate balance needs to be found between residence time and flow rate, which impacts mixing effects and reaction time. Batch control experiments corroborate the significant effects that mixing has on DCPD polymerization (Table S3.3). With DCPD, we found that higher flow rates, but shorter residence times were necessary for good conversions, observing 61% conversion for 0.56 mL/min total flow rate versus 34% and 50% conversion for 0.19 and 0.25 mL/min total flow rates, respectively (Table 1, entry 5; Table S3.2, entries 4 and 5). In flow experiments with DCPD performed in a cooled flow setup without a temperature equilibration zone, we observed low (< 30%) monomer conversions (Table S3.2, entry 2)), which we attribute to premature initiation of the polymerization before sufficient cooling.

After achieving successful polymerizations of both NB and DCPD, we extended our results to longer experiments, larger molecular weights, higher conversions, and different (co)polymerizations. By extending the flow parameters of the DCPD homopolymerization to the copolymerization of NB and DCPD, we achieved 68% conversion of DCPD, 83% conversion of NB, and 75% total monomer conversion at 20 °C (Table 1, entry 7; Table S3.4 entry 4). We were also able to maintain the DF-N_2 setup for 5 hours and achieved similar conversions to the 1-hour

experiments (82% for NB, 55% for DCPD, and 74% for NB-*co*-DCPD Table 1, entries 2, 6, and 8). With these 5-hour experiments, a slight drift in conversion was observed presumably due to increased moisture exposure of the storage vessel, which filled with air as reaction solution pumped through the reactor (see Figure S3.6). We then extended our optimized DF-N_2 conditions to increased loadings of NB, to increased conversions of NB, and to TD. For NB, we achieved 74% monomer conversion and reached a number average molecular weight of 19.3 kDa (notably above NB's entanglement molecular weight) at a polymer dispersity of 1.3 (Table 1, entry 3). We also lowered loadings of NB while increasing residence time to achieve 95% monomer conversion via DF-N_2 (Table 1, entry 4). For TD after adjusting solvent and reagent concentrations to accommodate pTD's solubility behavior, we achieved a similarly successful flow polymerization, reaching 74% monomer conversion at a projected output of 10 g/day of pTD (Table 1, entry 9).

Table 1. Summarized Results of MF-ROMP via DF-N_2

entry[a]	NB:DCPD:TD:1:2	residence time (min)	Conv[b] (%)	M_n[c] [kDa]	$Đ$	output[d] (g/day)
1	65:0:0:1:0.05	28	88 ± 1	8.1 ± 0.6	1.3 ± 0.0(4)	24 ± 1
2[e]	65:0:0:1:0.05	30	82	7.7	1.3	22
3	200:0:0:1:0.05	30	74	19.3	1.3	20
4	25:0:0:1:0.05	45	95	3.3	1.3	17
5[f]	0:25:0:1:0.07	45	61 ± 7	3.9 ± 0.7	1.3 ± 0.1	11 ± 1
6[e,f]	0:25:0:1:0.07	45	55	3.4	1.4	10
7[f]	25:25:0:1:0.07	45	75 ± 2	8.4 ± 1.0	1.4 ± 0.1	25 ± 1
8[e,f]	25:25:0:1:0.07	45	74	8.4	1.4	17
9[g]	0:0:25:1:0.07	50	74	5.8	1.5	10

[a]Run at room temperature during a 1-h experiment at a liquid flow of 0.2−0.3mL/min in a 25 mL active flow loop, unless otherwise noted. Values shown as an average of two trials ± standard deviation when applicable. [b]Monomer conversion determined from ^{1}H NMR spectroscopy. [c]Number-average molecular weights (M_n) determined by GPC equipped with multiangle light-scattering detector and a measured d*n*/dc, as described in the supporting information. [d]Projected polymer output calculated as described in the supporting information. [e]5-h experiment. [f]Run at −20°C. [g]Run in *ortho*-dichlorobenzene.

Conclusions

After finding suitable setups for the NB, DCPD, and NB-*co*-DCPD polymerizations with respect to flow rate, residence time, and temperature, we were able to compare the observed flow performance trends, as summarized in Figure 4 and Table 1. In all cases, we saw that the DF-N_2 setup performed the best in terms of monomer conversion, reaching up to 95% for NB, 61% for DCPD, and 75% for NB-*co*-DCPD. Regarding polymer output, the continuous flow setup tended to do well because of its larger liquid flow rate, but the DF-N_2 setup was competitive in terms of output for DCPD-containing polymers, reaching up to 24 g/day for pNB, 11 g/day for pDCPD, and 25 g/day for pNB-*co*-DCPD. We confirmed that these flow experiments could be conducted for 5 hours while maintaining similarly successful monomer conversions and polymer outputs. We also demonstrated that the DF-N_2 setup is compatible above the entanglement number-average molecular weight of NB, reaching 74% monomer conversion and achieving a number average molecular weight of 19.3 kDa and molecular weight dispersity of 1.3. Lastly, we then extended our optimized DF-N_2 conditions to TD where we achieved successful flow polymerization, reaching 74% monomer conversion at a projected output of 10 g/day of pTD.

We compared different flow setups for MF-ROMP using NB, DCPD, and TD monomer conversion as well as projected output as measurements of success. Through this process, we found that droplet flow configurations for MF-ROMP can translate results from small-scale batch experiments to flow processes. For polymerization of each monomer, droplet flow achieved higher conversion than continuous flow, which is attributed to better quality of mixing in the former. On the other hand, within the constraints of the current scale, continuous flow gave greater quantities of projected daily polymer output due to the higher liquid flow rate in comparison with droplet

flow. We found that lowering the reactive volume temperature was easily accommodated in flow, which offered benefits for MF-ROMP of DCPD. Similarly, solvent changes to enable MF-ROMP of TD were found to be straightforward. Moving forward, the reactor designs described herein can enable further scaleup of MF-ROMP while offering the operational and safety benefits of flow techniques for synthesis.

Appendix C: Chapter 4 Experimental Procedures and Supporting Information

1. General Information

1.1 Reagents

1.1.1 Materials and General Considerations. Dichloromethane, 1,2-dichloroethane (DCE), and orthodichlorobenzene (oDCB) were dried over 3Å molecular sieves prior to use. Tetrahydrofuran (THF) was obtained from an LC Technology solvent purification system. Norbornene (NB) was purchased from Sigma-Aldrich and sublimed prior to use. Dicyclopentadiene (DCPD) was purchased from Sigma-Aldrich as a 97:3 mixture of the *endo*:*exo* isomer and sublimed prior to use. Tetracyclododecene was provided by Promerus as a 95:5 mixture of the *endo-endo*:*endo-exo* isomer and used as is. 2,4,6-Tris(4-methoxyphenyl)pyrylium tetrafluoroborate (2) was prepared according to literature procedures with modifications. All other reagents and solvents were acquired from commercial sources and used without purification unless otherwise noted. All batch polymerizations were conducted in standard 2- dram borosilicate glass vials with PTFE-lined screw cap as purchased from Fisher Scientific. Irradiation of photoredox mediated ROMP was done in batch with 100 mW/cm^2 Norman Lamps MR16-4W blue LEDs (450 nm) and in flow with 20 mW/cm^2 Creative Lighting Solutions Blue Flexible LED Strips, 5M Spool-12vdc, Sapphire Blue (Figure S5.1). If cooling was needed, an EYELA PSL-2000 low temperature chiller with magnetic stirring was used with ethanol as the coolant.

1.1.2 Characterizations. ^{1}H NMR spectra were recorded on Bruker Avance III 400, 500, or 600 MHz spectrometers. Chemical shifts are reported in delta (δ) units, expressed in parts per million (ppm) downfield from tetramethylsilane using protio-solvent (residual) as internal standard ($CDCl_3$, δH = 7.26 ppm for ^{1}H NMR). Data are reported as chemical shift (δ). Gel permeation chromatography (GPC) was performed using the following setup: an Agilent Technologies Infinity Series II pump, either 2 or 3 inline columns, and Wyatt Technology miniDAWN light scattering (LS) and Optilab T-rEX refractive index (RI) detectors using THF as the mobile phase with a flow rate of 1 mL/min. The weight-average molecular weights were determined by the d*n*/d*c* value of polynorbornene in THF (0.1507 mL/g), polydicyclopentadiene in THF (0.1759 mL/g), 1:1 statistical copolymer of norbornene-*co*-dicyclopentadiene in THF (0.1632 mL/g), and polytetracyclododecene in THF (0.1668 mL/g). Values of each polymer's d*n*/d*c* were determined using Wyatt's ASTRA software assuming 100% mass recovery from the GPC columns.

1.2 Photocatalyst and Polymer Synthesis

1.2.1 2,4,6-Tris(4-methoxyphenyl)pyrylium tetrafluoroborate (2). 2 was prepared according to our previous procedure with minor modification.[13] To a 50 mL round bottom flask containing p-anisaldehyde (2.50 mL, 20.6 mmol, 1 eq) and p-acetylanisole (6.17 g, 41.2 mmol, 2 eq) was added BF3•Et_2O (6.28 mL, 50.9 mmol, 2.4 eq) dropwise over 5 min under nitrogen. The solution was heated in an oil bath set to 100 °C for 2 h. After cooling down, the reaction mixture was diluted with acetone (100 mL) and water (7.5 mL), and subsequently precipitated into diethyl ether (125 mL). The resulting suspension was filtered to give the crude product as a rust-colored solid. Recrystallization of the solids from hot acetone gave 2 as an orange powder (2.39 g, 4.91 mmol, 24% yield). Spectral data were consistent with reported values in literature.

1.2.2 Norbornene (NB) MF-ROMP Solution. To a 100 mL amber glass vial containing a magnetic stir bar and pyrylium (21.6 mg, 0.0445 mmol, 0.05 eq) were added norbornene (5.49 g, 58.3 mmol, 65 eq), and CH_2Cl_2 (90.0 mL, dried over 3Å molecular sieves) under air. The mixture was stirred at room temperature for 1 – 3 min until the pyrylium salt dissolved. Then initiator ethyl propenyl ether (100. µL, 0.903 mmol, 1 eq) was added via micro-syringe. The vial was mixed and then sealed with a PTFE-lined screw cap. This vial was then used to (i) take a 2 mL aliquot for a batch reaction irradiated in a sealed 2 mL glass vial (see reference [13] for more information efficient batch polymerizations of NB) or (ii) feed the flow reactor. Upon completion, aliquots were taken for analysis to determine monomer conversion and crude molecular weight by ^{1}H NMR spectroscopy and GPC, respectively. The results are shown in Table S3.1. When further purification was necessary, the polymer sample was then diluted with CH_2Cl_2 and passed through basic alumina to remove any remaining pyrylium. The filtrate was concentrated to approximately 20 mL and added into cold MeOH (100 mL, 3 ℃), which resulted in formation of a precipitate. The precipitate was collected by filtration, washed with MeOH, and dried under vacuum to give a white powder.

1.2.3 Dicyclopentadiene (DCPD) MF-ROMP Solution. To a 100 mL amber glass vial containing a magnetic stir bar and pyrylium (44.2 mg, 0.0909 mmol, 0.07 eq) were added dicyclopentadiene (4.55 g, 34.4 mmol, 25 eq), and CH_2Cl_2 (72.0 mL, dried over 3Å molecular sieves) under air. The mixture was stirred at room temperature for 1 – 3 min until the pyrylium salt dissolved. Then initiator ethyl propenyl ether (155 µL, 1.40 mmol, 1 eq) was added via micro-syringe. The vial was mixed and then sealed with a PTFE-lined screw cap. This vial was then used to (i) take a 2 mL aliquot for a batch reaction irradiated in a -20 °C sealed 2 mL glass vial (see reference [32] for more information efficient batch polymerizations of DCPD) or (ii) feed the flow reactor. Upon completion, aliquots were taken for analysis to determine monomer conversion and crude molecular weight by ^{1}H NMR spectroscopy and GPC, respectively. The results are shown in Tables S3.2 and S3.3. When further purification was necessary, the polymer sample was then diluted with CH_2Cl_2 and passed through basic alumina to remove any remaining pyrylium. The filtrate was concentrated to approximately 20 mL and added into cold MeOH (100 mL, 3 ℃), which resulted in formation of a precipitate. The precipitate was collected by filtration, washed with MeOH, and dried under vacuum to give a white powder.

1.2.4 Norbornene-*co*-Dicyclopentadiene MF-ROMP Solution. To a 100 mL amber glass vial containing a magnetic stir bar and pyrylium (31.2 mg, 0.0641 mmol, 0.07 eq) were added norbornene (2.22 g, 23.6 mmol, 25 eq), dicyclopentadiene (3.13 g, 23.6 mmol, 25 eq), and CH_2Cl_2 (68.0 mL, dried over 3Å molecular sieves) under air. The mixture was stirred at room temperature for 1 – 3 min until the pyrylium salt dissolved. Then initiator ethyl propenyl ether (105 µL, 0.948 mmol, 1 eq) was added via micro-syringe. The vial was mixed and then sealed with a PTFE-lined screw cap. This vial was then used to (i) take a 2 mL aliquot for a batch reaction irradiated in a -20 °C sealed 2 mL glass vial (see reference [32] for more information efficient batch polymerizations of NB-*co*-DCPD) or (ii) feed the flow reactor. Upon completion, aliquots were taken for analysis to determine monomer conversion and crude molecular weight by ^{1}H NMR spectroscopy and GPC, respectively. The results are shown in Table S3.4. When further purification was necessary, the polymer sample was then diluted with CH_2Cl_2 and passed through basic alumina to remove any remaining pyrylium. The filtrate was concentrated to approximately 20 mL and added into cold MeOH (100 mL, 3 ℃), which resulted in formation of a precipitate.

The precipitate was collected by filtration, washed with MeOH, and dried under vacuum to give a white powder.

1.2.5 Tetracyclododecene (TD) MF-ROMP Solution. To a 100 mL amber glass vial containing a magnetic stir bar and pyrylium (28.2 mg, 0.0580 mmol, 0.065 eq) were added tetracyclododecene (3.60 g, 22.5 mmol, 25 eq), and oDCB (86.0 mL, dried over 3Å molecular sieves) under air. The mixture was stirred at room temperature for 5 min. Then initiator ethyl propenyl ether (102 µL, 0.921 mmol, 1 eq) was added via micro-syringe. The vial was mixed and then sealed with a PTFE-lined screw cap. This vial was then used to (i) take a 2 mL aliquot for a batch reaction irradiated in a sealed 2 mL glass vial or (ii) feed the flow reactor. Upon completion, aliquots were taken for analysis to determine monomer conversion and crude molecular weight by ^{1}H NMR spectroscopy and GPC, respectively. The results are shown in Table S3.5. When further purification was necessary, the polymer sample was then diluted with CH_2Cl_2 and passed through basic alumina to remove any remaining pyrylium. The filtrate was concentrated to approximately 20 mL and added into cold MeOH (100 mL, 3 ℃), which resulted in formation of a precipitate. The precipitate was collected by filtration, washed with MeOH, and dried under vacuum to give a white powder.

1.3 Monomer and Polymer Analysis

All monomer conversions discussed in the main text and SI were determined via ^{1}H NMR and analyzed as follows. All projected outputs in the main text and SI were determined as described as follows.

1.3.1 Polymer Output Analysis

$$\textbf{Projected polymer output} = \left(\mathbf{1440}\frac{\mathbf{min}}{\mathbf{day}}\right)(\mathbf{10^{-3}}\frac{\mathbf{L}}{\mathbf{mL}}) * \boldsymbol{F_{liq}} * \sum[\boldsymbol{i}]_0 * \boldsymbol{X_i} * \boldsymbol{MW_i}$$

$\boldsymbol{F_{liq}}$ = liquid flow rate of reaction solution [mL/min]; $[\boldsymbol{i}]_0$ = initial concentration of monomer *i* [mol/L]; $\boldsymbol{X_i}$ = conversion of monomer *i*; $\boldsymbol{MW_i}$ = molecular weight of monomer *i* [g/mol].

Example calculations:

Table S1.3 Sample Values for Polymerization in Flow

NB:DCPD	[NB] (M)	monomer conversion (%)	liquid flow (mL/min)	total flow (mL/min)	projected polymer output (g/day)
24:25	0.33	75 total 68 DCPD 83 NB	0.3	0.55	25

$$\textbf{Projected polymer output} = \left(\mathbf{1440}\frac{\mathbf{min}}{\mathbf{day}}\right)\left(\mathbf{10^{-3}}\frac{\mathbf{L}}{\mathbf{mL}}\right)\left(\mathbf{0.3}\frac{\mathbf{mL}}{\mathbf{min}}\right) *$$
$$\left[\left(\mathbf{0.33}\frac{\mathbf{mol}}{\boldsymbol{L}}\right)(\mathbf{83\%})\left(\mathbf{94.2}\frac{\mathbf{g}}{\mathbf{mol}}\right) + \left(\frac{\mathbf{25}}{\mathbf{24}} * \mathbf{0.33}\frac{\mathbf{mol}}{\boldsymbol{L}}\right)(\mathbf{68\%})\left(\mathbf{132.2}\frac{\mathbf{g}}{\mathbf{mol}}\right)\right] = \mathbf{25}\frac{\mathbf{g}}{\mathbf{day}}$$

1.3.2 Norbornene conversion analysis.

The region X from 5.9-6.1 ppm (corresponding to 2 protons from the monomer) was compared to the region Y at 2.3-3.1 ppm (corresponding to 2 protons from the monomer and 2 protons from the polymer).

$$\textbf{NB conversion} = \frac{\textbf{area}_{\textbf{Y}} - \textbf{area}_{\textbf{X}}}{\textbf{area}_{\textbf{Y}}}$$

Example calculations:

$$\textbf{NB conversion} = \frac{(\mathbf{5.53}) - (\mathbf{1.00})}{(\mathbf{5.53})} = \mathbf{82\%}$$

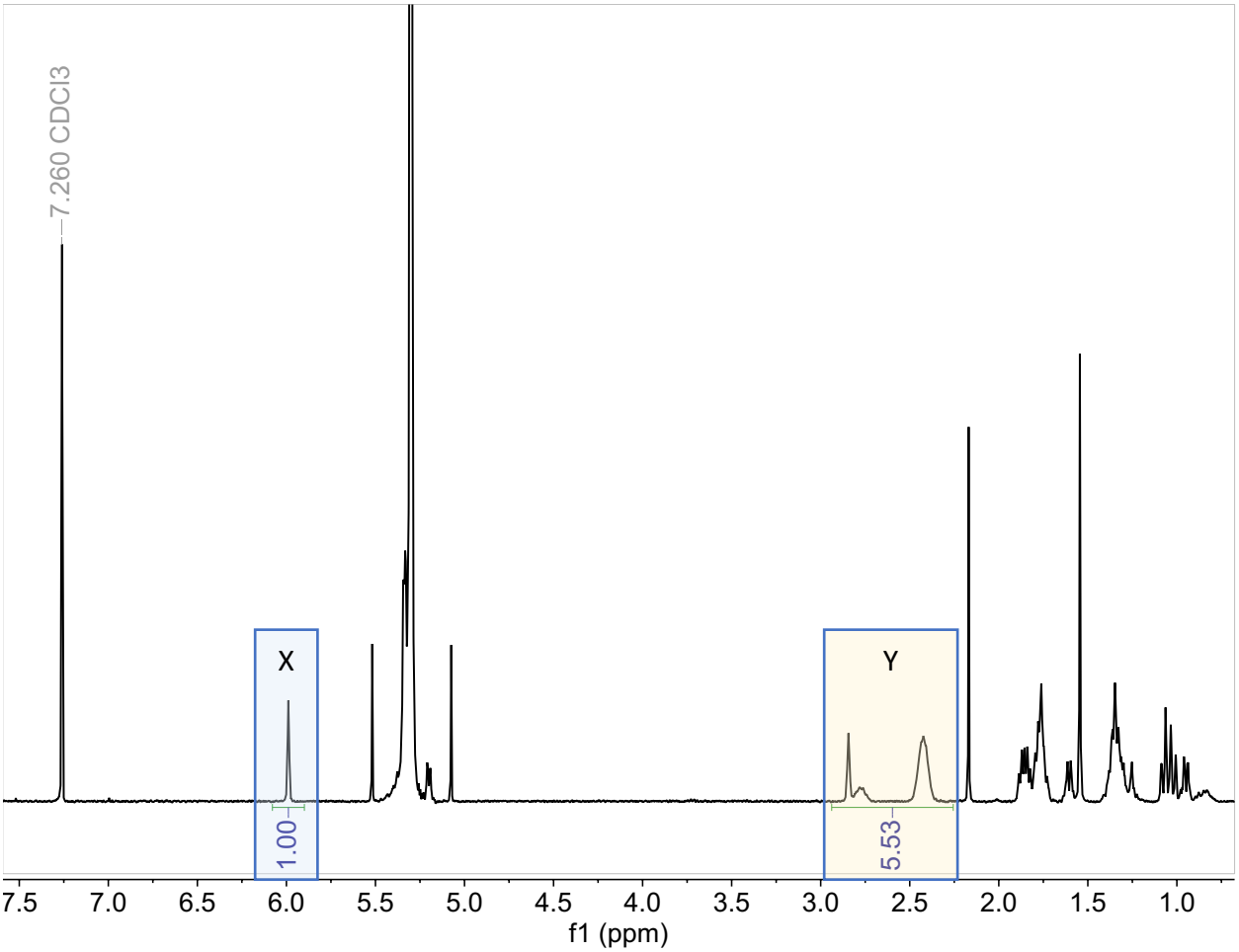

Figure S1.3.2. Crude pNB ^{1}H NMR for example calculation.

1.3.3 Dicyclopentadiene conversion analysis.

The region X from 5.8-6.1 ppm (corresponding to 2 protons from the monomer) was compared to the region Y at 5.6-5.8 ppm (corresponding to 1 proton from the polymer) and to region Z at 3.1-3.35 ppm (corresponding to 1 proton from the monomer and 1 proton from the polymer). Solvent signal can overlap with region Y, so the analysis method using only regions X and Z are most frequently used.

$$\textbf{DCPD conversion} = \frac{\textbf{area}_Z - \frac{1}{2}\textbf{area}_X}{\textbf{area}_Z} = \frac{\textbf{area}_Y}{\textbf{area}_Y + \frac{1}{2}\textbf{area}_X} = \frac{\textbf{area}_Y}{\textbf{area}_Z}$$

Example calculations:

$$\textbf{DCPD conversion} = \frac{(1.36) - \frac{1}{2}(1.00)}{(1.36)} = \frac{(0.86)}{(0.86) + \frac{1}{2}(1.00)} = \frac{(0.86)}{(1.36)} = 63\%$$

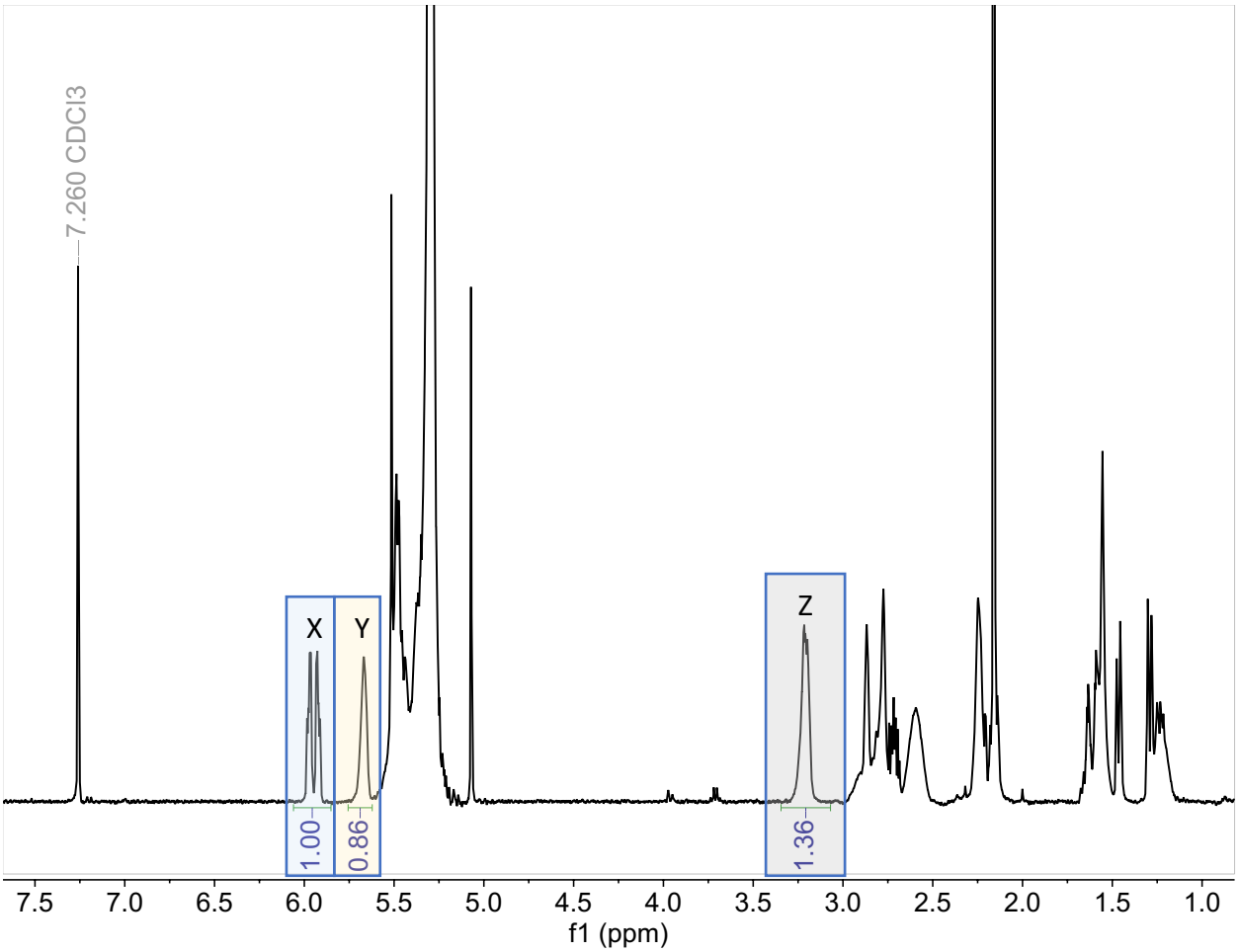

Figure S1.3.3. Crude pDCPD ^{1}H NMR for example calculation.

1.3.4 Norbornene-*co*-dicyclopentadiene conversion analysis.

The region V from 5.88-5.935 ppm (corresponding to 1 proton from DCPD) and region W from 5.935-6.02 ppm (corresponding to 1 proton from DCPD and 2 protons from NB) was compared to the region X at 5.6-5.8 ppm (corresponding to 1 proton from the polymeric DCPD), region Y at 3.1-3.35 ppm (corresponding to 1 proton from DCPD and 1 proton from the polymeric DCPD) and to region Z at 1.67-1.95 ppm (corresponding to 3 protons from the polymeric NB). Solvent signal can overlap with region Y, so the analysis method using only regions X and Z is most frequently used, and will be the only one shown for simplicity.

$$\mathbf{DCPD\ conversion} = \frac{\mathbf{area_Y} - \mathbf{area_V}}{\mathbf{area_Y}}$$

$$\mathbf{NB\ conversion} = \frac{\frac{\mathbf{1}}{\mathbf{3}}\mathbf{area_Z}}{\frac{\mathbf{1}}{\mathbf{3}}\mathbf{area_Z} + \frac{\mathbf{1}}{\mathbf{2}}[\mathbf{area_W} - \mathbf{area_V}]}$$

$$\mathbf{Total\ conversion} = (\mathbf{mol\ \%\ of\ feed\ NB}) * (\mathbf{NB\ conv}) + (\mathbf{mol\ \%\ of\ feed\ DCPD}) * (\mathbf{DCPD\ conv}) = \frac{\frac{\mathbf{1}}{\mathbf{3}}\mathbf{area_Z} + \mathbf{area_Y} - \mathbf{area_V}}{\frac{\mathbf{1}}{\mathbf{3}}\mathbf{area_Z} + \frac{\mathbf{1}}{\mathbf{2}}[\mathbf{area_W} - \mathbf{area_V}] + \mathbf{area_Y}}$$

Example calculations:

$$\mathbf{DCPD\ conversion} = \frac{(\mathbf{3.53}) - (\mathbf{1.00})}{(\mathbf{3.53})} = \mathbf{72\%}$$

$$\mathbf{NB\ conversion} = \frac{\frac{\mathbf{1}}{\mathbf{3}}(\mathbf{9.76})}{\frac{\mathbf{1}}{\mathbf{3}}(\mathbf{9.76}) + \frac{\mathbf{1}}{\mathbf{2}}[(\mathbf{1.65}) - (\mathbf{1.00})]} = \mathbf{91\%}$$

$$\mathbf{Total\ conversion} = (\mathbf{50\%}) * (\mathbf{91\%}) + (\mathbf{50\%}) * (\mathbf{72\%}) = \frac{\frac{\mathbf{1}}{\mathbf{3}}(\mathbf{9.76}) + (\mathbf{3.53}) - (\mathbf{1.00})}{\frac{\mathbf{1}}{\mathbf{3}}(\mathbf{9.76}) + \frac{\mathbf{1}}{\mathbf{2}}[(\mathbf{1.65}) - (\mathbf{1.00})] + (\mathbf{3.53})} = \mathbf{81\%}$$

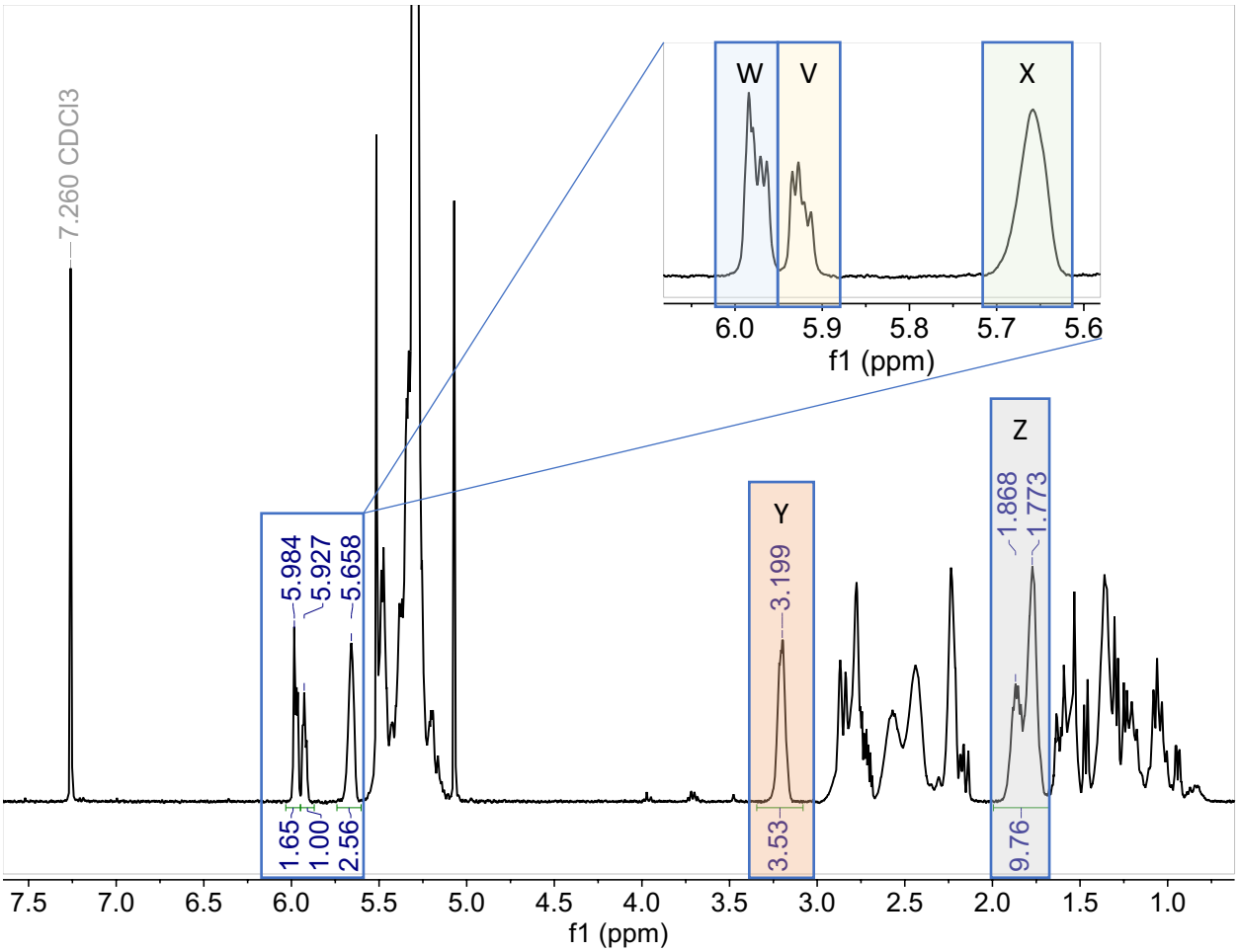

Figure S1.3.4. Crude pNB-*co*-DCPD ^{1}H NMR for example calculation.

1.3.5 Tetracyclododecene conversion analysis.

The region X from 5.85-6.15 ppm (corresponding to 2 protons from TD) was compared to the region Y from 5.25-5.70 ppm (corresponding to 2 protons from TD and 2 protons from pTD) or region Z at 2.60-3.20 ppm (corresponding to 2 protons from pTD **and 2 protons from pTD)**. Solvent signal can overlap with region Y, so the analysis method using only regions X and Z are most frequently used.

$$\textbf{TD conversion} = \frac{\textbf{area}_\textbf{Z} - \textbf{area}_\textbf{X}}{\textbf{area}_\textbf{Z}} = \frac{\textbf{area}_\textbf{Y} - \textbf{area}_\textbf{X}}{\textbf{area}_\textbf{Y}}$$

Example calculations:

$$\textbf{TD conversion} = \frac{(\mathbf{10.31}) - (\mathbf{1.00})}{(\mathbf{10.31})} = \frac{(\mathbf{10.37}) - (\mathbf{1.00})}{(\mathbf{10.37})} = \mathbf{90\%}$$

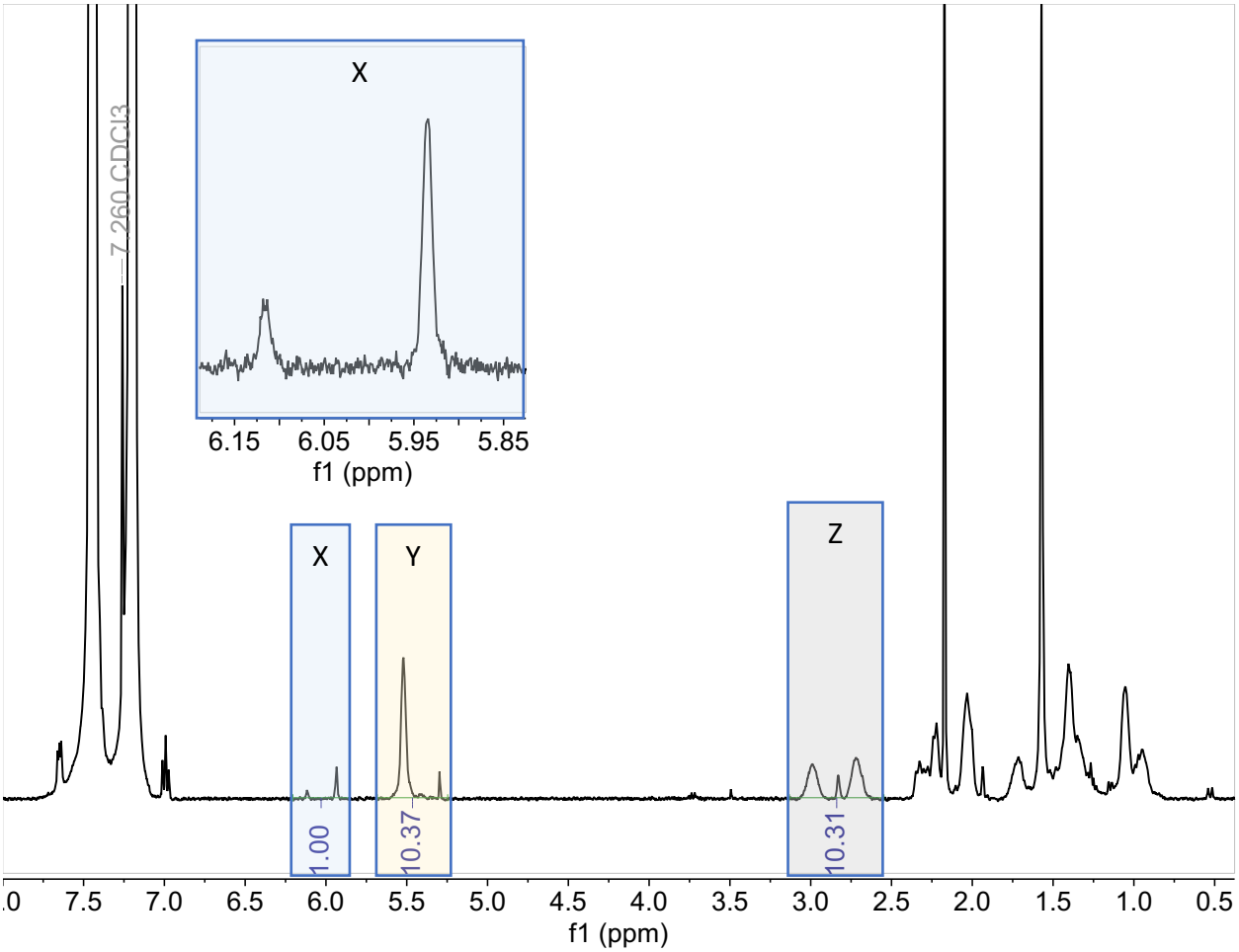

Figure S1.3.5. Crude pTD ^{1}H NMR for example calculation.

2. Flow Methodology

2.1 Flow Equipment

A: IDEX Micro Metering Valve Assembly for 1/16" OD With Fittings (P-445)
B: IDEX PFA Tubing Natural 1/8" OD x 1/16" ID x 50ft (P1507L); 25 mL internal volume for active flow loop (B1), 5 mL internal volume for temperature equilibration zone (B2)
C: Agilent Quaternary HPLC Pump (G7111b)
D: EYELA PSL-2000 low temperature chiller with magnetic stirring
E: Creative Lighting Solutions Blue Flexible LED Strips, 5M Spool-12vdc, Sapphire Blue
F: IDEX Back pressure regulators: 5 PSI, 20 PSI, 40 PSI (P-790, P-791, U-605)
G: W.A. Hammond Drierite Gas Drying Unit with Hose Barbs
H: Gas supply (N_2 cylinder, house air)
I: IDEX PEEK Low Pressure Tee Assembly 1/16" PEEK .020 thru hole (P-712)
J: Victor Model VTS250C Medium Duty Two Stage Regulator
K: 20 um pump filter
L: Opaque plastic housing used for temperature equilibration zone

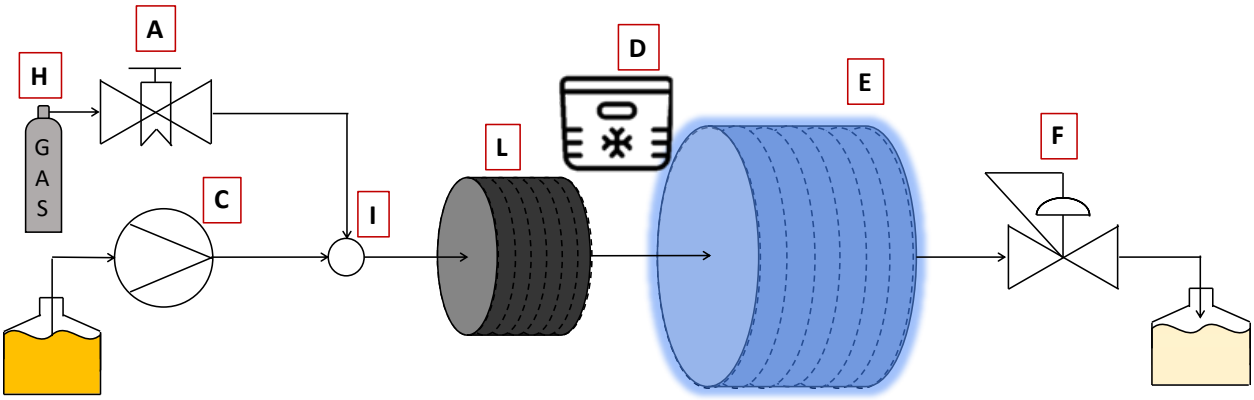

Figure S2.1. Labeled scheme of flow reactor setup. In the following images of the flow reactor setup, temperature equilibration loop L and active flow loop E are shown out of chiller D for clarity, but during flow experiments, L and E are submerged in the chiller.

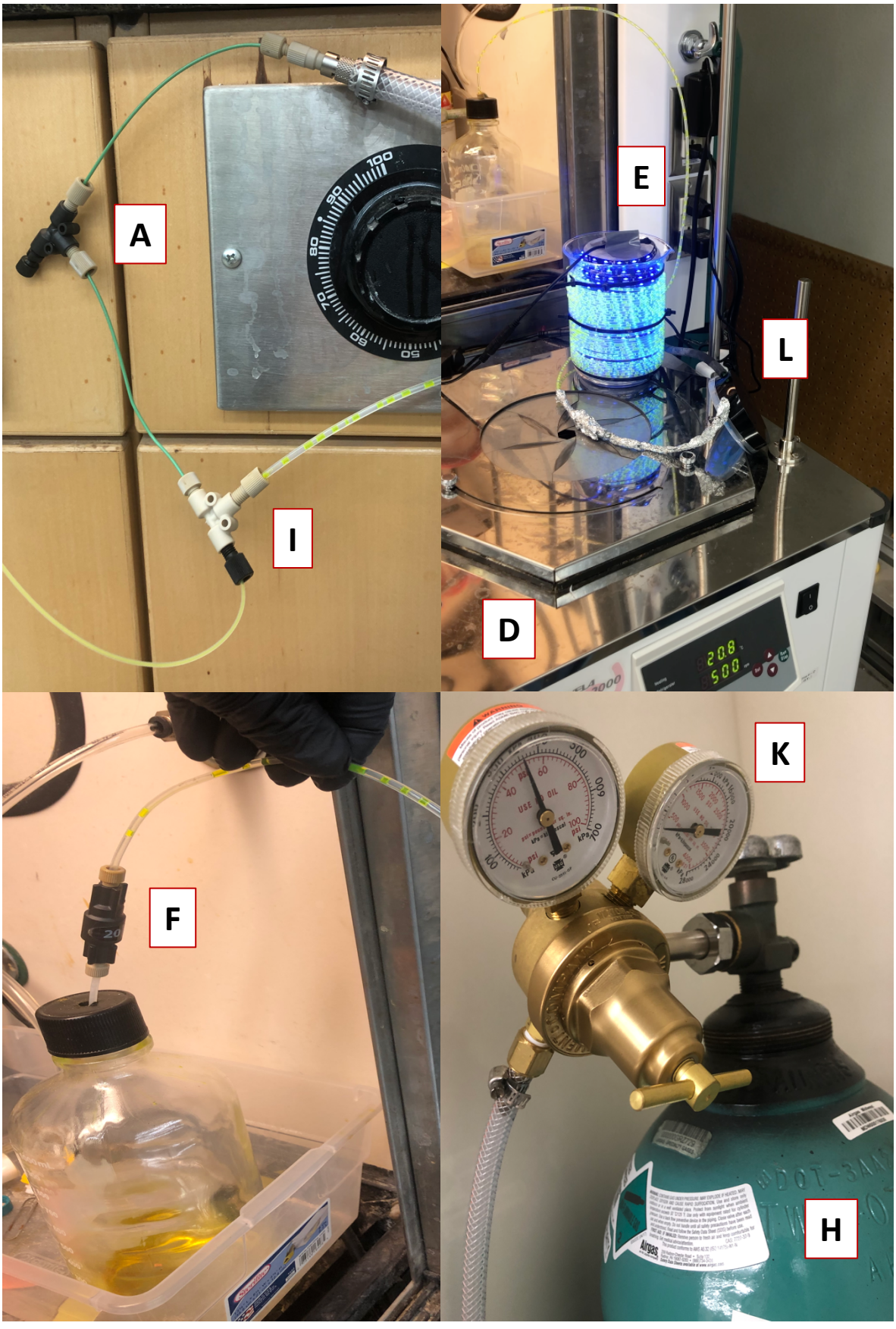
A
I
E
L
D
F
K
H

2.2 Flow Experiments

The chiller was turned on, set to the desired temperature, and allowed to thermally equilibrate. The magnetic stirring on the chiller was set to 500 RPM. The LEDs were switched on. The pump inlet was inserted into the reaction solution prepared in section 1.2. The liquid flow rate was then set to the desired liquid flow rate and allowed to equilibrate. The gas flow rate was then gradually increased to the desired value by visually comparing the liquid slug volume to gas slug volume. The residence time was measured by timing how long it took for the first slug to enter and leave the active flow loop; measured slug velocity was consistent with the measured residence time.

2.3 General Comments and Suggestions

Before entering the irradiated flow loop, there is an opaque section of tubing which allows for temperature equilibration when the reaction requires cooling. The temperature equilibration zone was essential for any polymerizations using DCPD. Additionally, the LEDs generated a significant amount of heat, making the chiller necessary for DCPD polymerizations. A dual stage gas regulator was found to provide a more steady source of pressure as opposed to a single stage gas regulator. Without a back pressure regulator, we observed unsteady flow and solvent evaporation within the tubing. The pump requires time to equilibrate after adding the gas stream. When working with droplet flow, note that changes in temperature (from cooling or from reaction thermodynamics) can affect the gas and total flow rate. At higher monomer and photocatalyst concentrations, be aware that the pyrylium can be insoluble and that there can be large changes in solution viscosity. When clogging was observed, it occurred at the BPR, which has a small ID. When we worked at higher monomer concentrations without a BPR in a DF-Air setup, we saw improved conversions relative to continuous flow, indicating that (i) droplet flow still provides improvement relative to continuous flow even at higher concentrations, and (ii) DF-Air setups can still be viable at lower pressures of O_2 (compare Table S3.1 entries 2 and 12). DCPD can be used without sublimation, but the results showed inconsistency in conversion across trials. DCPD polymerization shows greater sensitivity towards changes in temperature, humidity, and reactor design when compared to NB polymerization. Any discrepancies between batch conversions and flow conversions we attribute to a worse mixing quality and a reduced photocatalyst concentration due to the pump filter.

3. Extended Polymerization Data

For the following section contained in supplementary section 3, $\boldsymbol{\tau}$ = residence time; M_n = number average molecular of polymer as determined by GPC equipped with multiangle light-scattering detector and a measured dn/dc; $Đ$ = polymer molecular weight dispersity as determined by GPC equipped with multiangle light-scattering detector and a measured dn/dc; “2mL batch” refers to a 2 mL batch reactor setup as described in SI section 1.2; “1h CF” refers to a continuous flow setup run for 1 hour as described in section 2.2; “1h DF-Air” refers to a droplet flow air setup run for 1 hour as described in section 2.2; “1h DF-N_2” refers to a droplet flow N_2 setup run for 1 hour as described in section 2.2; “5h DF-N_2” refers to a droplet flow N_2 setup run for 5 hours as described in section 2.2.

3.1 NB Flow Experiments

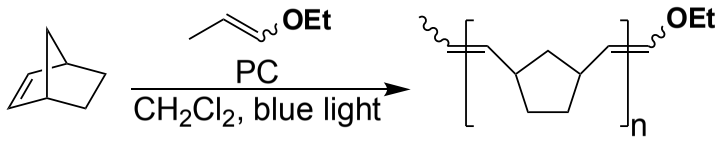

Table S3.1 NB Flow Reactor Results

entry[a]	NB:1:2	[NB] (M)	NB conversion (%)	τ (min)	liquid flow (mL/min)	total flow (mL/min)	reactor setup	BPR Pressure (PSI)	M_n [kDa]	$Đ$	projected polymer output (g/day)
1	65:1:0.050	0.66	95	20	n. a.	n. a.	2mL batch	n. a.	7.8	1.4	--
2	63:1:0.050	1.39	91	22	0.3	1.1	1h DF-Air	No BPR	7.6	1.4	51
3[b]	65:1:0.047	0.66	91	20	0.3	1.3	1h DF-Air	No BPR	n.m.	n.m.	24
4[b]	65:1:0.053	0.66	78	22	0.3	1.1	1h DF-N2	No BPR	n.m.	n.m.	21
5	65:1:0.050	0.65	67	30	0.3	0.8	1h DF-Air	5	5.7	1.4	18
6	63:1:0.051	0.64	83	35	0.3	0.7	1h DF-N2	5	6.5	1.2	22
7	65:1:0.050	0.66	56 ± 6	27	0.3	0.9	1h DF-Air	20	4.0 ± 1.2	1.5 ± 0.1	15 ± 2
8	65:1:0.050	0.66	88 ± 1	28	0.3	0.8	1h DF-N2	20	8.1 ± 0.6	1.3 ± 0.0(4)	24 ± 1
9[c]	63:1:0.051	0.64	29	25	0.5	1.0	1h DF-Air	40	n.m.	n.m.	12
10	63:1:0.050	1.37	51	20	0.3	1.3	1h DF-Air	40	n.m.	n.m.	28
11	63:1:0.051	0.65	82	30	0.5	0.8	1h DF-N2	40	4.7	1.3	36
12	63:1:0.05	0.66	80 ± 4	29	0.85	0.85	1h CF	20	8.3 ± 0.5	1.5 ± 0.1	61 ± 2
13	65:1:0.05	0.65	82	30	0.3	0.8	5h DF-N2	20	7.7	1.3	22
14	200:1:0.05	0.65	74	30	0.3	0.8	1h DF-N2	20	19	1.3	20
15	25:1:0.05	0.44	95	45	0.3	0.55	1h DF-N2	20	3.3	1.3	17

a: Run at room temperature in 25 mL flow loop with temperature equilibration zone unless otherwise stated. b: Unsteady flow observed.
c: Run at 0 °C. n.m. = not measured.

3.2 DCPD Flow Experiments

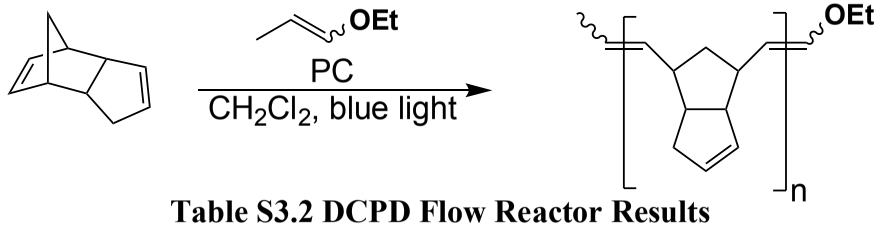

Table S3.2 DCPD Flow Reactor Results

entry	DCPD:1:2	[DCPD] (M)	DCPD conv (%)	τ (min)	liquid flow (mL/min)	total flow (mL/min)	reactor setup	BPR pressure (PSI)	M_n [kDa]	$Đ$	polymer output (g/day)
1	25:1:0.07	0.45	65	50	n. a.	n. a.	2mL batch	--	n.m.	n.m.	--
2[a]	25:1:0.03	0.27	23	30	0.1	0.4	1h DF-Air	No BPR	n.m.	n.m.	1
3	25:1:0.07	0.45	23 ± 13	45	0.2	0.6	1h DF-Air	20	n.m.	n.m.	5 ± 2
4	25:1:0.07	0.45	50	135	0.1	0.19	1h DF-N2	20	n.m.	n.m.	4
5	25:1:0.06	0.44	34	100	0.1	0.25	1h DF-N2	20	n.m.	n.m.	3
6	25:1:0.07	0.46	61 ± 7	45	0.2	0.56	1h DF-N2	20	3.9 ± 0.7	1.3 ± 0.1	11 ± 1
7	25:1:0.07	0.45	37 ± 7	125	0.2	0.2	1h CF	20	n.m.	n.m.	19 ± 4
8	25:1:0.07	0.45	32	45	0.55	0.55	1h CF	20	n.m.	n.m.	15
9	25:1:0.07	0.45	55	45	0.2	0.6	5h DF-N2	20	3.4	1.4	9

n. m. = not measured. All flow reactions run at -20 °C in 25 mL loop with temperature equilibration zone unless otherwise noted. a: Run in 15 mL flow loop without temperature equilibration zone.

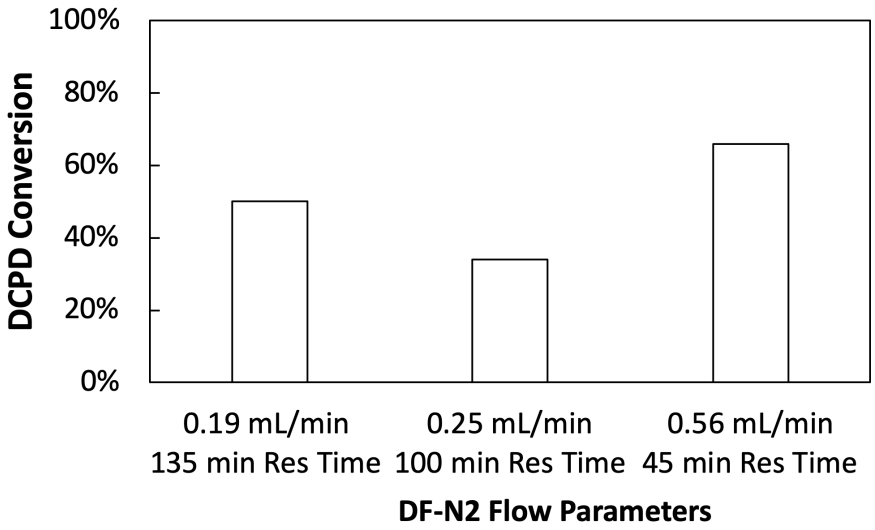

Figure S3.2. Flow rate versus residence time for MF-ROMP of DCPD in DF-N_2. Uses entries 4, 5, and 6 from Table S3.2.

3.3 DCPD Control Experiments

In batch controls of DCPD we found that the quality of mixing greatly affected monomer conversion. Specifically, monomer conversion dropped from 75% to 39% when stirring was not conducted (cf. Table S3.3, entries 1 and 2). Stirring, but in a reaction vial that had no headspace, also resulted in significant reduction in conversion (21%, entry 3). These results suggest that mixing is necessary for successful polymerization of DCPD, most likely due to a combination of uneven photoinitiation, decreased effective monomer concentration around the propagating species, and decreased heat transfer in an unmixed sample. Experiments where DCE was used as solvent instead of CH_2Cl_2, different monomer concentrations were used, and different monomer:initiator loadings were used all showed similar trends, supporting the hypothesis that mixing and potentially air exposure plays a role in polymer conversion. Using ultrasonication instead of mechanical mixing method did not lead to improved conversions.

Table S3.3 DCPD Batch Reactor Controls

entry[a]	DCPD:1:2	[DCPD] (M)	DCPD conversion	mixing method	headspace
1[b]	10:1:0.02	0.45	43 %	none	air
2[b,d]	13:1:0.02	0.58	47 %	sonication	air
3	10:1:0.02	0.45	52 %	none	air
4	25:1:0.03	0.68	39 %	none	air
5[c]	27:1:0.03	0.64	34 %	none	air
6[d]	13:1:0.02	0.58	57 %	sonication	air
7	10:1:0.02	0.34	22 %	stir bar	none
8	25:1:0.03	0.68	21 %	stir bar	none
9[c]	27:1:0.03	0.64	29 %	stir bar	none
10[d]	13:1:0.02	0.58	28 %	sonication	none
11[e]	17:1:0.024	0.70	83 %	stir bar	N_2
12	10:1:0.02	0.45	89 %	stir bar	air
13[e]	17:1:0.024	0.70	80 %	stir bar	air
14	25:1:0.03	0.68	75 %	stir bar	air
15[c]	27:1:0.03	0.64	58 %	stir bar	air

a: Run for 60 minutes at -20 °C unless otherwise noted. b: Run stationary in flow loop. c: DCE as solvent. d: Run at 3 °C. e: Run for 75 minutes.

3.4 NB-*co*-DCPD Flow Experiments

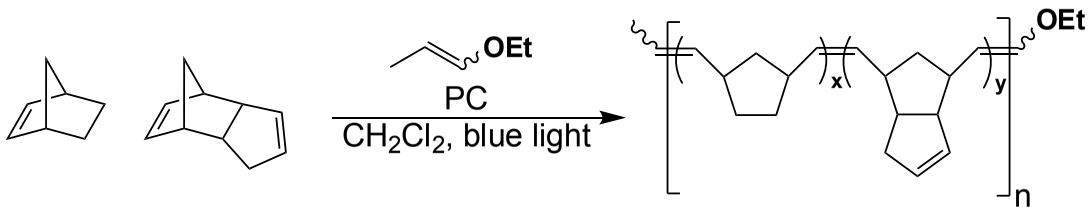

Table S3.4 NB-*co*-DCPD Flow Reactor Results

entry	NB:DCPD:1:2	[NB] (M)	monomer conversion (%)	τ (min)	liquid flow (mL/min)	total flow (mL/min)	reactor setup	BPR Pressure (PSI)	M_n [kDa]	$Đ$	projected polymer output (g/day)
1	27:25:1:0.06	0.27	80 total 69 DCPD 89 NB	50	n. a.	n. a.	2mL batch	n. a.	8.1	1.5	--
2	25:25:1:0.07	0.33	22 ± 4 total 20 ± 2 DCPD 25 ± 6 NB	45	0.3	0.55	1h DF-Air	20	6.5	1.5	7 ± 3
3	25:25:1:0.07	0.33	54 total 45 DCPD 64 NB	29	0.85	0.85	1h CF	20	6.5	1.5	48
4	24:25:1:0.07	0.33	75 ± 2 total 68 ± 3 DCPD 83 ± 5 NB	45	0.3	0.55	1h DF-N2	20	8.4 ± 1.0	1.4 ± 0.1	25 ± 1
5	26:25:1:0.07	0.32	57 ± 1 total 53 ± 0 DCPD 60 ± 0 NB	45	0.55	0.55	1h CF	20	7.3 ± 0.1	1.5 ± 0.0	32 ± 2
6	25:25:1:0.07	0.33	74 total 70 DCPD 78 NB	45	0.2	0.55	5h DF-N2	20	8.4	1.4	16

Run at -20 °C in 25 mL flow loop with temperature equilibration zone unless otherwise stated. n. m. = not measured

3.5 TCD Flow Experiments

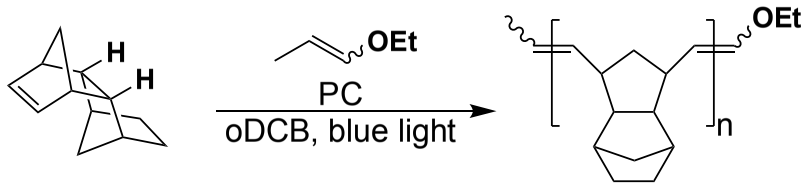

Table S3.5 TD Flow Reactor Results

entry	TD:1:2	[TD] (M)	Conv (%)	τ (min)	liquid flow (mL/min)	total flow (mL/min)	reactor setup	BPR pressure (PSI)	M_n [kDa]	$Đ$	projected polymer output (g/day)
1	25:1:0.07	0.3	90	60	n.a.	n.a.	2mL batch	--	n.m.	n.m.	--
2	25:1:0.07	0.3	74	50	0.2	0.55	1h DF-N2	20	5.8	1.5	10

Run at room temperature in 25 mL flow loop with temperature equilibration zone unless otherwise stated. n. m. = not measured.

3.6 Five-hour droplet flow experiments

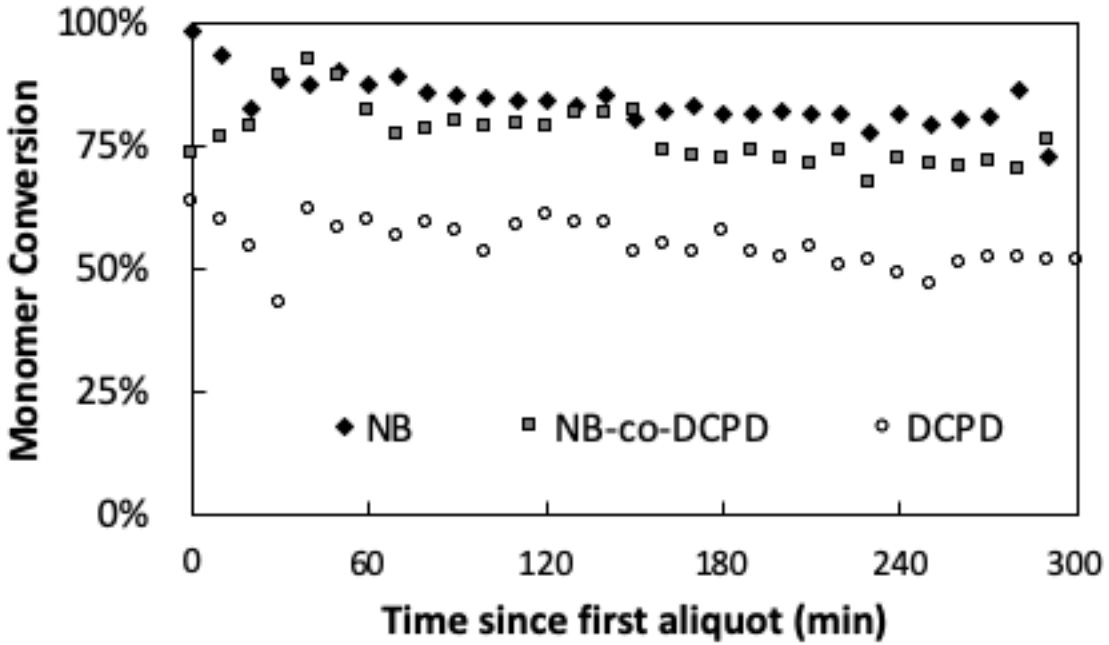

Figure S3.6. 5-hour Droplet Flow N_2 Experiments. NB conversion during homopolymerization (black diamond), DCPD conversion during homopolymerization (white circle), total monomer conversion during 1:1 NB:DCPD copolymerization. For reaction conditions, see Table S3.1, entry 13; Table S3.2, entry 9; Table S3.4, entry 6.

4. Additional Oxygen Experiments and Commentary

The following experiments were conducted to explore the role of oxygen in batch MF-ROMP. A FireSting GO_2 sensor in reaction solution was used to measure the solution's oxygen depletion in sealed batch experiments. The measured dissolved O_2 concentration drops linearly and rapidly within the first few minutes of polymerization before becoming completely consumed. Monomer conversion and initiator conversion do not seem to be impacted by the O_2 concentration before and after consumption. The O_2 concentration does not regenerate while irradiation occurs (see Figure S4.1). The rate of O_2 consumption was also linearly correlated with the intensity of incident light (see Figure S4.2). In control experiments that used photocatalyst and monomer without initiator, oxygen consumption was significantly slower. We also notice significant catalyst photobleaching of during polymerization. These data suggest O_2 is reacting when the radical cationic pathway is active, perhaps in a deleterious pathway with the reduced photocatalyst.

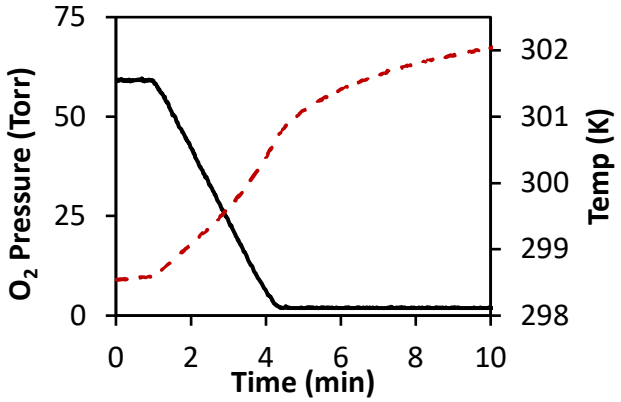

Figure S4.1. Dissolved oxygen consumption in MF-ROMP. NB:**1**:**2** = 30:1:0.05 at [NB] = 0.6 M in CH_2Cl_2 at room temperature. Irradiated from t = 1–10 min with blue LED. Solid, black trace shows dissolved O_2 concentration in Torr; dotted red trace shows temperature increase over the course of reaction.

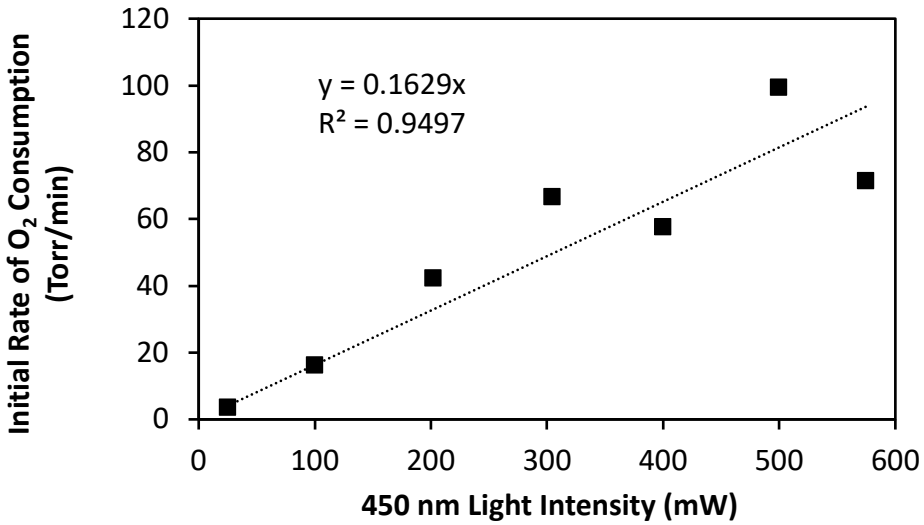

Figure S4.2. Initial oxygen consumption rates in MF-ROMP at different 450 nm light intensities. NB:**1**:**2** = 0:1:0.05 at [**1**] = 0.1 mM in CH_2Cl_2 at room temperature.

5. LED Emission Spectra, NMR Spectra, and GPC Traces

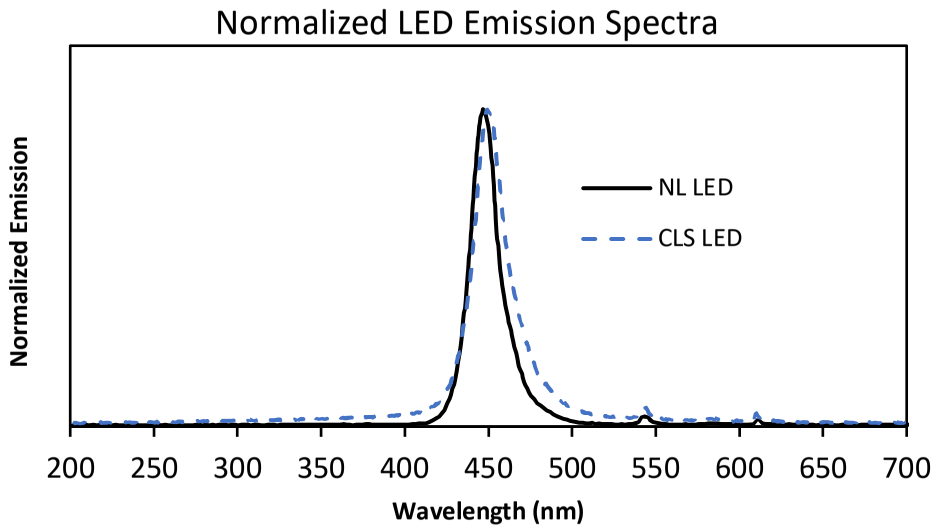

Figure S5.1. Normalized LED emission spectra of Norman Lamps LED (solid, black) and Creative Lighting Solutions LED (dotted, blue). Taken using Ocean Optics FLAME-S-XR1 Extended Range Spectrometer Assembly. The light intensity of the Norman Lamps LED was measured to be 100 mW/cm^2 at 455 nm. The light intensity of the Creative Lighting Solutions LED was measured to be 20 mW/cm^2 at 455 nm. Light intensities were measured with a G&R Labs Model 100 UV Light Meter with a 455 nm probe.

^{1}H NMR of 2,4,6-Tris(4-methoxyphenyl)pyrylium tetrafluoroborate (**2**) in d6-DMSO

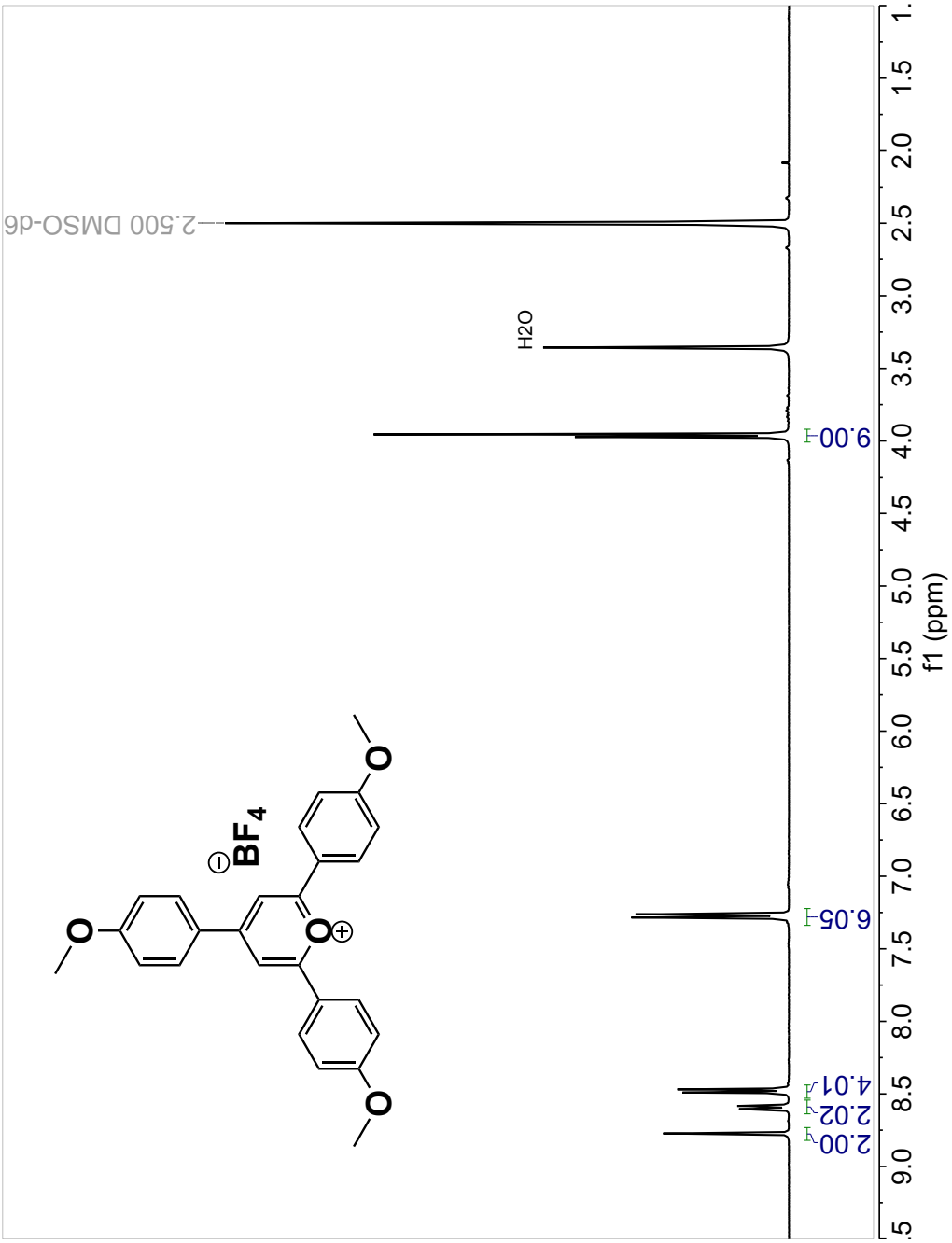

^{1}H NMR of ethyl propenyl ether (**1**) in $CDCl_3$

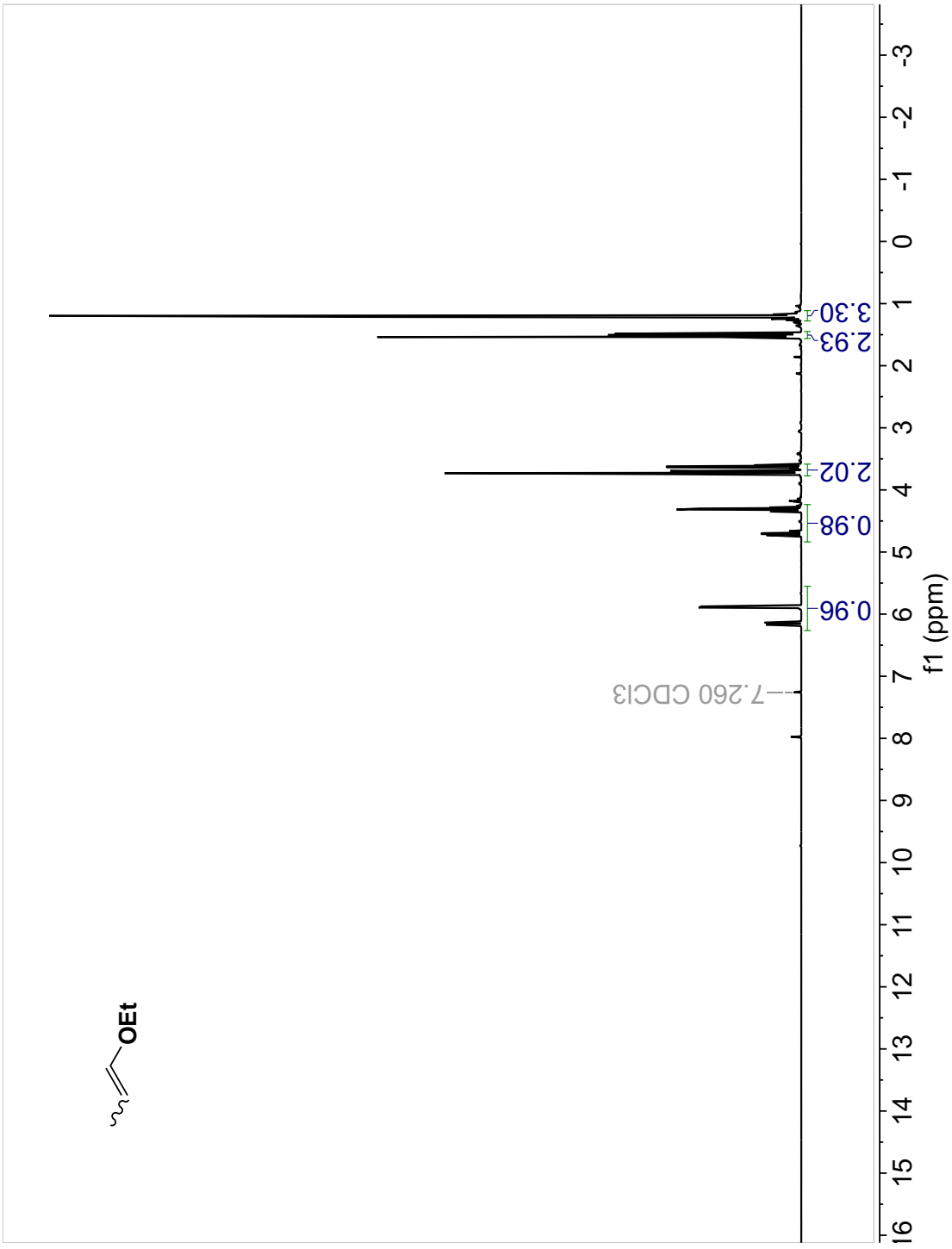

^{1}H NMR of Norbornene (NB) in $CDCl_3$

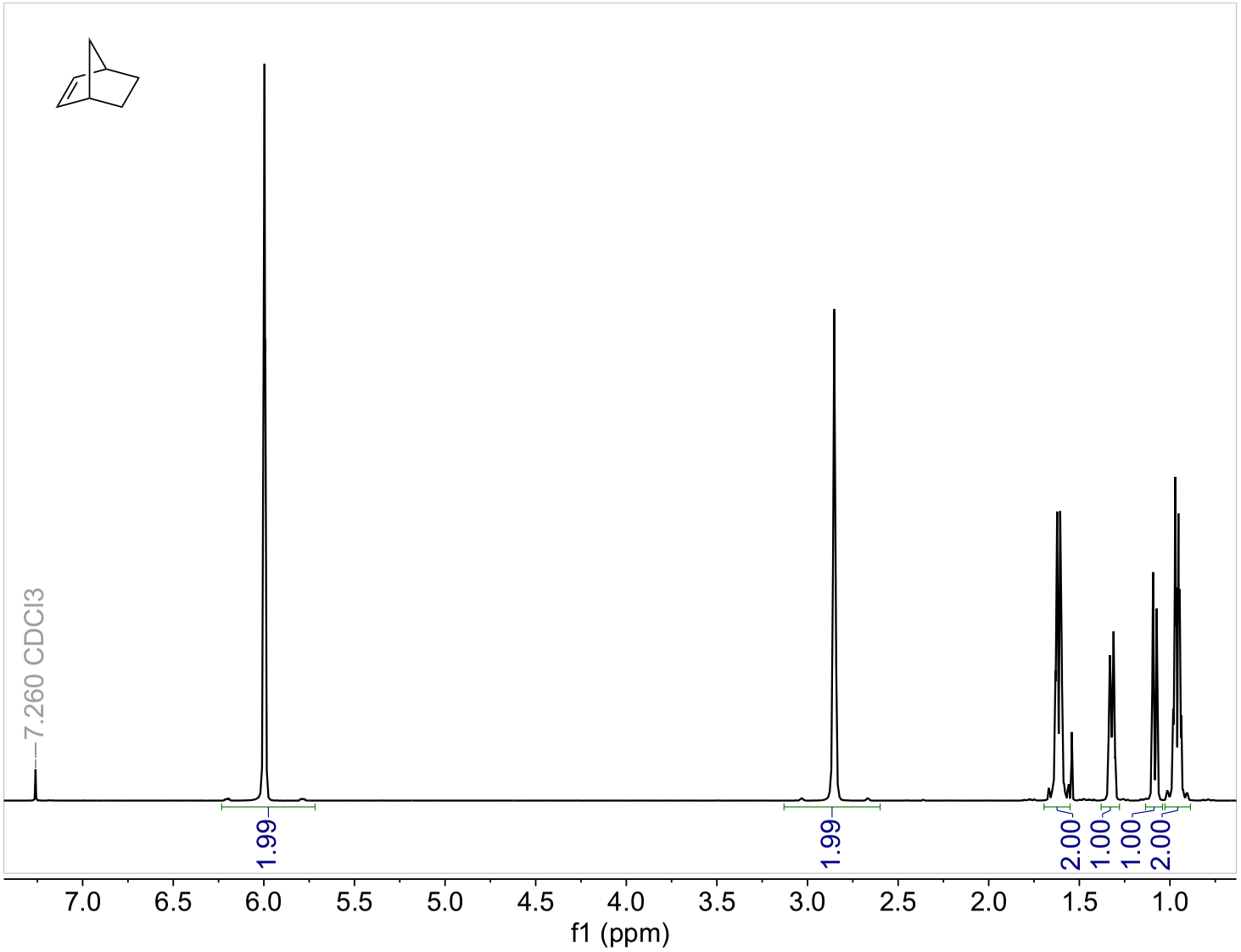

^{1}H NMR of Dicyclopentadiene (DCPD) in $CDCl_3$

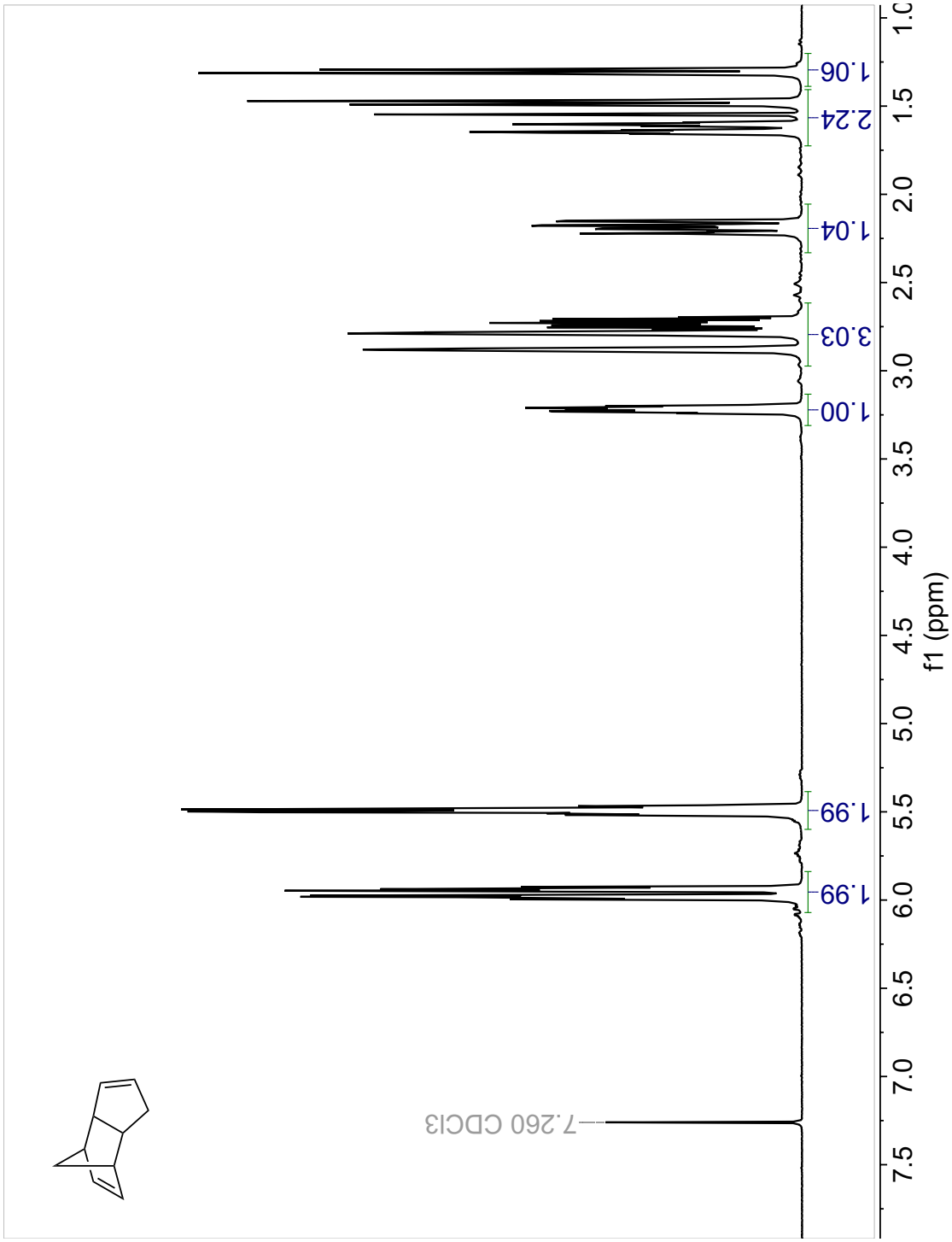

^{1}H NMR of Tetracyclododecene (TD) in oDCB and $CDCl_3$

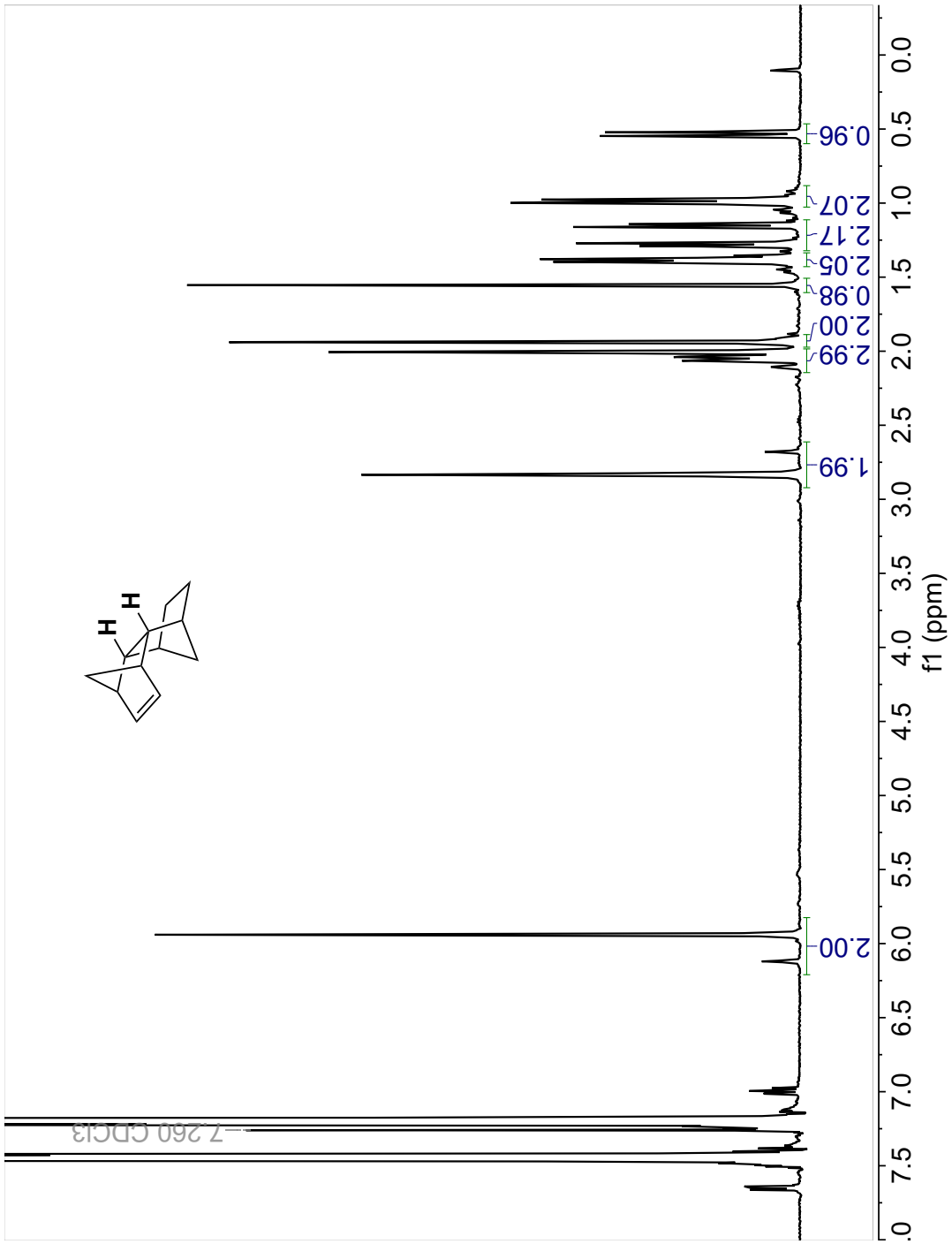

^{1}H NMR of pNB in $CDCl_3$

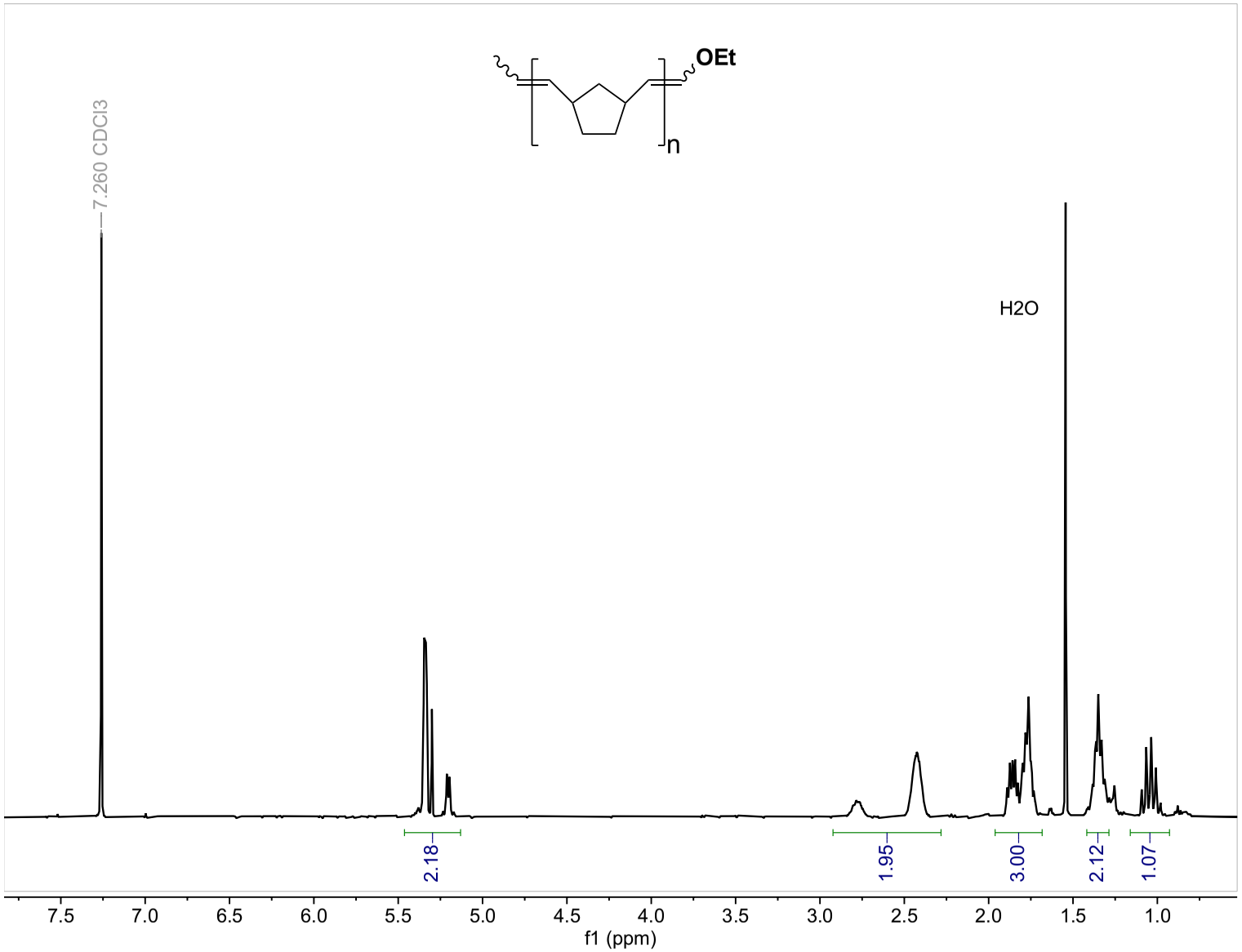

^{1}H NMR of pDCPD in $CDCl_3$

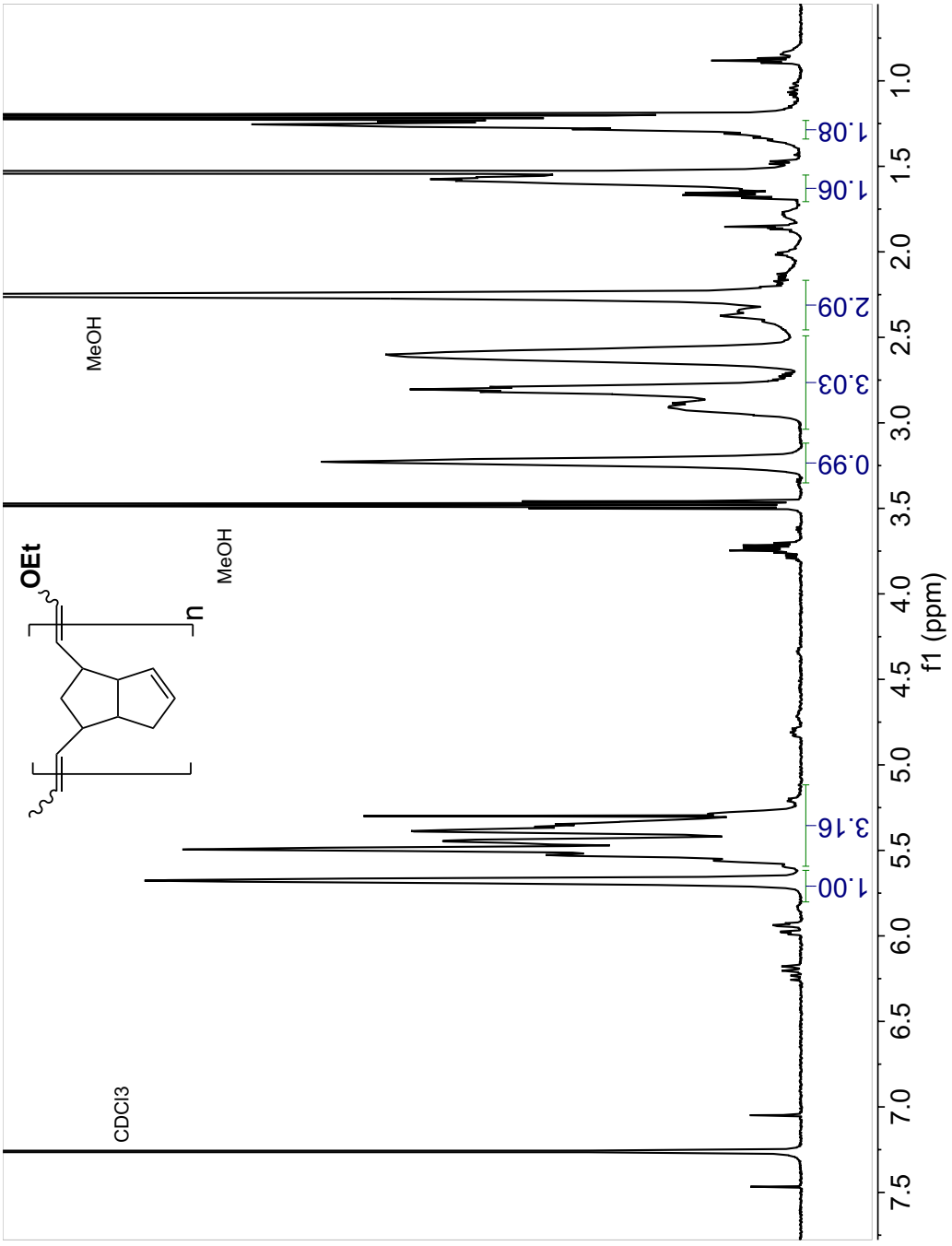

^{1}H NMR of pNB-*co*-DCPD in $CDCl_3$

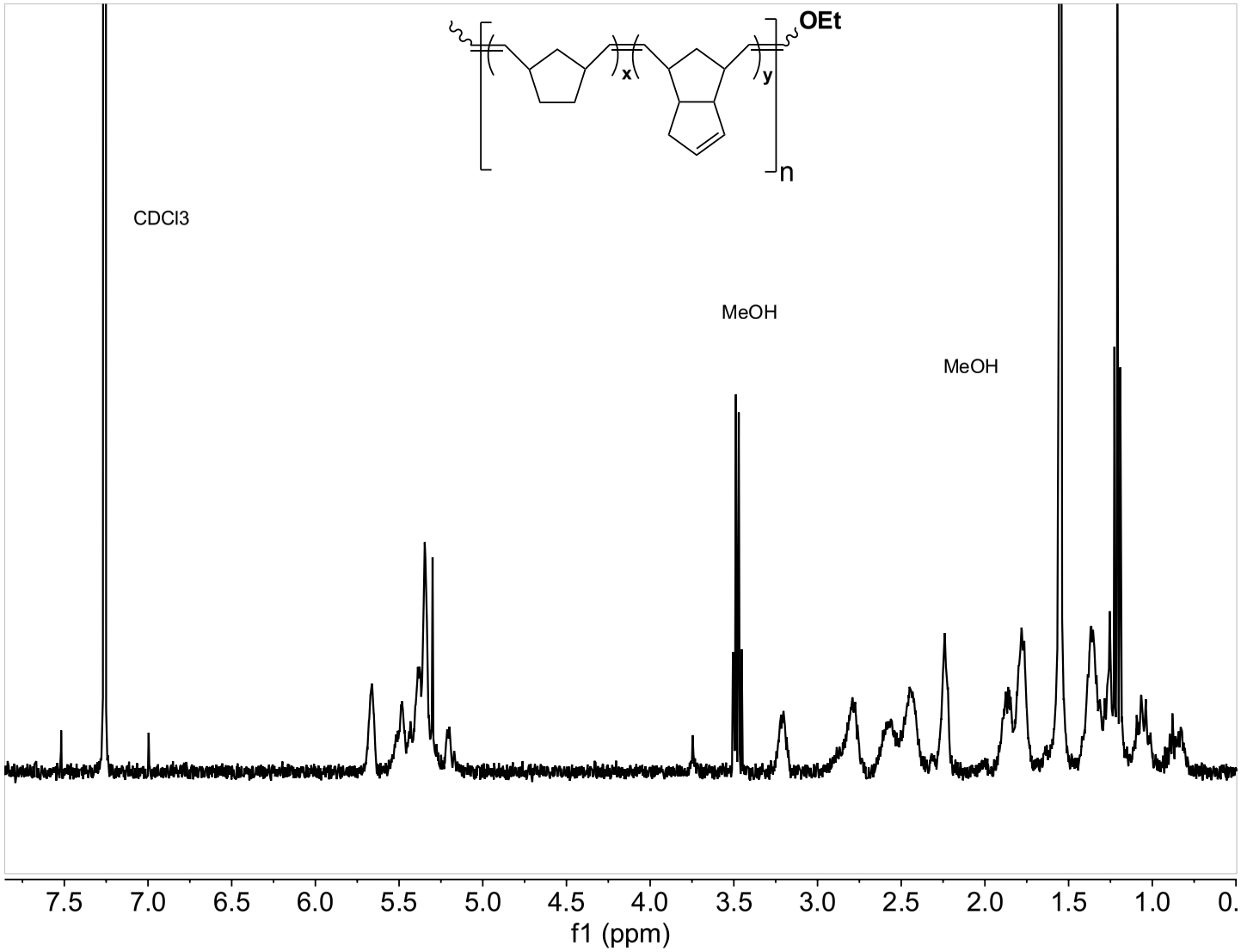

101

^{1}H NMR of pTD in $CDCl_3$

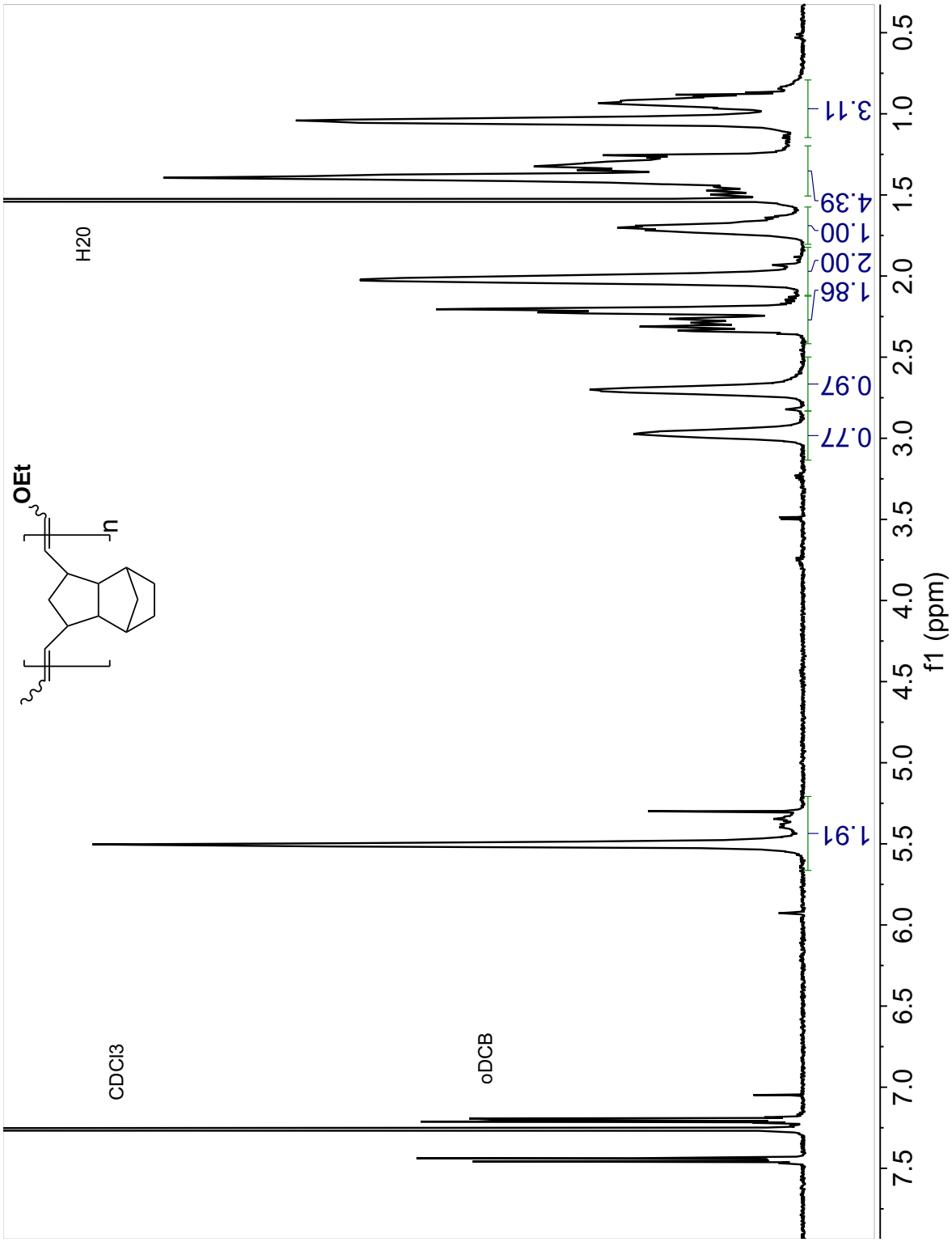

Representative ^{1}H NMR Spectrum and GPC Trace of crude pNB in $CDCl_3$

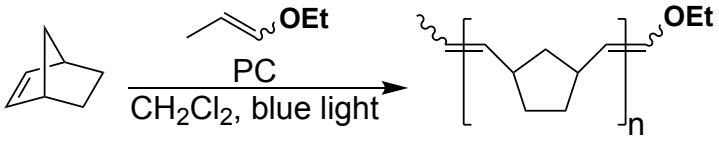

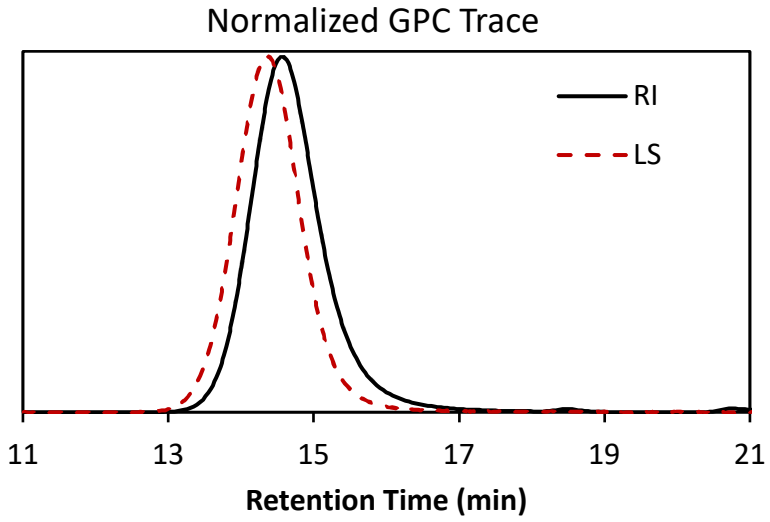

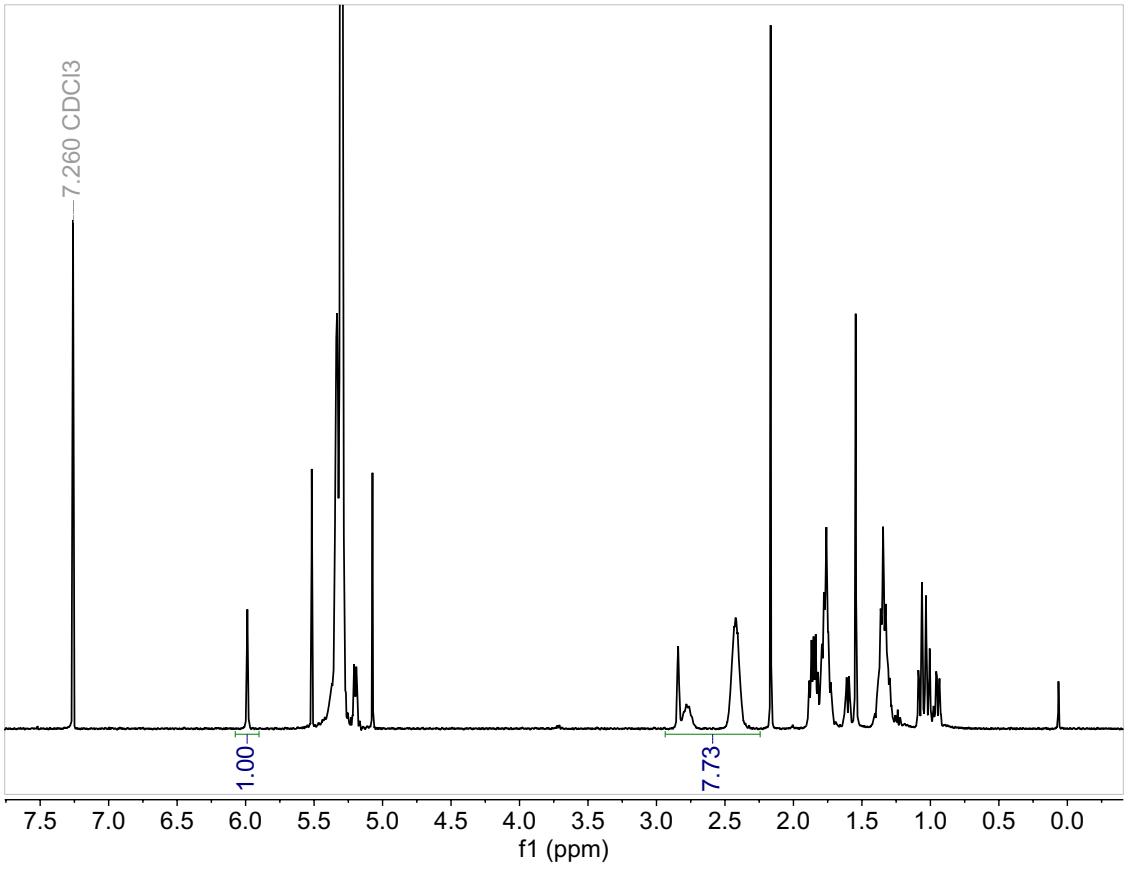

Representative ^{1}H NMR Spectrum and GPC Trace of crude pDCPD in $CDCl_3$

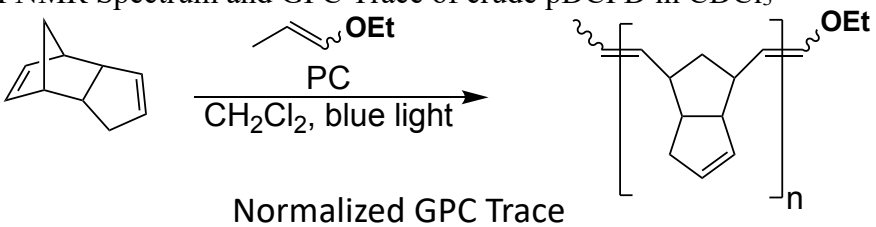

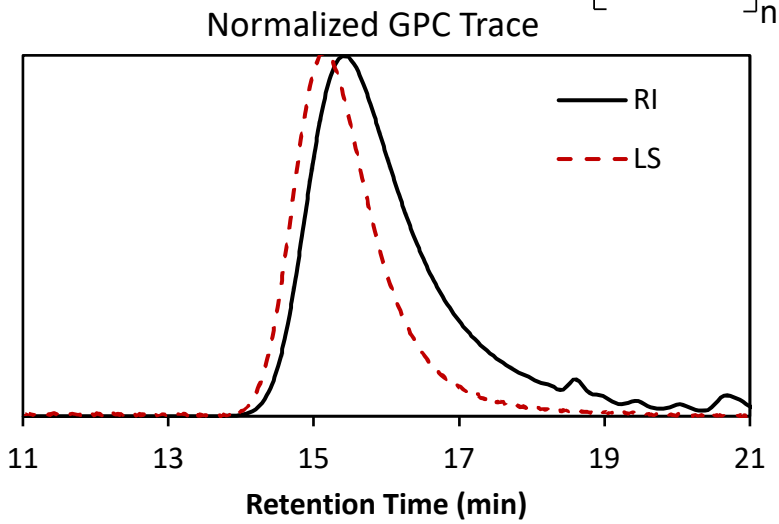

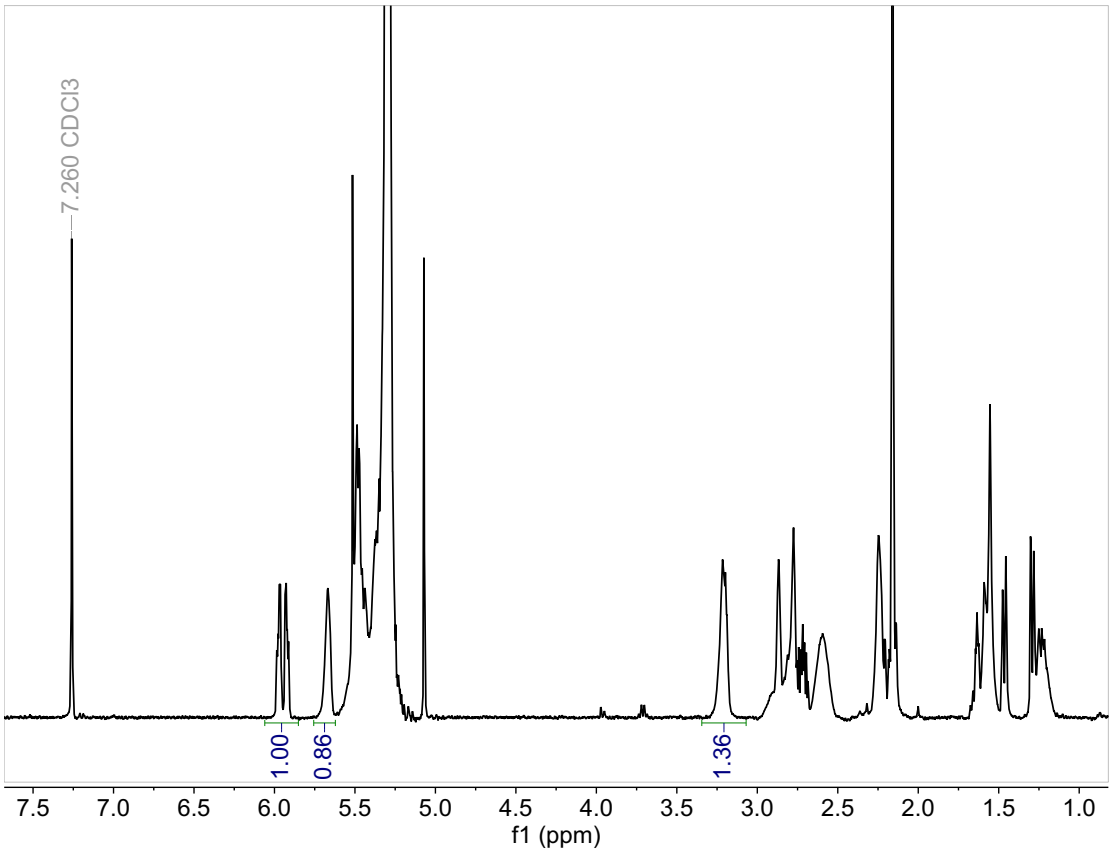

Representative ^{1}H NMR Spectrum and GPC Trace of crude pNB-*co*-DCPD in $CDCl_3$

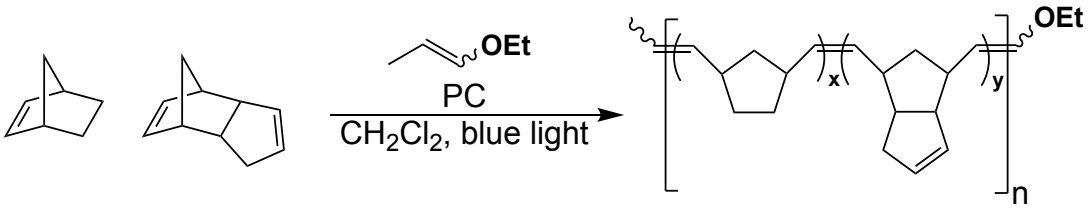

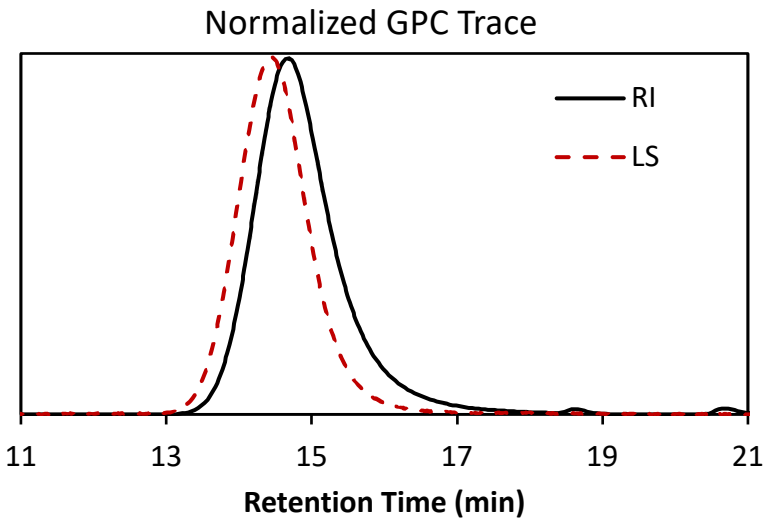

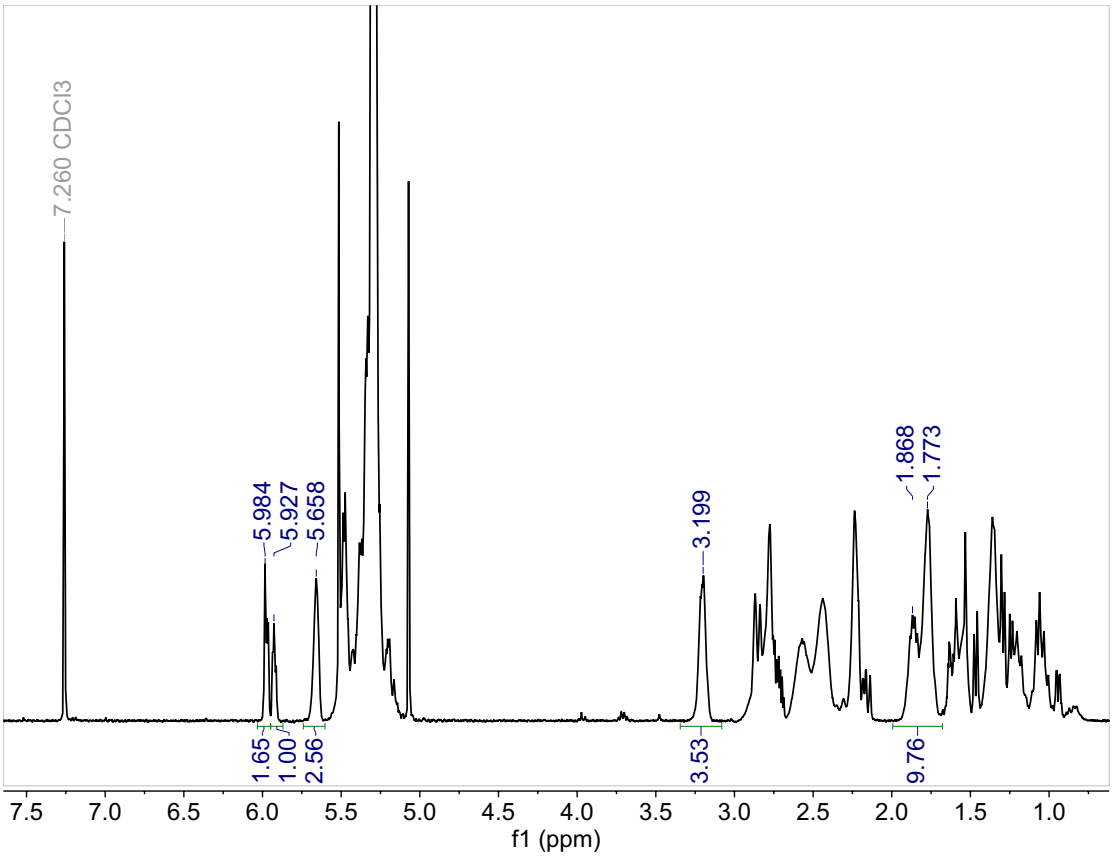

Representative ^{1}H NMR Spectrum and GPC Trace of crude pTD in $CDCl_3$

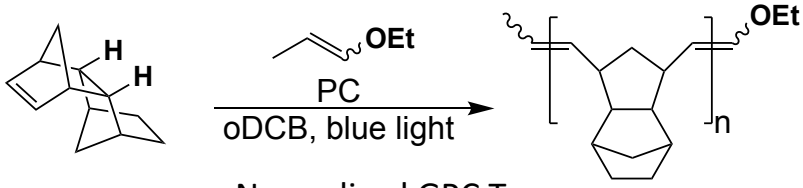

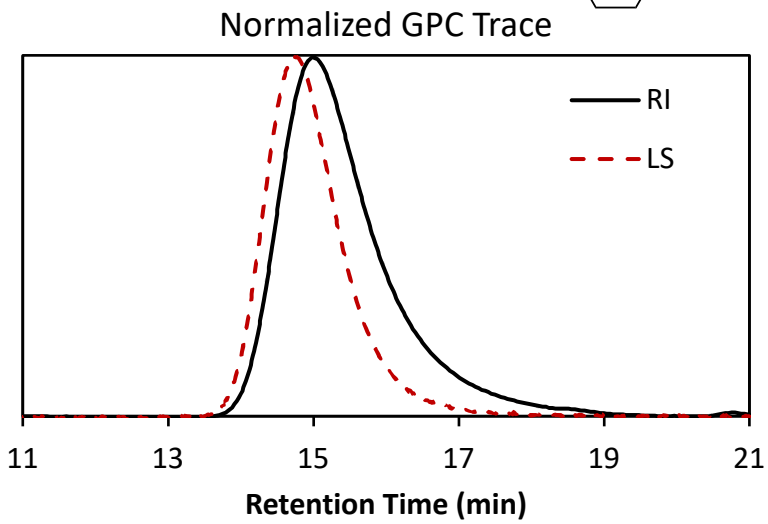

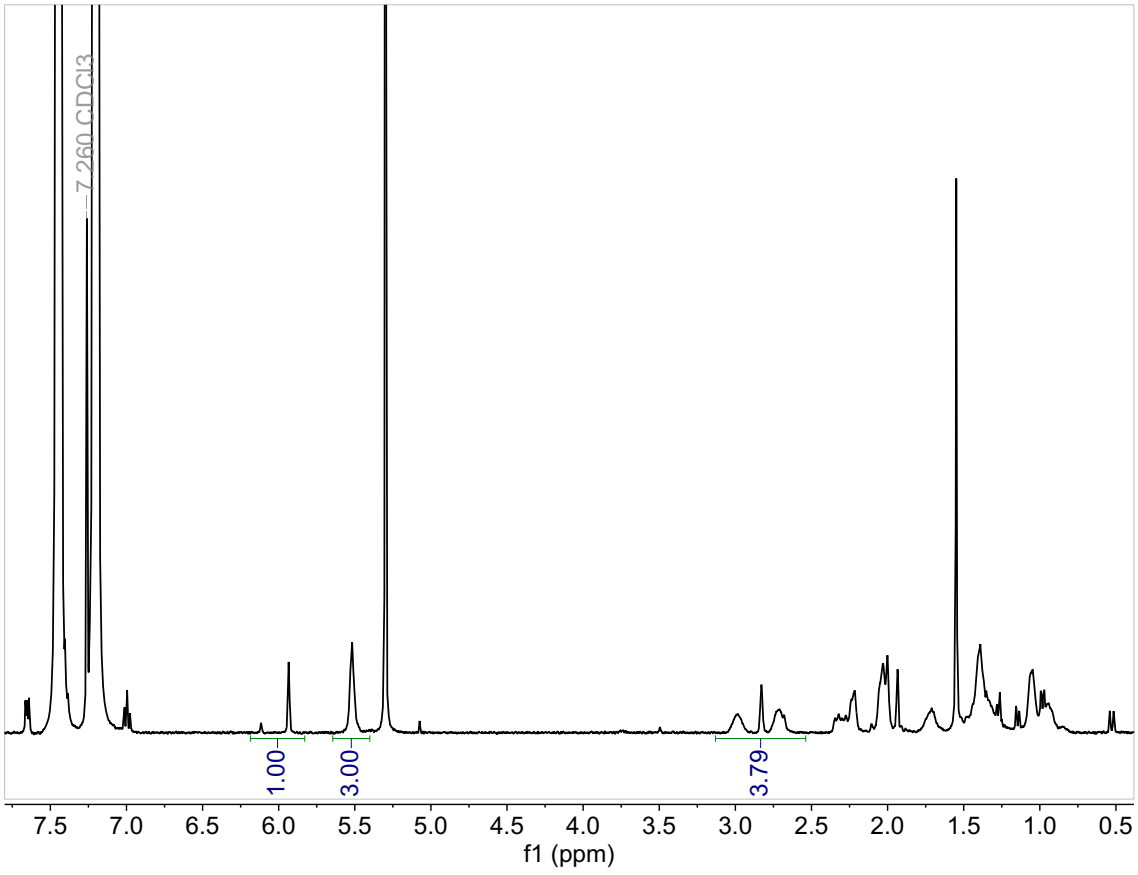

Chapter 4. References

1) Mol, J. C. Industrial applications of olefin metathesis. *Journal of Molecular Catalysis A: Chemical* **2004,** *213,* 39–45.

2) Schrock, R. R. Synthesis of stereoregular polymers through ring-opening metathesis polymerization. *Acc. Chem. Res.* **2014**, *47*, 2457−2466.

3) Sutthasupa, S.; Shiotsuki, M.; Sanda, F. Recent advances in ring-opening metathesis polymerization, and application to synthesis of functional materials. *Polym. J.* **2010**, *42*, 905−915.

4) Bielawski, C. W.; Grubbs, R. H. Living ring-opening metathesis polymerization. *Prog. Polym. Sci.* **2007**, *32*, 1−29.

5) Rosebrugh, L. E.; Marx, V. M.; Keitz, B. K.; Grubbs, R. H. Synthesis of highly cis, syndiotactic polymers via ring-opening metathesis polymerization using ruthenium metathesis catalysts. *J. Am. Chem. Soc*. **2013**, *135*, 10032−10035.

6) Jeong, H.; Kozera, D. J.; Schrock, R. R.; Smith, S. J.; Zhang, J.; Ren, N.; Hillmyer, M. A. Z-Selective Ring-Opening Metathesis Polymerization of 3-Substituted Cyclooctenes by Monoaryloxide Pyrrolide Imido Alkylidene (MAP) Catalysts of Molybdenum and Tungsten. *Organometallics* **2013**, *32*, 4843−4850.

7) Forrest, W. P.; Axtell, J. C.; Schrock, R. R. Tungsten oxo alkylidene complexes as initiators for the stereoregular polymerization of 2, 3-dicarbomethoxynorbornadiene. *Organometallics* **2014**, *33*, 2313−2325.

8) Chauvin, Y. Olefin metathesis: The early days (Nobel lecture). *Angew. Chem., Int. Ed*. **2006**, *45*, 3740−3747.

9) Schrock, R. R. Multiple metal–carbon bonds for catalytic metathesis reactions (Nobel lecture). *Angew. Chem., Int. Ed*. **2006**, *45*, 3748−3759.

10) Grubbs, R. H. Olefin-metathesis catalysts for the preparation of molecules and materials (Nobel lecture). *Angew. Chem., Int. Ed.* **2006**, *45*, 3760−3765.

11) Autenrieth, B.; Schrock, R. R. Stereospecific Ring-Opening Metathesis Polymerization (ROMP) of Norbornene and Tetracyclododecene by Mo and W Initiators. *Macromolecules* **2015**, *48*, 2493–2503.

12) Subnaik, S. I.; Hobbs, C. E. Flow-facilitated ring opening metathesis polymerization (ROMP) and post-polymerization modification reactions. *Polym. Chem*. **2019**, *10*, 4524–4528.

13) Ogawa, K. A.; Goetz, A. E.; Boydston, A. J. Metal-Free Ring-Opening Metathesis Polymerization. *J. Am. Chem. Soc.* **2015**, *137*, 1400–1403.

14) Tonhauser, C.; Natalello, A.; Löwe, H.; Frey, H. Microflow Technology in Polymer Synthesis. *Macromolecules* **2012**, *45*, 9551−9570.

15) Parida, D.; Serra, C. A.; Gomez, R. I.; Garg, D. K.; Hoarau, Y.; Bouquey, M.; Muller, R. Atom Transfer Radical Polymerization in Continuous Microflow: Effect of Process Parameters. *J. Flow Chem.* **2014**, *4*, 92−96.

16) Den Haese, M.; Gemoets, H. P. L.; Van Aken, K.; Pitet, L. M. Fully biobased triblock copolymers generated using an unconventional oscillatory plug flow reactor. *Polym. Chem.* **2022**, *13*, 4406–4415.

17) Fortelný, I.; Juza, J. Description of the Droplet Size Evolution in Flowing Immiscible Polymer Blends. *Polymers* **2019**, *11*, 761.

18) Reis, M. H.; Leibfarth, F. A.; Pitet, L. M. Polymerizations in Continuous Flow: Recent Advances in the Synthesis of Diverse Polymeric Materials. *ACS Macro Lett.* **2020**, *9*, 123−133.

19) Plutschack, M. B.; Pieber, B.; Gilmore, K.; Seeberger, P. H. The Hitchhiker's Guide to Flow Chemistry. *Chem. Rev.* **2017**, *117*, 11796−11893.

20) Junkers, T. Precise Macromolecular Engineering via Continuous- Flow Synthesis Techniques. *J. Flow Chem.* **2017**, *7*, 106−110.

21) Hu, X.; Zhu, N.; Fang, Z.; Guo, K. Continuous Flow Ring- Opening Polymerizations. *React. Chem. Eng.* **2017**, *2*, 20−26.

22) Elliott, L. D.; Berry, M.; Harji, B.; Klauber, D.; Leonard, J.; Booker-Milburn, K. I. A Small-Footprint, High-Capacity Flow Reactor for UV Photochemical Synthesis on the Kilogram Scale. *Org. Process Res. Dev.* **2016**, *20*, 1806−1811.

23) Herrero-Gomez, E.; van der Loo, C. H. M.; Rioz-Martínez, A.; Keene, N. F.; Li, B.; Pouwer, K.; Allais, C. Photo-oxidation of Cyclopentadiene Using Continuous Processing: Application to the Synthesis of (1R,4S)-4-Hydroxycyclopent-2-en-1-yl Acetate. *Org. Process Res. Dev*. **2020**, *24*, 2304−2310.

24) Aroh, K. C.; Jensen, K. F. Efficient kinetic experiments in continuous flow microreactors. *React. Chem. Eng*. **2018**, *3*, 94–101.

25) González-Esguevillas, M.; Fernández, D. F.; Rincón, J. A.; Barberis, M.; Frutos, O.; Mateos, C.; García-Cerrada, S.; Agejas, J.; MacMillan, D. W. C. Rapid Optimization of Photoredox Reactions for Continuous-Flow Systems Using Microscale Batch Technology. *ACS Cent. Sci.* **2021**, *7*, 1126–1134.

26) Rehm, T. H. Reactor Technology Concepts for Flow Photochemistry. *ChemPhotoChem* **2020**, *4*, 235–254.

27) Sun, A. C.; Steyer, D. J.; Allen, R. A.; Payne, E. M.; Kennedy, R. T.; Stephenson, C. R. J. A droplet microfluidic platform for high-throughput photochemical reaction discovery. *Nat. Commun.* **2020** *11*, 6202.

28) Harper, K. C.; Moschetta, E. G.; Bordawekar, S. V.; Wittenberger, S. J. A Laser Driven Flow Chemistry Platform for Scaling Photochemical Reactions with Visible Light. *ACS Cent. Sci.* **2019**, *5*, 109−115.

29) Andrews, S. R.; Becker, J. J.; Gagné, M. R. A Photoflow Reactor for the Continuous Photoredox-Mediated Synthesis of C-Glycoamino Acids and C-Glycolipids.

30) Su, Y.; Straathof, N. J. W.; Hessel, V.; Noël, T. Photochemical Transformations Accelerated in Continuous-Flow Reactors: Basic Concepts and Applications. *Chem. Eur. J.* **2014**, *20*, 10562−10589.

31) Straathof, N. J. W.; Su, Y.; Hessle, V.; Noël, T. Accelerated gas-liquid visible light photoredox catalysis with continuous-flow photochemical microreactors. *Nature Protocols* **2016,** *11,* 10–21.

32) Yang, X.; Murphy, L. M.; Haque, F. M.; Grayson, S. M.; Boydston, A. J. A highly efficient metal-free protocol for the synthesis of linear polydicyclopentadiene. *Polym. Chem*., **2021**, *12*, 2860–2867.

33) Goetz, A. E.; Pascual, L. M. M.; Dunford, D. G.; Ogawa, K. A.; Knorr, D. B.; Boydston, A. J. Expanded Functionality of Polymers Prepared using Metal-Free Ring-Opening Metathesis Polymerization. *ACS Macro Lett.* **2016**, *5*, 579–582.

34) Goetz, A. E.; Boydston, A. J. Metal-Free Preparation of Linear and Cross-Linked Polydicyclopentadiene. *J. Am. Chem. Soc.* **2015**, *137*, 7572–7575.

35) Kensy, V. K.; Tritt, R. L.; Haque, F. M.; Murphy, L. M.; Knorr, D. B.; Grayson, S. M.; Boydston, A. J. Molecular Weight Control via Cross Metathesis in Photo-Redox Mediated Ring-Opening Metathesis Polymerization. *Angew. Chem., Int. Ed.*, **2020**, *59*, 9074–9079.

36) Lu, P.; Kensy, V. K.; Tritt, R. L.; Seidenkranz, D. T.; Boydston, A. J. Metal-Free Ring-Opening Metathesis Polymerization: From Concept to Creation. *Acc. Chem. Res*. **2020**, *53*, 2325–2335.

37) Abadie, M. J.; Dimonie, M.; Couve, C.; Dragutan, V. New catalysts for linear polydicyclopentadiene synthesis. *Eur. Polym. J.* **2000**, *36*, 1213–1219.

38) Autenrieth, B.; Jeong, H.; Forrest, W. P.; Axtell, J. C.; Ota, A.; Lehr, T.; Buchmeiser, M. R.; Schrock, R. R. Z-Selective and Syndioselective Ring-Opening Metathesis Polymerization (ROMP) Initiated by Monoaryloxidepyrrolide (MAP) Catalysts. *Macromolecules* **2015**, *48*, 2480–2492.

39) Hayano, S.; Kurakata, H.; Tsunogae, Y.; Nakayama, Y.; Sato, Y.; Yasuda, H. Stereospecific Ring-Opening Metathesis Polymerization of Cycloolefins Using Novel Molybdenum and

Tungsten Complexes Having Biphenolate Ligands. Development of Crystalline Hydrogenated Poly(endo-dicyclopentadiene) and Poly(norbornene). *Macromolecules* **2003**, *36*, 7422–7431.

40) Hayano, S.; Takeyama, Y.; Tsunogae, Y.; Igarashi, I. Hydrogenated Ring-Opened Poly(endo-dicyclopentadiene)s Made via Stereoselective ROMP Catalyzed by Tungsten Complexes: Crystalline Tactic Polymers and Amorphous Atactic Polymer. *Macromolecules* **2006**, *39*, 4663–4670.

41) Dono, K.; Huang, J.; Ma, H.; Qian, Y. Ring opening metathesis polymerization of dicyclopentadiene catalyzed by titanium tetrachloride adduct complexes with nitrogen-containing ligands. *J. Appl. Polym. Sci*. **2000**, *77*, 3247–3251.

42) Steese, N. D.; Barvaliya, D.; Poole, X. D.; McLemore, D. E.; DiCesare, J. C.; Schanz, J. J. Synthesis and thermal properties of linear polydicyclopentadiene via ring-opening metathesis polymerization with a third generation grubbs-type ruthenium-alkylidene complex. *J. Polym. Sci., Part A: Polym. Chem*. **2018**, *56*, 359–364.

43) Dumrath, C.; Dumrath, A.; Neumann, H.; Beller, M.; Kadyrov, R. Practical Ruthenium Catalysts for the Synthesis of Cyclic Olefin Oligomers, Polymers, and their Hydrogenated Derivatives. *ChemCatChem* **2014**, *6,* 3101–3104.

44) Yao, Z. Wang, Z.; Yu, Y.; Zeng, C.; Cao, K. Facile synthesis and properties of the chemo-reversible and highly tunable metallogels based on polydicyclopentadiene. *Polymer* **2017**, *119*, 98–106.

45) Straathof, N. J. W.; Noël, T. Accelerating Visible-Light Photoredox Catalysis in Continuous-Flow Reactors. In *Visible Light Photocatalysis in Organic Chemistry*; Stephenson, C. R. J., Yoon, T. P., MacMillan, D. W. C., Eds.; Wiley-VCH: Weinheim, Germany, 2018; Chapter 13, pp 389−410.

46) Knowles, J. P.; Elliott, L. D.; Booker-Milburn, K. I. Flow photochemistry: Old light through new windows. *Beilstein J. Org. Chem.* **2012**, *8*, 2025–2052.

47) Aillet, T.; Loubiere, K.; Dechy-Cabaret, O.; Prat, L. Photochemical synthesis of a “cage” compound in a microreactor: Rigorous comparison with a batch photoreactor. *Chem. Eng. Process.* **2013**, *64*, 38–47.

48) Hook, B. D. A.; Dohle, W.; Hirst, P. R.; Pickworth, M.; Berry, M. B.; Booker-Milburn, K. I. A Practical Flow Reactor for Continuous Organic Photochemistry. *J. Org. Chem*. **2005**, *70*, 7558–7564.

49) Ramsey, B. L.; Pearson, R. M.; Beck, L. R.; Miyake, G. M. Photoinduced Organocatalyzed Atom Transfer Radical Polymerization Using Continuous Flow. *Macromolecules* **2017**, *50*, 2668−2674.

50) Buss, B. L.; Miyake, G. M. Photoinduced Controlled Radical Polymerizations Performed in Flow: Methods, Products, and Opportunities. *Chem. Mater.* **2018**, *30*, 3931−3942.

51) Rubens, M.; Latsrisaeng, P.; Junkers, T. Visible light-induced iniferter polymerization of methacrylates enhanced by continuous flow. *Polym. Chem.* **2017,** *8,* 6496–6505.

52) Lauterbach, F.; Rubens, M.; Abetz, V.; Junkers, T. Ultrafast PhotoRAFT Block Copolymerization of Isoprene and Styrene Facilitated through Continuous-Flow Operation. *Angew. Chem. Int. Ed.* **2018**, *57*, 14260–14264.

53) Corrigan, N.; Almasri, A.; Taillades, W.; Xu, J.; Boyer, C. Controlling Molecular Weight Distributions through Photoinduced Flow Polymerization. *Macromolecules* **2017**, *50*, 8438–8448.

54) Chen, K.; Zhou, Y.; Han, S.; Liu, Y.; Chen, M. Main-Chain Fluoropolymers with Alternating Sequence Control via Light-Driven Reversible-Deactivation Copolymerization in Batch and Flow. *Angew. Chem. Int. Ed.* **2022**, *61*, e202116135.

55) Davidson, C. L. G. IV; Lott, M. E.; Traschel, L.; Wong, A. J.; Olson, R. A.; Pedro, D. I.; Sawyer, W. G.; Sumerlin, B. S. Inverse Miniemulsion Enables the Continuous-Flow Synthesis of Controlled Ultra-High Molecular Weight Polymers. *ACS Macro Lett.* **2023,** *12,* 1224–1230.

56) Song, H.; Chen, D. L.; Ismagilov, R. F. Reactions in Droplets in Microfluidic Channels. *Angew. Chem. Int. Ed.* **2006**, *45*, 7336–7356.

57) i Solvas, X. C.; Droplet microfluidics: recent developments and future applications. *Chem. Commun.* **2011**, *47*, 1936–1942.

58) Lima, M. J.; Silva, A. M. T.; Silva, C. G.; Faria, J. L.; Lopes, J. C. B.; Dias, M. M. An innovative static mixer photoreactor: Proof of concept. *Chem. Eng. J.* **2016,** *287,* 419–424.

59) Gobert, S. R. L.; Kuhn, S.; Braeken, L.; Thomassen, L. C. J. Characterization of Milli- and Microflow Reactors: Mixing Efficiency and Residence Time Distribution. *Org. Process Res. Dev.* **2017**, *21*, 531−542.

60) Danckwerts, P. V. Continuous flow systems: Distribution of residence times. *Chem. Eng. Sci.* **1953**, *2*, 1−13.

61) Angeli, P.; Gavriilidis, A. Hydrodynamics of Taylor flow in small channels: a review. Proceedings of the Institution of Mechanical Engineers, Part C: Journal of Mechanical Engineering Science **2008**, 222, 737–751.

62) Villermaux, E. Mixing Versus Stirring. *Annual Review of Fluid Mechanics* **2019**, *51*, 245–273.

63) Rhee, M.; Burns, M. A. Membranous Bypass Valves for Discrete Drop Mixing and Routing in Microchannels. *Sensors & Transducers Journal* **2008,** *3*, 37–46.

64) Chen, C.; Zhao, Y.; Wang, J.; Zhu, P.; Tian, Y.; Xu, M.; Wang, L. Huang, X. Passive Mixing inside Microdroplets. *Micromachines* **2018**, *9*, 160.

65) Loizou, K.; Wong, V. L.; Hewakandamby, B. Examining the Effect of Flow Rate Ratio on Droplet Generation and Regime Transition in a Microfluidic T-Junction at Constant Capillary Numbers. *Inventions* **2018**, *3*, 54.

66) Reis, M. H.; Varner, T. P.; Leibfarth, F. A. The Influence of Residence Time Distribution on Continuous-Flow Polymerization. *Macromolecules* **2019**, *52*, 3551−3557.

67) Lu, S.; Wang, K. Kinetic study of TBD catalyzed δ-valerolactone polymerization using a gas-driven droplet flow reactor. *React. Chem. Eng*. **2019**, *4*, 1189–1194.

68) Schrimpf, M.; Esteban, J.; Warmeling, H.; Färber, T.; Behr, A.; Vorholt, A. J. Taylor-Couette reactor: Principles, design, and applications. *AIChE J.* **2021**; *67*, e17228.

69) Russum, J. P.; Jones, C. W.; Schork, F. J. Impact of Flow Regime on Polydispersity in Tubular RAFT Miniemulsion Polymerization. *AIChE J*. **2006,** *52*, 1566–1576.

70) Zhou, Y.; Gu, Y.; Kunming, J.; Chen, M. Droplet-Flow Photopolymerization Aided by Computer: Overcoming the Challenges of Viscosity and Facilitating the Generation of Copolymer Libraries. *Macromolecules* **2019**, *52*, 5611−5617.

71) Zhou, Y.; Fu, Y.; Chen, M. Facile Control of Molecular Weight Distribution via Droplet-Flow Light-Driven Reversible-Deactivation Radical Polymerization. *Chin. J. Chem.* **2022**, *40*, 2305–2312.

72) Martiny, M.; Steckhan, E.; Esch, T. Cycloaddition Reactions Initiated by Photochemically Excited Pyrylium Salts. *Chem. Ber.* **1993,** *126*, 1671-1682.

Chapter 5

Polymer Chemistry for the General Public

Section 0: Who's this chapter for, and why is science communication important?

This chapter is meant for anyone interested in learning more about chemistry and what chemists do! The preceding chapters of my thesis that describe my research are written with chemists as the audience, so there are various technical, chemistry terms thrown around which make it harder for non-chemists to follow these chapters. In this chapter, I'll describe my research (mainly from dissertation chapters 1 and 4) for **anyone** that's interested but doesn't want to be slowed down by scientific jargon.

Describing one's own research so that a wide audience can follow is a huge skill called science communication, and I've worked hard to develop this skill over the course of my graduate schooling. Science communication is a vital skill for any scientist, because at some point we hope that non-scientists will be able to use our research. This means we need to explain the motivation behind our research and how to use our research to people that are interested in listening.

Science communication is also important to me as an educator. Students that take general chemistry and organic chemistry (usually not because the students want to but because their major requires it), walk away never wanting to look at chemistry again. This is a problem that educators need to address. We see chemistry as a beautiful, logical science, but we still have trouble motivating learning students that don't see the full picture yet. I strive to describe my science in interesting (but still accurate) ways because when I eventually teach science, I want everyone to have the opportunity to love chemistry just as much as I do.

Section 1: What are polymers, how do you make them, and why are they important?

The word “polymer” comes from the Greek words “poly” (meaning many) and “mer” (meaning parts). A polymer is a molecule formed by stringing together smaller molecules called monomers (“mono” meaning single in Greek). You can make a polymer by taking a molecule and then combining it with itself over and over again.

Making polymers is like using LEGO building blocks at the molecular level (see Figure 1 on the next page for an illustration of this analogy). You can combine these different little pieces and make them into a variety of structures to achieve a multitude of material and chemical properties. The length, sequence, and structure of the polymer can greatly affect its characteristics, and the ability to combine these molecules in many different ways to create many different properties is why we frequently encounter polymers in everyday life. Plastics, spandex, rubber, Kevlar, tree bark, and even DNA—these are all examples of polymers!

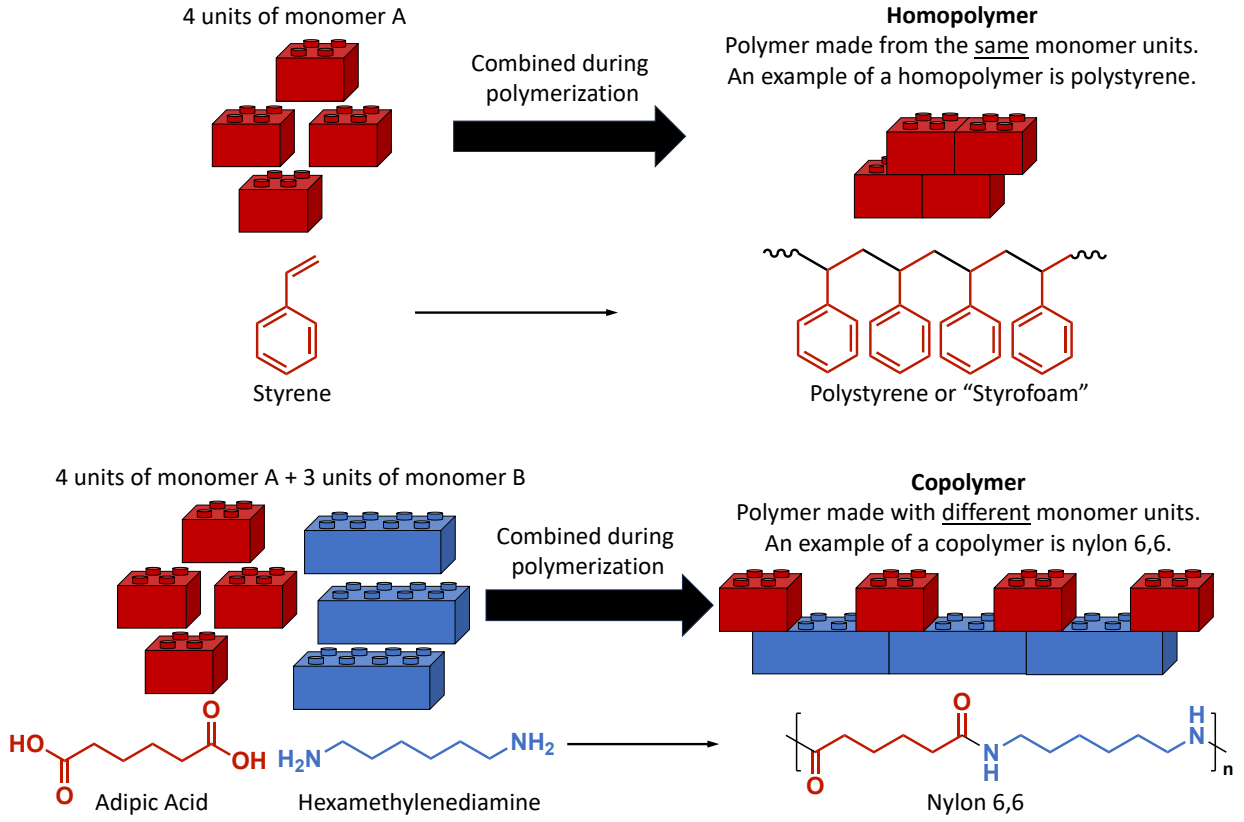

Figure 1. Comparing polymers to LEGOs. Polymers are very similar to LEGOs—both are made from smaller units and can be combined in different ways to make a multitude of different products. Shown is an example of a homopolymer ("homo" meaning same) and copolymer ("co" meaning together). The homopolymer consists of the same one monomer combined over and over again, while the copolymer consists of many different monomers combined together. Polystyrene, (commonly called Styrofoam, the material frequently used for coffee cups) is a homopolymer. Nylon 6,6 (the clothing material) is a copolymer made from the monomers adipic acid and hexamethylenediamine. Fun fact: LEGOs are actually made from the copolymer ABS (acrylonitrile butadiene styrene, a polymer made with 3 different monomer units).

Section 2: What's the role of a polymer chemist, and what are the problems they solve?

Polymer chemists have this really interesting job. We make polymers, study their properties, and figure out ways to more easily manufacture them. To study polymers, we use different types of equipment to determine molecular properties (like how long each polymer is) and physical properties (like how strong the polymer is). We then try to figure out how these different properties are related so we can design polymers with specific properties.

The polymer chemistry field also has a challenging problem: we need to make enough polymers to meet the ever-growing demand for polymer products, which is projected to reach over one billion tons by 2050, but we also need to do this sustainably, because we don't want plastic trash everywhere, and we want to make sure our polymers aren't environmentally toxic.

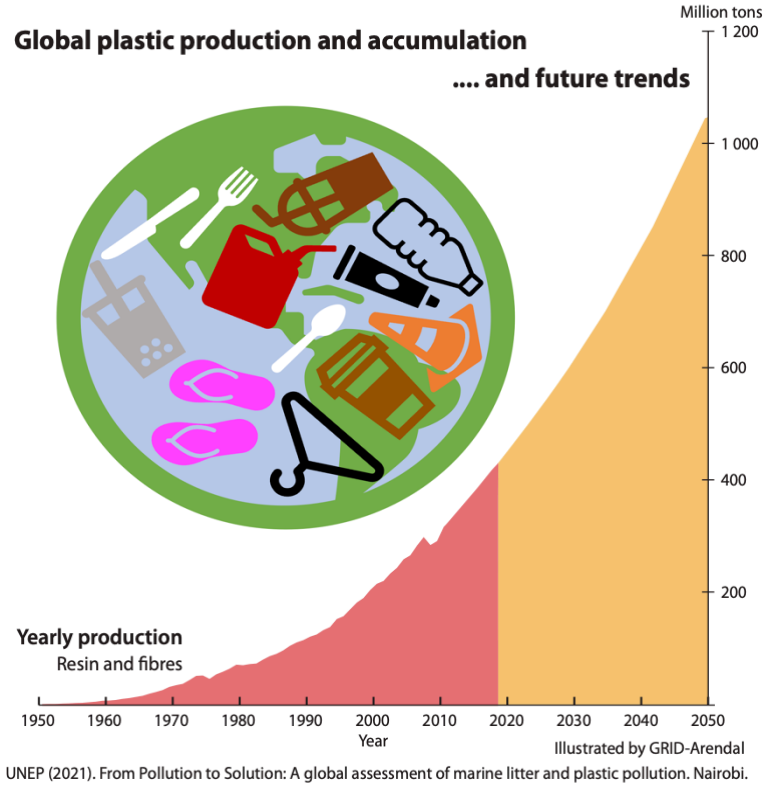

Figure 2. Plastic production forecast through 2050. Red area represents measured data, orange area represents forecasted data. Reproduced from Grid-Arendal UNEP (2021).

Section 3: What research are you working on, and how are you solving these polymer sustainability problems?

My primary research goal is to prepare a polymerization performed in a small-scale university laboratory for a large-scale industrial laboratory or factory. I optimize the polymerization process by testing different reactor setups making it safer, greener, and more efficient. For example, I may take a product stirred in a small glass jar the size of a thumb, and mix it in an even bigger glass jar the size of a refrigerator. Or if you don't need to stir it, I can run the reaction mixture through something called a flow reactor, which is just some tubing that allows your reaction to occur (a flow reactor is similar to a water faucet except instead of water coming out of the faucet, the polymer product comes out). In flow reactors, scaling up production just requires faster flow speeds (like turning the faucet on higher) instead of larger reactor volumes. But the specific polymerization that I'm studying is a bit trickier to make efficient.

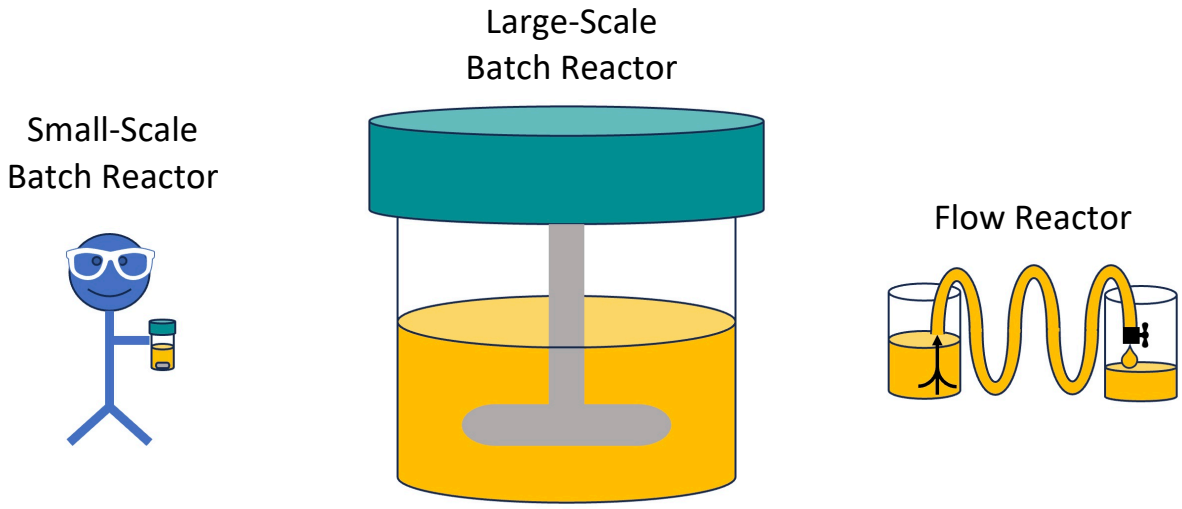

Figure 3. Graphic of small-scale batch, large-scale batch, and flow reactor setups. Approximately to scale.

I'm studying a polymerization where the building blocks are molecular rings and the polymer is made by breaking open these rings and stitching them to the next ring. Normally, the rings are hard to break apart, like opening a nut with only your hands. Fortunately, we can use molecular nutcrackers—reactive, toxic metals—to crack open up the donuts. After these rings are opened, the metal also stitches them together. But since we use toxic metals in the polymerization, (1) you can't use these polymers in any biological applications and (2) discarding them becomes an environmental hazard (this ring-opening chemistry is so effective and efficient that it won the 2005 Nobel Prize for Chemistry). To avoid using these reactive metals, my research group found an alternative way to open these rings: we use visible light to crack them! Now that we use light instead of metals for the polymerization, we can use these polymer products for any application we want, and it's safer for the environment.

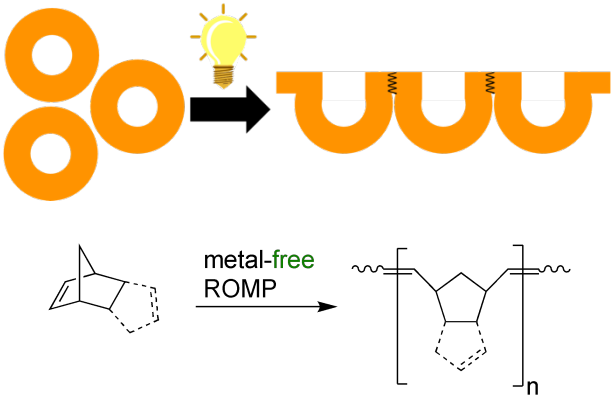

Figure 4. My polymerization of focus. It's called metal-free ring-opening metathesis polymerization (MF-ROMP), which is the scientific way to describe that the polymerization involves opening up molecular rings! The product polymer can be used as sound-proofing material, car plastic, clothing padding, or even oil-spill cleanup material.

However, using light adds an obstacle towards scaling up the polymer production. How we make the polymer is by stirring a liquid in a small glass vial and then shining a bright blue LED

on it. But if we try using a bigger glass jar, the light isn't strong enough and won't reach the center of the jar. (You can think about it like trying to use a flashlight on a faraway object at night—even when you use a laser pointer, your light can't reach the moon!). This is problematic because then the polymerization will only occur on the exposed side of the reactor, making the process really inefficient.

Another alternative to a bigger batch reactor is using an unstirred flow reactor. In this case, the tubing is usually narrow enough so light penetration isn't an issue, but now the reaction is inefficient for a different reason. Since we can't stir the reaction solution, the only mixing that occurs comes from diffusion (the natural tendency of liquids to mix themselves, try dropping food dye in water and watching it mix itself), which creates a significant amount of inconsistency in the polymerization process. It's like adding all the ingredients of cake into an oven without mixing it—you won't make a very good cake!

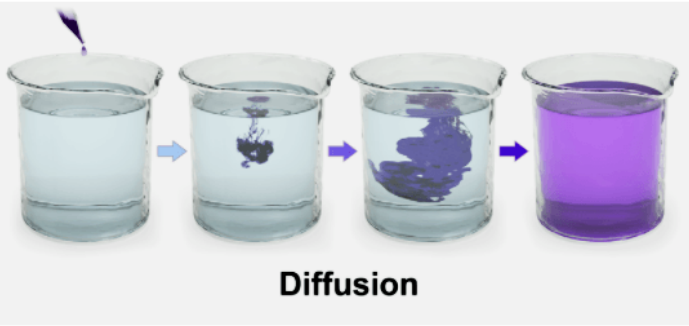

Figure 5. Graphic of diffusion using purple food dye in water. The leftmost image shows the water right before the food dye was added. The adjacent images show how the dye mixes into the water via diffusion over time until the dye looks evenly distributed within the water (Even at this last point diffusion occurs, but we can no longer observe it because it no longer produces a color change). Graphic from BruceBlause CC By 3.0 via Wikimedia Commons.

So we can't achieve an efficient polymerization using a large-scale batch reactor (because of light penetration) or a conventional flow reactor (because of mixing issues). So I looked at ways the scientists get better mixing in flow reactors, and found something interesting… There's a reactor design where you mix a flow reactor! It's called droplet flow, and you pump liquid and gas through your flow reactor at the same time. This forms liquid droplets sandwiched between gas, and doing this actually causes your droplets to mix themselves. **Figure 7** shows this droplet flow reactor in use; you can see the yellow reaction solution sandwiched between the gas. Even after discovering this reactor setup, the polymerization wasn't efficient yet—I had to figure out what gas, temperature, light, and amounts work best. Let's think about cakes again. To make a great cake recipe, you need to know exactly how much of each ingredient to add, what oven temperature to use, and how long to cook your cake. You figure this out by comparing to others' cake recipes, learning from your past attempts, and harnessing your baker's intuition. This is basically how I came up with the final reactor optimizations!

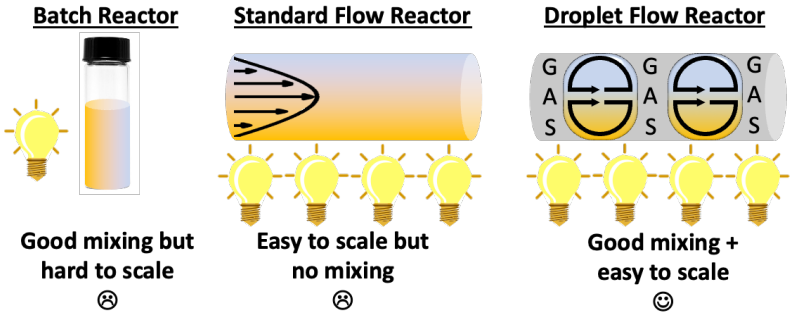

Figure 6. Comparison of the different reactor setups specifically for a polymerization that uses light.

Section 4: What excites you about this research project? What are the results of your research?

Throughout this research project, I worked on the cutting edge of polymer science, photoredox chemistry, and reaction engineering, and I got to learn new strategies and techniques every day. I'm also proud that this is the most efficient setup to make polymers this way as of 2023. You can reach 95% polymer conversion (the percentage of donuts that become polymer), and you can actually make a few pounds of polymer a month this way! I've been in contact with a company that's interested in adopting my reactor setups to help make their polymers more sustainable.

Figure 7. Image of the droplet flow reactor in use.

Section 5: Acknowledgments

I would like to thank the Wisconsin Initiative for Science Literacy (WISL) at UW-Madison for providing this opportunity in science communication, and for sponsoring and supporting the creation of this chapter. I'd like to specifically acknowledge Professor Bassam Shakhashiri, Elizabeth Reynolds, and Cayce Osborne for their valuable feedback and encouragement.

I would also like to thank the DELTA Program (including Dr. Devin Wixon and Dr. Jess Maher), CIRTL Network (including Kate Diamond), chemical education community at UW-Madison (including the Pazicni Group and Stowe Group), the UW-Madison Chemistry Teacher's Tea crew (including Dr. Liana Lamont, Dr. Brian Esselman, and Dr. Nick Hill), and the Boydston Group for teaching me how to be an effective science communicator.